MATERIALS SCIENCES CORPORATION

NASA CR-145308

(MSC/TFR/806/1025)

EVALUATION AND EXPANSION OF AN ANALYTICAL MODEL FOR FATIGUE OF NOTCHED COMPOSITE LAMINATES

R. L. Ramkumar, S. V. Kulkarni,
and R. B. Pipes

MATERIALS SCIENCES CORPORATION
Blue Bell, PA 19422

Prepared under Contract No. NAS1-13931

March 1978

National Aeronautics and
Space Administration

Langley Research Center
Hampton, Virginia 23665

MATERIALS SCIENCES CORPORATION

MSC/TFR/806/1025

EVALUATION AND EXPANSION OF AN ANALYTICAL MODEL FOR FATIGUE OF NOTCHED COMPOSITE LAMINATES

Prepared for:

National Aeronautics and
Space Administration
Langley Research Center
Hampton, VA 23665

Approved by:

B. Walter Rosen
President

Under Contract No. NAS1-13931

March 1978

BLUE BELL OFFICE CAMPUS • MERION TOWLE HOUSE • BLUE BELL, PA. 19422 • 215-542-8400

FOREWORD

This report summarizes the work accomplished by the Materials Sciences Corporation under NASA Contract NAS1-13931. Mr. G. L. Roderick (US AAMRDL, Langley Directorate) was the NASA Project Engineer.

The Program Manager and Principal Investigator for Materials Sciences Corporation were Dr. S. V. Kulkarni and Dr. R. L. Ramkumar, respectively. The experimental program was conducted at the University of Delaware under the supervision of Professor R. Byron Pipes. The authors would like to acknowledge the many helpful discussions they had with Dr. B. W. Rosen and Mr. G. L. Roderick during this program.

TABLE OF CONTENTS

TABLE OF CONTENTS (contd.)

SYMBOLS

a	width of notch
a_o	width of the overstressed region
a_2	width of the average stress region
c	superscript indicating compressive stress
C_i	constants
d, d_1, d_2	interlaminar boundary layer thicknesses
E_x, E_{xu1}, E_{xu2}	longitudinal modulus of the laminate
E_{xi}	longitudinal modulus of the i^{th} lamina
F	applied laminate force in the axial dire direction
G_{xyi}	axial shear modulus of the i^{th} lamina in the xy coordinate system
G_{xy}, G_{xy12}, G_{12}	axial shear modulus of the laminate in the xy coordinate system
$G_{xz}, G_{xz12}, G_{xz23}$	transverse shear moduli
G_{90}	modified shear modulus of 90° lamina
G'_{90}	contribution of fiber bending stiffness to the modified shear modulus G_{90} of the 90 degree lamina
h	laminate thickness
h_i	thickness of the i^{th} lamina
i	subscript indicating lamina number
N	number of cycles
R	$\sigma_{min.}/\sigma_{max.}$, stress ratio

SYMBOLS (Continued)

S	cyclic maximum stress/static failure strength
t	superscript indicating tensile stress
u	superscript indicating ultimate value
u_{0i}	axial displacement of the i^{th} lamina inside the core region
u_1	axial displacement in the overstressed region
u_2	axial displacement in the average uniformly stressed region
w	total width of the laminate
x, y	laminate coordinate system
y	superscript indicating yield value
α	axial inelastic length
γ_{xy}^{ult}	axial shear failure strain
ζ	axial crack length
$\sigma_x, \sigma_y, \sigma_z$	applied gross laminate stress in the x, y and z direction
σ_T	applied laminate stress at which transverse crack propagates from notch tip
σ_{xy}	inplane shear stress
σ_x^t	unnotched laminate tensile strength
σ_x^c	unnotched laminate compressive strength
τ_{xyi}	shear stress in the i^{th} lamina in the xy coordinate system

SYMBOLS (Continued)

$\bar{\tau}_{xyi}$	yield value of shear stress in the i^{th} lamina in the xy coordinate system
$\bar{\tau}_{xz12}, \bar{\tau}_{xz23}$	yield value of interlaminar shear stress between layers 1 and 2, and 2 and 3, respectively.

EVALUATION AND EXPANSION OF AN ANALYTICAL MODEL FOR FATIGUE OF NOTCHED COMPOSITE LAMINATES

R. L. Ramkumar, S. V. Kulkarni*
and R. B. Pipes**

Materials Sciences Corporation

SUMMARY

This report describes the analytical and experimental study performed to expand the existing static and fatigue failure analysis. The analytical effort extended the analysis to include interlaminar effects, while the experimental effort developed methods to obtain basic experimental data required as input to the analysis.

The static failure analysis for notched laminates was modified to include interlaminar effects near the notch. The interlaminar effects were included by discretizing the laminate into laminae in the region of the projection of the notch width along the axial direction. This discretization produced additional degrees of freedom which were used to analyze axial in-plane shear damage or crack in each lamina and axial interlaminar damage or delamination at the laminae interfaces. Because a large number of damage zones is possible when elastic-perfectly plastic behavior in in-plane and interlaminar shear is considered, the analysis was simplified by assuming a secant modulus representation of the nonlinear shear stress-shear strain curve. The growth of damage by both the above-mentioned approaches is calculated for various realistic T-300 Gr/Ep laminates ($[0_2/\pm45]_s$, $[0/\pm45/90]_s$) and compared with earlier experimental observations.

Three-dimensional elastic and two-dimensional elastic-plastic finite element analyses were also performed for some

---

*Presently a Consultant.

**Associate Professor, University of Delaware, and Affiliate Staff Member, Materials Sciences Corporation.

notched laminates for the purposes of (i) developing an understanding of the behavior of interlaminar stresses around the notch, and (ii) determining the nature of the 2-D elastic-plastic stress distribution adjacent to the notch when the maximum attainable stresses or combinations thereof for the laminate are governed by a yield criterion. The results obtained from task (i) provided a guideline for qualitatively assessing the approximate stress analysis procedure. Task (ii) determined how appropriate some of the postulates (such as the average stress concentration region being a function of of laminate anisotropy) of the basic failure model are.

The experimental effort was directed at several different tasks: (i) determining static/fatigue (S-N) curve data for interlaminar shear and normal stresses; (ii) assessing the effect of (a) the interaction between in-plane shear and transverse compression on the wearout rates for strength and stiffness in a $[\pm 45]_s$ laminate subjected to uniaxial loading, and (b) the transverse restraint (as provided by 90° layers in a $[0_i/90_j]_s$ laminate) on the failure mode and wearout rates for strength and stiffness for a unidirectional layer when subjected to compression/compression fatigue; and finally (iii) designing the experiments and specimens to obtain the required data.

INTRODUCTION

The use of composite materials for primary aerospace structural applications requires that they have adequate safety margins and lifetimes under all anticipated environments. Accordingly, a sound understanding of the fracture and fatigue behavior of these materials is needed, and the materials must also be well characterized by soundly based experimental data. To characterize materials by tests alone is expensive; analyses which correlate successfully among data points can greatly reduce the number of tests needed and guide the testing methods to provide more useful experimental results.

The development of such analyses was initiated in reference 1 in which a methodology was developed for predicting the growth of cracks and ultimate failure under fatigue loading of fiber composite laminates containing through-the-thickness notches or holes. This framework was based on knowledge of the static and fatigue behavior of a unidirectional layer of the material. Specifically, the analysis assumes that lamina fatigue behavior within the notched laminate is predictable from fatigue data obtained from tests of unnotched laminae.

To verify this analysis, and develop a semi-empirical capability for the fatigue analysis of notched, fiber-composite laminates, the predictions derived from reference 1 were compared in reference 2 with experimental fatigue data for notched $[0_2/\pm 45]_s$ Boron/epoxy laminates containing a 0.635 cm diameter circular hole. The specific phenomena studied were:

(1) initiation of fatigue damage, and growth as a function of load cycles;

(2) fatigue life and mode of failure; and

(3) residual strength and mode of failure after a predetermined number of cycles.

The residual strength after fatigue loading, and both axial and transverse damage growth, were measured quantitatively for correlation with the analytical predictions.

Correlation between analysis and experiment was hampered, however, by the following factors:

(1) delamination of the 0° surface layers in the region of the longitudinal projection of the notch diameter;

(2) lack of a statisitically significant data base for lamina fatigue properties in general; and, particularly,

(3) absence of lamina axial compression fatigue data.

The principal deficiency in the analysis appeared to be the lack of a capability to predict the growth of the delaminations. A primary objective of the present study is to correct this deficiency. The approach used is to modify the existing static failure analysis (ref. 3) to permit the effects of interlaminar shear stress to be taken into account. This is achieved by discretizing the laminate into laminae in the vicinity of the notch. Significant features of the analytical developments are described in the section "Description of the Failure Model," and the mathematical details are presented in Appendix A. The analysis has been incorporated into a computer program for calculation of damage growth and residual strength.

To assess the degree of realism associated with the assumptions in the analysis, the calculated stresses have been compared to those obtained from 2-D and 3-D finite element analyses. These comparisons are discussed in the section "Finite Element Analysis of Notched Composite Laminates."

An experimental program was conducted to demonstrate the feasibility of obtaining the data required as input to the analysis. Inadequacies of the existing data base for lamina fatigue properties (already noted during the analysis-experiment correlation study in reference 2) are compounded by the need to incorporate consideration of interlaminar effects into the fatigue analysis. Exploratory testing to develop methods for obtaining lamina properties from simple

laminates instead of unidirectional samples therefore has been initiated as follows:

(i) $[\pm 45]_s$ laminate uniaxial compression/compression fatigue tests have been made to determine the nature of the interaction between in-plane shear and transverse compression in a lamina and to compare the wearout rate with that of a $[\pm 45]_s$ uniaxial tension/tension fatigue test;

(ii) $[0_i/90_j]_s$ laminate uniaxial compression/compression fatigue tests have been made to ascertain the effect of transverse restraint (provided by the 90-degree laminae) on the failure mode and the wearout rate for a unidirectional lamina in compression/compression fatigue;

(iii) $[\pm 25_2/90]_s$ laminate specimens were used to obtain the S-N curve for interlaminar normal tensile stress; and

(iv) Partially notched $[\pm 45_i/0_j]_s$ laminates were used for determining the behavior of interlaminar shear stress in fatigue.

Highlights of the tests and their implications in the light of the analysis as extended herein are discussed in the section entitled "Experimental Program." The test specimen design is outlined in Appendix B.

FAILURE MODEL FOR NOTCHED COMPOSITE LAMINATES INCLUDING INTERLAMINAR EFFECTS

DISCUSSION OF PREVIOUS MODEL

The prior analysis (ref. 2, see fig. 1) was based on two concepts: (1) Failure in the presence of a notch can result from cracks propagating along planes of weakness parallel to the fibers or perpendicular to them; (2) The notched laminate may be divided into regions having simple, approximate stress states. The first of these concepts is utilized unchanged in this study. The second is extended to take into account through-the-thickness effects.

In reference 2, the laminate was considered as an assemblage of discrete regions; namely, the strip containing the notch; the overstress region adjacent to this strip; the intermediate, shear-overstress region; and the undisturbed or average stress region. In the thickness direction, the laminate was treated as a homogeneous material. Consequently, the predictions of interlaminar stresses and the resulting delaminations were beyond the scope of the analysis. To take into account the interlaminar stresses, the laminate was considered herein divided into laminae in the local regions where the effect of interlaminar stresses is most pronounced. Resultant changes in the analysis and its failure-prediction capability are discussed in the following section.

DESCRIPTION OF THE NEW FAILURE MODEL

Static Failure Analysis

The static failure model, at the laminate level, is divided, as before (ref. 1), into three regions: (i) a central core region which is the projection of the notch in the loading direction; (ii) an overstressed region of average stress concentration, adjacent to the core region; and (iii) an average stress region (fig. 1). As mentioned in the earlier sections,

this model adequately predicts the gross heterogeneous behavior of the laminate in the overstressed and average stress regions. The stress state in the vicinity of the notch, though, indicates the presence of high interlaminar stresses. In some laminates, these interlaminar stresses are large enough to cause a delamination or "peeling off" of one ply from another (ref. 2). This necessitates discretization of the core region to the lamina level so that interlaminar stresses may be quantified and the corresponding failure mode predictive capability built into the model (fig. 2).

The predictable failure modes in the analysis comprise: (i) an axial in-plane crack in any layer in the core region; (ii) an interlaminar debond between any two layers in the core region; and (iii) a transverse crack across the laminate, through the specimen thickness, normal to the loading direction. The failure modes are thus predicted at the lamina level in contrast to the gross laminate failure modes of the earlier model (fig. 3).

The governing equations for the laminates that exhibit the above failure modes form five coupled equations (Appendix A). The core region is assumed to have three different plies above the midplane. The mathematical complexity introduced by the actual nonlinear shear behavior of the individual laminae is overcome by assuming an elastic-perfectly plastic behavior and an ultimate strain criterion for crack initiation. Alternatively, an elastic, secant modulus behavior may also be assumed. The latter approach reduces the computational efforts by a considerable amount. The words "defect" and "damage" are used to refer to in-plane and interlaminar plastic regions, and in-plane crack and interlaminar delaminations, in general. This facilitates a general discussion on both the elastic-plastic approach and the elastic, secant modulus approach. The governing equations and their solutions for regions in the laminate with different damage zones are given in Appendix A.

The elastic solution for the notched laminate (Appendix A) estimates the maximum in-plane and interlaminar shear stresses at the notch. A comparison of these stresses, normalized with respect to the corresponding yield values, determines the type and number of defects that initiate and grow simultaneously in the initial damage zone and the corresponding magnitude of the load. Two or more defects that occur in succession due to a small change in the applied loading are assumed to initiate and grow together to enhance the predictive capability of the model. The growth of the initial damage zone is predicted through the solutions to the modified governing equations (Appendix A). These solutions are compatible with the elastic solutions at the boundary of the two regions (fig. 4). The normalized maximum shear stresses and shear strains at the notch are computed for each increment of the first damage zone size to predict the initiation of the second damage zone and the corresponding load.

The second damage zone in the notched laminate may have additional inelastic layers and interfaces, or may have a crack or debond in a layer or interface that was inelastic in the first damage zone. The growth of the second damage zone size with the applied loading involves solutions for three regions that are continuous at two boundaries (fig. 4). This procedure can be extended to many successive damage zones till the laminate fails. A transverse failure is marked by a crack across the specimen, through the thickness, normal to the loading direction. An axial failure is determined by an unstable growth of a crack/debond with the applied loading.

Figure 5 shows the various possible sequences of defects in a general notched laminate. The branching of defects is a strong function of the laminate material and geometric properties. The solutions for any damage zone depend on the solutions for the regions that preceded it. Consequently, generalization of the solution procedure is very tedious when more

than two damage zones exist in the laminate. However, this is alleviated by eliminating a few damage sequences that are unlikely to occur. It is assumed that, before too many damage zones appear, the load will be large enough to cause a transverse failure or one of the earlier defects will precipitate an axial failure. This is where the simplicity in the application of the elastic, secant modulus approach is obvious. The elimination of the inelastic regions leaves only cracks and delaminations to be accounted for.

In many laminate constructions, a degenerate region is created whenever the applied loading reaches a critical value. Degeneracy sets in when one or more layers in the core region are surrounded by stress-free surfaces and/or inelastic surfaces. In the elastic-plastic approach, one or more degenerate layers have a linear variation of axial strain in the degenerate region. The degenerate layers in the elastic, secant modulus approach are stress free and are essentially "carried" by adjacent load-carrying regions. In a degenerate region, the solutions for the degenerate layers are uncoupled from the five basic governing equations. The solutions change for different types of degeneracies (Appendix A). Hence, if all types of laminate behavior are to be included in the solution procedure, programming of the solution becomes tedious.

Fatigue Failure Analysis

A "mechanistic wearout" concept used in earlier studies (ref. 2) underlines the basic philosophy of the laminate fatigue behavior. On fatigue loading, material property degradation is predominant in the vicinity of the notch due to stress concentration effects. An experimental characterization of the lamina fatigue data helps estimate the degradation in the laminate properties due to cyclic loading. The material property degradation on fatigue loading, when incorporated into the static failure model described earlier, could lead to fatigue failure modes and strengths that are very different from the static predictions.

Figure 6 shows a flow chart of the program developed to predict the failure modes and strengths of notched laminates subjected to cyclic loading.

DISCUSSION OF RESULTS

The approximate failure analysis for notched laminates which considers the effects of interlaminar stresses was utilized to investigate the damage growth in some T-300/5208 laminates. Table 1 lists the various data sets utilized in the failure analysis. The trial data are used to illustrate the extent of the predictive capability of the analysis when laminate failure in the transverse direction is prevented.

Tables 2 and 3 indicate the results of the analysis for T-300/5208 $[0_2/\pm45/\bar{0}]_s$ and $[\pm45/0_2/\bar{0}]_s$ laminates, respectively, for different values of interlaminar boundary layer zone size "d" and the trial data. In the table, the distance "d" is the interlaminar boundary layer region which assumes two values: (i) half the lamina thickness (typical for Boron/epoxy); and (ii) one-tenth the lamina thickness (typical for Graphite/epoxy). Figure 7 shows a typical variation of the in-plane displacement as obtained in reference 4. The figure explains the meaning of the parameter "d". In the present analysis, the axial displacements in the various layers are piecewise uniform, and hence, discontinuous at the interfaces. The ratio of the displacement discontinuity to "d" - the transverse shear strain - should match the slope of the continuous displacement curve at the interface obtained from a higher order analysis. For the $[0_2/\pm45/\bar{0}]_s$ laminate, the in-plane plastic zone is initiated almost simultaneously in the 0_2 and $\bar{0}$ laminae ($\alpha_{xyl,3}>0$). Also, the next damage zone - a plastic zone - appears in the ±45 laminae ($\alpha_{xy2}>0$) because the interlaminar shear stress (τ_{xzl2}) is not large enough to form an interlaminar inelastic region. Thus, the approximation that the axial, in-plane plastic zone grows uniformly through-the-thickness (ref. 3) may reflect the actual behavior for this laminate. After both the plastic zones have grown over a

certain distance, an in-plane crack is initiated in the 0_2 and $\bar{0}$ layers. Note, however, that the interlaminar shear stresses are high and may eventually give rise to a delamination. In tables 2 and 3, the results for the $[0_2/\pm45/\bar{0}]_s$ laminate are essentially the same as for the $[\pm45/0_2/\bar{0}]_s$ laminate except that the magnitude of the interlaminar shear stress (τ_{xz12}) is increased by about 25%.

An important conclusion which can be drawn from the above results is that the number of combinations of different damage zones (inelastic regions as well as cracks) is large (fig. 5). The factors which affect this number are the material properties, stacking sequence, and notch size. An automated numerical scheme to "track" the various possible damage growth combinations is a tedious task. Also, the solution procedure expands with the initiation of plastic zones. Thus the analysis is further complicated. Consequently, the analytical procedure was modified to eliminate the need to consider plastic zones by considering linear approximations of the nonlinear in-plane and interlaminar shear stress-strain curves as shown in figure 8. Such an analysis would, however, still consider the growth of in-plane shear cracks and interlaminar debonds, but the number of combinations of the different damage zones is drastically reduced. The various damage growth combinations are illustrated in figure 5.

Figures 9 and 10 illustrate the progressive damage growth for $[0_2/\pm45/\bar{0}]_s$ and $[0/\pm45/90]_s$ T-300/5208 Graphite/epoxy laminates, respectively, based on the trial data in table 1. The force represents the applied laminate force and "α" indicates the cumulative sum of the damage zones. In figure 9, two inelastic in-plane axial damage zones are predicted before an axial crack in the 0° layers appears. Figure 10 illustrates a similar pattern of damage growth, except that no in-plane crack occurs in the 90° layer and an interlaminar inelastic zone is initiated at a higher value of the applied force. Figure 11 shows the effect of notch size on the damage

growth in a $[\pm 45/0/0]_s$ laminate for the trial data input. The $[\pm 45/0/0]_s$ notation is used for a $[\pm 45/0_2]_s$ laminate, which is treated by the analysis as a "±45° layer" and two 0° layers. If the ±45 layup is treated as two layers (a +45 layer and a -45 layer) in the analysis, the Poisson effect causing an increase in the shear modulus will not be accounted for. Figures 9 to 11 show the capability of the approximate analysis procedure to predict damage regions on a lamina level. However, as has been noted earlier, the analysis is not capable of predicting all combinations of damage growth because of a significant increase in the complexity of the computation procedure.

The variation of failure load with notch size is studied in figure 12 for a $[\pm 45/0/0]_s$ laminate for the actual data input. The following conclusions can be drawn from the figure:

(i) Damage zone size increases with increase in notch size.

(ii) In-plane damage occurs only in the 0° layers.

(iii) Laminate fails by transverse crack propagation.

(iv) At failure, the maximum in-plane shear stress in the ±45 laminae is higher for larger notch sizes than that for smaller notch sizes, thus indicating the increased probability of through-the-thickness axial crack propagation for larger notch sizes.

(v) The transverse failure values predicted by the secant modulus approach are close to those predicted by the elastic-plastic analysis.

Figure 13 illustrates the results for a $[0/0/\pm 45]_s$ laminate with the allowable interlaminar shear stress value reduced to account for the presence of interlaminar normal tension stress at the 0/±45 interface. The obvious result is the initiation of an interlaminar inelastic zone followed by in-plane plasticity in the 0° layers.

In figure 14 the results for a $[0/\pm45/90]_s$ laminate for different notch sizes are shown for the actual data. Since this laminate is more isotropic than the $[0_2/\pm45]_s$ laminate, the inelastic damage zones are smaller. Also, failure occurs by transverse crack propagation.

Figure 14 is an illustration of the predictive capability of the secant modulus analysis. As shown in the previous figure, the $[0/\pm45/90]_s$ laminate fails in the transverse direction before any crack appears when the secant modulus approach was used. In figure 15, the damages are made to grow by preventing a transverse failure. Table 4 shows the effect of the interlaminar boundary layer thickness on the damage growth for the same laminate.

Figure 16 illustrates an interesting interlaminar damage growth in a $[0/0/\pm45]_s$ laminate for a reduced value of interlaminar stress that causes delamination. The reduction accounts for the effect of interlaminar normal tensile stress. A high value of σ_T, the applied stress at which transverse failure occurs, is chosen to prevent that failure mode. It is seen that the delamination that initiates at the $0/\pm45$ interface grows in an unstable fashion to failure. The 0° plies thus separate away from the ±45 plies in the notch region. This result was observed experimentally (fig. 17) in the first phase of the program (ref. 2). This qualitative agreement between the failure prediction of the analytical model and the experimental observation justifies the approach taken in building the model.

In the results discussed above, the ultimate failure stress for the ±45 laminate has been obtained from "netting analysis." The netting analysis predictions may be significantly higher than first-ply failure predictions because fiber failure within a ply is required in "netting analysis." Also, a through-the-thickness axial crack cannot propagate in a ±45 laminate unless the fibers fail. Laminate failure stress corresponding to the fracture of ±45 layer fibers is

synonymous to the netting analysis failure stress. Hence, the upper-bound predictions of the netting analysis may be realistic when considering the incipient conditions required for the initiation and growth of through-the-thickness axial cracks.

FINITE ELEMENT ANALYSIS OF NOTCHED COMPOSITE LAMINATES

The failure predictive capability of the analytical model was based on a few simplifying assumptions. Justification of these assumptions is essential to extend the model application to any general laminate.

A three-dimensional finite element analysis was carried out to predict the in-plane and interlaminar stresses in a notched laminate. The primary objectives of the 3-D finite element analysis were (i) to substantiate the assumptions made in the approximate model and (ii) to provide guidance for any modification. This elastic analysis aimed at establishing a qualitative agreement with the model stress predictions, and also establishing the predominance of the axial normal and interlaminar shear stresses over the other stresses. A two-dimensional, elastic-perfectly plastic finite element analysis was carried out to verify the inelastic damage growth predictions of the analytical model for various notched laminates.

THREE-DIMENSIONAL ELASTIC ANALYSIS

The present analytical modeling philosophy considers the physics of the problem without accounting for the detailed stress distribution. Thus, only those stress fields (and the appropriate equations of equilibrium) are considered which have a predominant effect on the observed failure modes. The driving force for this approximate approach has been the complexity of the three-dimensional nonlinear stress analysis and the associated failure prediction. However, the use of simplified models (which neglect the effects of some stress fields) can be justified only if there exists qualitative, and to a limited extent, quantitative correlation with the more exact stress analyses. To that end, a three-dimensional finite element anlaysis of notched laminates was carried out to check the assumptions made in the approximate stress analysis procedure.

The computer code SAP-IV was used to carry out the finite element analysis (ref. 5). An octant of the notched laminate was considered and each layer above the reference midplane was discretized into the mesh form shown in figure 18. A minimum of eight and a maximum of twenty-one nodes were chosen to describe the general three-dimensional isoparametric element used in the analysis. The element was used to represent orthotropic, elastic media. Laminate analysis was used to apply the appropriate loads in each layer so that a far-field uniform strain state existed in the laminate.

In figure 19, σ_{yz} obtained from the approximate analysis, at the $0/\pm45$ interface, is compared with the σ_{yz} variation from the 3-D finite element analysis (the average value at the face centroids). The comparison is made at two axial locations. As shown in figure 19, the average stresses from the approximate analysis compare qualitatively with the 3-D finite element results.

Figure 20 shows the axial normal stress variation in the load-carrying direction agreeing qualitatively with the analytical prediction. Figure 21 shows the variation of the same stress, σ_{yy}, in the elements just above the x axis. A comparison with the applied stress in each layer (fig. 18) gives a measure of the stress concentration in each of the three layers of the $[0/+45/-45]_s$ laminate. These stress concentration values show good agreement with the value predicted by the analytical model.

The number of integration points to be used in the numerical evaluation of integrals over volumes is referred to as the integration order in SAP-IV. Different orders of integration may be chosen in the plane of the element and through its thickness. The orders of integration chosen in the finite element analysis affect the cost of the run and the magnitude of the results. Figures 22 and 23 show that for two different orders of integration (2 and 4), the σ_{yz} variations with y at the 0/45 interface for a $[0/\pm45/-45]_s$ laminate have good qualitative agreement along with a quantitative difference.

The approximate analysis, discussed in the previous chapter, treats notches of any geometry as equivalent slit notches since the notched strength for composite laminates is not strongly dependent on the notch shape (ref. 3). The 3-D finite element analysis was used to verify this. Figure 24 compares the shear stress variations for a circular hole and a slit notch of the same width at the ±45/-45 interface of the $[0/\pm45/-45]_s$ laminate. The results show a slight difference only in the vicinity of the notch, justifying the notch geometry assumption in the simplified analytical model.

The 3-D finite element results indicate that the variation of in-plane stresses (σ_{yy} and σ_{xy}) justifies the assumption of an average stress concentration region and a localized region of shear stress transfer. The finite element solutions also justify the approximate analysis assumption of a uniform value of σ_{yz} (independent of the x-coordinate but a function of the y-coordinate) in the notched region and a zero value in the other regions of the laminate. The non-zero value of σ_{yz} predicted by the 3-D finite element analysis in the region away from the notch is of little significance because it does not contribute to the precipitation of failure.

2-D ELASTIC-PLASTIC FINITE ELEMENT ANALYSIS

As an additional task conducted during the present study, a 2-D elastic-plastic finite element analysis was performed for some notched laminates. Because of the consideration of elastic-perfectly plastic behavior in shear in the basic fracture model, the elastic-plastic finite element analysis was used to investigate the damage growth and stress distribution near the notch and to ascertain the effect of laminate anisotropy on damage propagation. The PLANE finite element program (developed at Grumman, ref. 6) was used for this purpose.

Figure 25 illustrates the finite element mesh and the loading for a laminate containing a slit notch. Input values

of moduli and strength (ref. 7) for various laminates are shown in table 5. Note that the failure stresses satisfy the stability condition for the Hill's yield criterion (ref. 8). Results of the finite element analysis are presented for a $[0/\pm45]_s$ laminate in figures 26 and 27. The notch blunting effect due to plasticity is evident in both the figures. The figures also show the change in the notch blunting effect on varying the applied load. Subsequently, the plastic region growth is investigated for laminates with various anisotropies. The critical value of the loads (a multiple for the applied load vectors) at which plasticity is initiated for the [0], $[0/90]_s$ and $[0_2/\pm45]_s$ T-300/5208 laminates is tabulated in table 6. As expected, the load is lower for the [0] and $[0/90]_s$ laminates. In figures 28 through 30 are shown the elements which have yielded for all the three laminates for similar load levels. It is evident that the yield zones are most prominent for the $[0/90]_s$ and [0] laminates, in that order. However, it has been observed in experiments with Boron/epoxy laminates that the axial inelastic damage zone is more pronounced in the [0] laminates than in the $[0/90]_s$ laminate (ref. 9). This is also predicted by the static failure model, when the effective in-plane shear modulus is modified for laminates containing 90° layers in order to reflect the local bending effects of 90° fibers in the vicinity of the notch (ref. 3). The 2-D finite element analysis does not account for these changes. Hence, it appears that the elastic-plastic finite element analysis is not capable of predicting accurately the growth of damage zone for the [0] laminate. Table 7 shows the variation of an approximate measure of stress concentration factor with increasing load for different laminates. The stress concentration shows a decrease with increasing load for the $[0/90]_s$ and $[0_2/\pm45]_s$ laminate, while, for the [0] laminate, it increases. This increase is contrary to the well-known notch blunting effect when there is a growth of the inelastic region in the axial direction.

EXPERIMENTAL PROGRAM

The experimental tasks conducted during this program have been defined by the observations made during the previous analysis-experiment correlation study and the expansion of the basic failure model to include interlaminar effects. The tests are of an exploratory nature and were performed for the specific purpose of defining the requirements of basic data to be utilized as input in the analysis.

The thrust of the earlier experimental program (ref. 2) was to provide Boron/epoxy lamina static/fatigue data to be used as input into the fatigue analysis and to generate static/fatigue data for notched Boron/epoxy laminates to be utilized in the fatigue failure model. However, in the previous programs several items were not investigated.

Consequently, there is a need for uniaxial compression fatigue data, even for a tension/tension fatigue loading of a notched laminate. To that end, [0] coupon compression tests were performed. However, since failure in a [0] longitudinal compression test is accelerated by the presence of longitudinal cracks, the residual strength/stiffness data obtained may not be representative of a unidirectional layer in a multi-layered laminate, because of the absence of the restraining effect provided by the adjacent layers. Hence, utilization of the unidirectional compression data alone to predict laminate fatigue response is questionable. Alterations in failure modes for static compression have been observed in reference 10 on providing a nominal lateral reinforcement. For these reasons, it may be imperative to obtain the compressive fatigue data in the presence of transverse restraint. Indeed, just as the $[\pm 45]_s$ specimens are used for shear data, another simple laminate may be required for other layer properties. For axial compression, the $[0_i/90_j]_s$ laminate provided a means to do this. Comparison of $[0_i/90_j]_s$ and [0] laminate compression fatigue test results will indicate the effect of lateral constraint on residual properties. (Note that the residual properties for the

0° layers in the $[0_i/90_j]$ specimen have to be extracted by filtering out the contribution of 90° layers).

Combined stress effects upon wearout have not been evaluated experimentally and have been modeled approximately in the fatigue model. Hence, initial assessment of the magnitude of this problem was obtained from compression fatigue tests on $[\pm 45]_s$ laminates. These results can be compared with those obtained from tension fatigue tests on similar laminates. Thus axial in-plane shear combined with transverse tensile stress will be compared with the same shear and transverse compressive stress.

Important parameters in the analysis which considers debond propagation are the interlaminar strengths (shear and normal tension). An estimate of the interlaminar shear strength may be obtained from the short beam test. Alternatively, the interlaminar shear strength was obtained from a $[\pm 45/0]_s$ laminate with a slit (transverse to the fibers) in the 0° layers. Also, as suggested in reference 11, the interlaminar (σ_z) normal tension strength was determined by utilizing a $[\pm 25_2/90]_s$ laminate. The $[\pm 25_2/90]_s$ laminate is optimized to yield a maximum value of σ_z.

The various tests and the specimen geometries are summarized in table 8.

MATERIALS FABRICATION AND QUALITY CONTROL

Fabrication of the composite laminates was accomplished with contemporary vacuum bag autoclave techniques with the proper cure cycle as supplied by the material producer. In order to evaluate process conditions for adequacy, lamina characterization tests were performed to determine fiber tension and in-plane shear properties. These properties are summarized in table 9. Review of the lamina characterization tests indicated that the fabricated T-300/5208 composite possessed an average fiber tensile strength of 1668 MPa, a Young's modulus of 141 GPa, and an in-plane shear modulus of 5 GPa. These properties are indicative of high-quality

laminate fabrication (ref. 7) and suggest that the processing conditions were adequate.

Each composite panel was subjected to ultrasonic inspection after fabrication. In this way, both defects could be isolated from test specimens. A typical "C" scan of a 32-ply $[\pm 45]_s$ laminate is shown in figure 31. The "C" scan reveals anomolies near the "raw" panel edges associated with variations in resin content or thickness due to edge effects. These regions of the panel were removed prior to specimen fabrication. Interior regions are revealed as uniform in both thickness and resin content.

All panels were fabricated from a single batch of the T-300/5208 prepreg. The panels were fabricated during the initial phase of the program and stored in dessicant for future use. Specimen fabrication was accomplished by first cutting the composite panel into sublaminates. The sublaminate was then mounted in a fixture for bonding tabs. After tabs were bonded to the sublaminates, test specimens were sawed to the proper geometry with a precision diamond saw facility. Each specimen was then engraved for identification as to laminate, sublaminate, and position within the sublaminate. Next, specimens were instrumented with electrical resistance strain gages and stored for subsequent testing.

TEST METHODS

The test methods developed in this study include methods for determination of 0° compression (constrained and unconstrained) fatigue properties, the in-plane shear fatigue properties in the presence of a compressive transverse stress, interlaminar shear fatigue properties, and interlaminar normal fatigue properties of the T-300/5208 material systems.

Compression Tests

The test method chosen for evaluation of the 0° compression and in-plane shear fatigue properties was a modified

IITRI wedge action grip test fixture shown in figure 32. The IITRI compression fixture consists of wedge action friction grips mounted in support blocks, with connecting rods and linear bearings which yield a concentric load path. While the IITRI fixture was originally designed for a narrow test specimen of 6.35 mm in width with an unsupported length of 6.35 - 12.7 inches, the fixture was modified to accept specimen widths up to 19.05 mm. In addition, specimen lateral deflection restraint was achieved by special roller supports attached to the wedge action grips as shown in figure 33.

In the evaluation of 0° compression strength of the T-300/5208 composite system, the test specimen geometry strongly influences test results. In addition to unsupported specimen length, the specimen width was found to affect compressive strength. For example, the average strength for a specimen geometry of 12.7 mm width and 28.575 mm unsupported length was 957 MPa, while the average strength for the 6.35 mm width specimen was 1134 MPa. By reducing the unsupported length of the 6.35 mm width specimen to 15.875 mm, the average compressive strength achieved was 1347 MPa with a corresponding modulus of 133 GPa. These results compared favorably with the tensile properties (1668 MPa and 141 GPa) and, therefore, the last specimen geometry was chosen for fatigue testing. The test specimen's unsupported length is important in the determination of compressive strength due to restraint of axial cracking rather than column instability about the axis of minimum moment of inertia. Indeed, the failure mode of the 0° compression test specimens was axial splitting followed by micro-instability of the segments formed by the axial cracking. It would appear, therefore, that the compressive properties developed in this effort are uniquely a function of the test specimen geometry. The actual compressive strength of the composite specimen is bonded by the Euler critical load for the total specimen and the strength achieved when axial cracking is fully constrained.

To investigate the influence of axial cracking upon the compressive strength of the composite, the $[0/90/0]_{2s}$ laminate was found to exceed a "rule of mixtures" prediction of strength (935 MPa) and thereby illustrate the synergistic influence of the 90° constraint layers. In order to minimize the influence of edge effects upon the behavior of the $[0/90/0]_{2s}$ test specimen, a specimen width of 19.05 mm was chosen. Since it was shown earlier that specimen width influenced the compressive strength of the $[0_{16}]$ test specimen, it should be expected that the large width would lead to conservative estimates of the $[0/90/0]_{2s}$ specimen strength. Hence, the difference between observed strength and "rule of mixtures" estimate (7%) could have been greater had the specimen width been smaller and the associated deleterious influence of edge effects been absent. In order to evaluate the influence of unsupported length upon compressive strength of the $[0/90/0]_{2s}$ laminate, specimen tests with unsupported lengths of 12.7 mm and 9.525 mm were conducted. The difference in average strengths for the two test lengths was less than one percent. It would appear, therefore, that the lateral support system was effective over such a variation in unsupported length and acted to insure compressive failure. It should be noted, however, that the typical stress-strain response revealed some bad eccentricity as exhibited by differences in apparent moduli between stress-strain responses of gages on opposite sides of the specimen. Failure commonly corresponded to an abrupt increase in strain on one side of the specimen and a corresponding decrease on the other side. This behavior would tend to imply an instability induced failure. However, the lateral constraint at the center of the specimen should preclude gross instability. Hence, the failure of the $[0/90/0]_{2s}$ specimen is considered to be initiated by a local instability of the outer 0° layers.

In order to investigate the in-plane shear fatigue properties of the T-300/5208 material system in the presence of

a compressive transverse normal stress, $[\pm 45_{16}]_s$ laminate specimens were loaded in compression. Since the compression response of the $[\pm 45]_s$ laminate is of nonlinear softening character, it was necessary to employ a 32-ply laminate in order to preclude instability induced failure. A specimen width of 19.05 mm was chosen in order to minimize the influence of edge effects upon laminate response. By introducing a teflon layer between specimen and tab adjacent to the test section, the test section could be effectively increased while maintaining the lateral constraint of the tab. In order to assess the influence of the transverse normal stress upon static in-plane shear strength, it is informative to compare the tensile and compressive strengths of the $[\pm 45]_s$ laminate. The average static compressive strength observed was 201 MPa with an average modulus of 18.9 GPa. The average static tensile strength for the identical specimen geometry was 170 MPa with a modulus of 18.8 GPa. The latter data show good agreement with the tensile response of the 8-ply $[\pm 45]_s$ laminate of 25.4 mm width and 152.4 mm test section length. Average tensile strength and modulus for this specimen geometry were found to be 150 MPa and 19.2 GPa, respectively. Hence, it would appear that there is a strong dependence of shear strength upon the sign of the transverse normal stress.

The $[\pm 45_{16}]_s$ laminate specimen was subjected to compression fatigue employing the modified IITRI test fixture shown in figure 33. Both fatigue life and residual strength data were developed with this test method. Residual strength test specimens were instrumented with longitudinal and transverse strain gages for determination of residual modulus and Poisson's ratio.

Tension Tests

Tensile test methods were developed and evaluated for determination of the interlaminar shear fatigue, and interlaminar normal fatigue properties. The interlaminar shear fatigue test specimens consisted of a $[\pm 45/0_3]_s$ laminate

wherein the 0° layers were discontinuous at the center of the specimen. Load carried by the 0° layers was transferred through interlaminar shear. Hence, failure was initiated at the discontinuity of the 0° layers in an interlaminar shear mode. Specimens were subjected to a fatigue loading (R = 0.1, 30 Hz) and the initiation of cracking detected visually. Static samples were instrumented with acoustic emission sensors for detection of interlaminar failure. Specimens were not tested beyond the initiation of damage.

The interlaminar normal stress fatigue properties were evaluated with the $[\pm 25_2/90]_s$ tensile coupon. Due to the large difference in Poisson's ratios between the 90° and ±25° layers, failure is initiated at the specimen edge in an interlaminar tensile mode. Fatigue specimens were subjected to tensile fatigue loadings of R = 0.1 at a rate of 30 Hz. Both acoustic emission and visual detection techniques were employed to establish failure initiation.

DISCUSSION OF RESULTS

As noted above, the objective of the uniaxial compression static/fatigue tests of $[\pm 45]_s$ Graphite/epoxy laminates is to determine the effect of interaction between in-plane shear and transverse stress (transverse tension plus in-plane shear for a tension test of $[\pm 45]_s$ laminate vs. transverse compression and in-plane shear for the compression test). To that end, static tension and compression tests were conducted for the $[\pm 45]_s$ laminate and the results are tabulated in table 10. It is seen that the average compression strength is higher than the average tension strength, although the moduli are almost identical. This is an expected result and is confirmed by analytical predictions. Thus the $[\pm 45]_s$ laminate cannot be used realiably for predicting shear strength because the mode of transverse stress has a noticeable effect on it.

Table 11 and figure 34 show the summary of the T-300/5208 $[\pm 45_{16}]_s$ laminate compression fatigue data. Note that there

is only a slight wearout of strength and stiffness. This is contrary to the significant wearout observed for the tension fatigue tests. Note also that the scatter is rather high for the lifetime data at S = 0.67. Figures 35 and 36 illustrate the failure modes in static tension, and static compression after fatigue, respectively. The failure in tension occurs primarily due to ply separation which is precipitated by transverse tension failure in the ±45 laminae. Microbuckling at the lamina level is the predominant failure mode for compression. An interesting failure mode is observed in figure 37 for a $[\pm 45]_s$ laminate subjected to compression. The surface ply has buckled in figure 37 resulting in further loss of stiffness and subsequent failure.

The static/fatigue data for interlaminar normal stress σ_z as obtained from a $[\pm 25_2/90]_s$ laminate are shown in tables 12 and 13 and in figure 38. In table 12, the initiation of failure at the free edges was monitored by acoustic emission and from the load-displacement chart. In figure 38, the scatter is rather large for S = 0.6. However, this is to be expected. The slope of the S-N curve does indicate a wearout rate that is consistent with a matrix-dominated behavior. The edge failure mode for this specimen is illustrated in figure 39.

The static/fatigue test data for the $[\pm 45/0_3]_s$ partially notched laminates are given in tables 14 and 15 and shown in figure 40. Failure is initiated in the interlaminar shear mode and this is evident from the C-scan in figure 41 and the photomicrograph in figure 42. Referring to the derivations in Appendix B and to table B1, the analytical prediction based on an interlaminar shear strength of 68.95 MPa is substantiated by this data. Interestingly enough, the scatter for S = 0.8 is rather significant while for S = 0.5, the data points are rather close. Because of the notch blunting effect during fatigue, the residual strength for the specimen at S = 0.6 is higher than the average static strength. Figures 43 and 44 illustrate the static and residual strength, and fatigue

failures, respectively. The fatigue failures, however, are visible only under magnification.

The static compression results for the [0] and $[0/90/0]_{2s}$ laminates are given in tables 16 and 17. The compression strength for the [0] laminate is consistent with the values reported in the literature. The modulus is also comparable to the [0] tension modulus as reported earlier in table 9. The compression strength and modulus for the $[0/90/0]_{2s}$ laminate is comparable to the values obtained by multiplying the corresponding quantities for the [0] laminate by 0.66 (percentage of 0 degree laminae in the laminate).

Lifetime and residual strength data for the [0] laminate are tabulated in table 18 and plotted in figure 45. An important feature of the [0] fatigue tests is that for most of the specimens, failures occurred by the separation of tabs because of the high stress levels. Hence only two fatigue failures were obtained. When a specimen experienced separation of tabs, it was removed from the fixture, the tabs were rebonded, and the specimen was tested statically to failure. Hence the result is a residual strength data point. Because of these difficulties, an S-N curve for the [0] laminate could not be obtained. Note also that the residual strength actually shows an increase in strength. This appears to be paradoxical. A probable explanation for this inconsistency is the scatter in the static strength data. The compression fatigue failures for the [0] laminate are illustrated in figure 46. The failure sequence is splitting in the axial direction, instability, and brooming.

The $[0/90/0]_{2s}$ compression fatigue test results are shown in table 19 and figures 47 and 48. Once again, the data points for S = 0.8 and 0.67 sometimes differ by two or three decades. While the residual strength for the [0] shows an increase for S = 0.5, that for the $[0/90/0]_{2s}$ laminates registers a small decrease. Note, however, that the failure modes for [0] and $[0/90/0]_{2s}$ laminates are different. In figure 49, the residual

strength test failure suggests the buckling of the surface 0 degree layer on an elastic foundation followed by overall instability and subsequent fracture. The fatigue failures in figure 49 for S = 0.8 occurred generally inside the tabs, suggesting that some of the data points in figure 47 are premature failures.

CONCLUDING REMARKS

The basic failure model for predicting through-the-thickness crack growth and ultimate failure of notched composite laminates (ref. 3) has been expanded to include the effects of interlaminar stresses in the vicinity of the notch. The modification was accomplished by locally discretizing the laminate into laminae in the region of the projection of the notch diameter along the direction of the loading. In-plane and interlaminar damage (inelastic region or crack) growth was calculated for various laminates ($[0_2/\pm45]_s$, $[0_2/\pm45/0]_s$ and $[0/\pm45/90]_s$) and stacking sequences.

Because of the possibility of a large combination of in-plane and interlaminar damage zones and the numerical complexity associated with "tracking" them, the capability of the failure model is restricted to the prediction of only a limited number of combinations of these regions. In order to simplify the analysis, a secant modulus approximation to the nonlinear in-plane and interlaminar shear stress-strain curves was considered in lieu of the elastic, perfectly plastic approximation. This eliminated the need to consider inelastic regions and damage was predicted as a crack in a layer or at the interface. This enhanced the capability of the analysis to predict axial crack growth in an unstable fashion or until failure.

Three-dimensional finite element analysis was performed in order to develop an understanding of the nature of the stress distribution around a hole in $[0/\pm45]_s$ and $[\pm45/0]_s$ laminates. Ths SAP-IV computer program was utilized for this purpose. The results obtained from the finite element analysis were compared with that of the approximate stress analysis procedure with the objective of qualitatively assessing the kinematic assumptions.

As an additional task, a 2-D elastic-plastic finite element analysis was conducted for some notched laminates.

Because of the consideration of inelastic effects in shear in the basic failure model, it appeared desirable to conduct such an analysis for the purpose of investigating the nature of the damage growth and the stress distribution in the vicinity of the notch, and to ascertain the effect of laminate anisotropy on damage propagation.

The experimental program basically consisted of the following exploratory tests:

(i) $[\pm 45]_s$ laminate uniaxial compression/compression fatigue tests to determine the nature of the interaction between in-plane shear and transverse compression in a lamina and to compare the wearout rates with that of a $[\pm 45]_s$ uniaxial tension/tension fatigue test. The results indicated that there is no noticeable wearout, thus suggesting that the sign of the transverse stress has an important effect.

(ii) $[0_i/90_j]_s$ laminate uniaxial compression/compression fatigue tests to ascertain the effect of transverse restraint (provided by the 90 degree laminae) on the failure mode and the wearout rate for a unidirectional lamina in compression/compression fatigue. The data scatter for the $[0/90/0]_{2s}$ laminate fatigue tests was rather large for S = 0.8 and specimen failures were experienced outside the gage section. Problems in the [0] laminate tests were premature failures along the bond between the specimen and the tabs, and an increase in the residual strength after fatigue. The former could be attributed to high stress level while the latter could be a result of a scatter in the static strength data. Because of these inconsistencies, an appropriate evaluation of the $[0/90/0]_{2s}$ laminate to obtain unidirectional compression fatigue data could not be made.

(iii) $[\pm 25_2/90]_s$ laminate specimen to obtain the S-N curve for interlaminar normal tensile stress.

(iv) Partially notched $[\pm 45_i/0_j]_s$ laminate for determining the behavior of interlaminar shear stress in fatigue.

The current analysis includes the effects of damage growth due to both in-plane and interlaminar shear stress behavior. The transverse stresses in the notched laminate are ignored in the analysis in comparison to the axial stresses. This assumption was validated by finite element analyses and experimental observations. The experimental observations on a notched $[0_2/\pm 45]_s$ laminate were predicted qualitatively by this analytical model using an elastic, secant modulus approach.

The shortcoming of the failure prediction methodology is the extensive effort needed to automate the numerical procedure to account for all possible damage sequences in a general laminate. A recommended alternative, for future research, would be the utilization of these defined damage and failure modes in a finite element analysis. This could provide a better understanding of the stress state around the notch and have the additional advantage of incorporating all the stresses for general in-plane loading into the failure prediction methodology.

APPENDIX A
FAILURE MODEL FOR NOTCHED COMPOSITE LAMINATES WITH INTERLAMINAR EFFECTS

Referring to figures 1 and 2 in the main text, the governing equilibrium equations for the various regions in the notched laminate may be written as shown below.

ELASTIC REGION

The basic approach utilized in formulating the present model is to discretize the laminate into laminae only in the region of the projection of the notch width. The remaining portion of the homogeneous laminate is divided into an average stress concentration region and a uniform stress region as in reference 2 . It is also assumed that the symmetric laminate has a maximum of six laminae. Equilibrium of each ply in the central core region and the adjacent overstressed region yields the following equations:

$$\frac{d^2u_{01}}{dx^2} - \frac{2G_{xy1}}{E_{x1}aa_0}(u_{01} - u_1) - \frac{G_{xz12}}{E_{x1}h_1d_1}(u_{01} - u_{02}) = 0 \qquad \text{(A1)}$$

$$\frac{d^2u_{02}}{dx^2} - \frac{2G_{xy2}}{E_{x2}aa_0}(u_{02} - u_1) + \frac{G_{xz12}}{E_{x2}h_2d_1}(u_{01} - u_{02}) - \frac{G_{xz23}}{E_{x2}h_2d_2}(u_{02} - u_{03}) = 0 \qquad \text{(A2)}$$

$$\frac{d^2u_{03}}{dx^2} - \frac{2G_{xy3}}{E_{x3}aa_0}(u_{03} - u_1) + \frac{2G_{xz23}}{E_{x3}h_3d_2}(u_{02} - u_{03}) = 0 \qquad \text{(A3)}$$

$$\frac{d^2u_1}{dx^2} + \frac{2G_{xy1}h_1}{E_{xu1}a_0^2h}(u_{01} - u_1) \frac{2G_{xy2}h_2}{E_{xu1}a_0^2h}(u_{02} - u_1)$$

$$+ \frac{G_{xy3}h_3}{E_{xu1}a_0^2h}(u_{03} - u_1) - \frac{G_{xy12}}{E_{xu1}a_0^2}(u_1 - u_2) = 0 \qquad \text{(A4)}$$

Note that the inplane shear stress transfer region is of width "a_0" for all layers and the interlaminar shear stress transfer is assumed to take place over a thickness "d". Axial force equilibrium in the laminate requires that:

$$2ah_1E_{x1}\frac{du_{01}}{dx} + 2ah_2E_{x2}\frac{du_{02}}{dx} + ah_3E_{x3}\frac{du_{03}}{dx}$$

$$+ 2a_0hE_{xu1}\frac{du_1}{dx} + 2a_2hE_{xu2}\frac{du_2}{dx} = F \qquad \text{(A5)}$$

Integrating equation (A5) with respect to x yields:

$$2a_2hE_{xu2}u_2(x) = Fx + C_{10} - 2ah_1E_{x1}u_{01}(x)$$

$$- 2ah_2E_{x2}u_{02}(x) - ah_3E_{x3}u_{03}(x) - 2a_0hE_{xu1}u_1(x) \qquad \text{(A6)}$$

where C_{10} is a constant of integration.

Substituting equation (A6) into (A4), the governing equations can be written in a matrix form as:

$$\frac{d^2\{u\}_e}{dx^2} - [B]_e\{u\}_e = (Fx + C_{10})\{D\} \qquad \text{(A7)}$$

where $\{u\}_e = \lfloor u_{01}\ u_{02}\ u_{03}\ u_1 \rfloor^T$ (A8)

and the subscript or a superscipt "e" represents the elastic region.

The general solution of equation (A7) is:

$$\{u\}_e = (C_{11}e^{-m_1x} + C_{16}e^{m_1x})\{U\}^{(1)} + (C_{12}e^{-m_2x} + C_{17}e^{m_2x})\{U\}^{(2)}$$

$$+ (C_{13}e^{-m_3x} + C_{18}e^{m_3x})\{U\}^{(3)} + (C_{14}e^{-m_4x}$$

$$+ C_{19}e^{m_4x})\{U\}^{(4)} + (Fx + C_{10})\{S\}_e \qquad \text{(A9)}$$

where $\{S\}_e = -[B]_e^{-1}\{D\}$, (A10)

m_1, m_2, m_3 and m_4 are the eigenvalues of the matrix $[B]_e$, $\{U\}^{(1)}$, $\{U\}^{(2)}$, $\{U\}^{(3)}$ and $\{U\}^{(4)}$ are the corresponding eigenvectors

and C_{10}, C_{11}, C_{12}, etc., are constants.

Finiteness of the stresses for large x is introduced by setting C_{16}, C_{17}, C_{18} and C_{19} equal to zero. Hence

$$\{u\}_e = C_{11}e^{-m_1x}\{U\}^{(1)} + C_{12}e^{-m_2x}\{U\}^{(2)} + C_{13}e^{-m_3x}\{U\}^{(3)}$$

$$+ C_{14}e^{-m_4x}\{U\}^{(4)} + (Fx + C_{10})\{S\}_e \, . \qquad \text{(A11)}$$

Five boundary conditions are required to solve for the five constants. If the applied load is such that the stresses in the laminate are in the elastic range, these conditions are the zero stress condition on the notch surface (x = 0) and symmetry

conditions in the u_1 and u_2 regions at the same location. That is,

$$\frac{du^e_{0i}(0)}{dx} = 0 \; ; \quad i = 1,3$$

and $u^e_1(0) = u^e_2(0) = 0$ (A12)

INELASTIC REGION(S) $(0 < x < \alpha)$

Three inplane and two interlaminar inelastic shear stress transfer regions are postulated in the discretized region. If, for example, the top layer (layer number 1) has an inplane inelastic region of length α (see fig. 1), equations (A1) and (A4) are modified in accordance with the elastic-perfectly plastic shear behavior assumption (fig. 6):

$$\frac{d^2u_{01}}{dx^2} - \frac{G_{xz12}}{E_{x1}h_1d_1}(u_{01} - u_{02}) = \frac{2\bar{\tau}_{xy1}}{E_{x1}a} \tag{A13}$$

$$\frac{d^2u_1}{dx^2} + \frac{2G_{xy2}h_2}{E_{xu1}a_0^2h}(u_{02} - u_1) + \frac{G_{xy3}h_3}{E_{xu1}a_0^2h}(u_{03} - u_1)$$

$$- \frac{G_{xy12}}{E_{xu1}a_0^2}(u_1 - u_2) = - \frac{2\bar{\tau}_{xy1}h_1}{E_{xu1}a_0h} \tag{A14}$$

Equations (A2), (A3) and (A5) remain unaltered.

For an inelastic region at an interface (see fig. 1), a similar modification is introduced. Assuming an interlaminar inelastic region between layers 1 and 2, for example, equations (A1) and (A2) are modified as shown below:

$$\frac{d^2u_{01}}{dx^2} - \frac{2G_{xy1}}{E_{x1}aa_0}(u_{01} - u_1) = \frac{\bar{\tau}_{xz12}}{E_{x1}h_1} \tag{A15}$$

$$\frac{d^2u_{02}}{dx^2} - \frac{2G_{xy2}}{E_{x2}aa_0}(u_{02} - u_1) - \frac{G_{xz23}}{E_{x2}h_2d_2}(u_{02} - u_{03})$$

$$= \frac{\bar{\tau}_{xz12}}{E_{x2}h_2} \tag{A16}$$

Equations (A3), (A4) and (A5) remain the same.

The governing equations for a region of the laminate where inelasticity is present may then be written as:

$$\frac{d^2\{u\}_p}{dx^2} - [B]_p\{u\}_p = (Fx + C_5)\{D\} + \{R\} \tag{A17}$$

where $\{R\}$ represents the inelastic contribution to the nonhomogeneous term. The solution for this set of equations is:

$$\{u\}_p = (C_1e^{-m_5x} + C_6e^{m_5x})\{U\}^{(1)} + (C_2e^{-m_6x} + C_7e^{m_6x})\{U\}^{(2)}$$

$$+ (C_3e^{-m_7x} + C_8e^{m_7x})\{U\}^{(3)} + (C_4e^{-m_8x}$$

$$+ C_9e^{m_8x})\{U\}^{(4)} + (Fx + C_5)\{S\}_p + \{T\} \tag{A18}$$

$$\text{where } \{T\} = -[B]_p^{-1}\{R\} \text{ and } \{S\}_p = -[B]_p^{-1}\{D\} \tag{A19}$$

and the subscript or the superscript "p" represents the inelastic region.

The eigenvalues $m_i (i = 5,8)$ and the corresponding eigenvectors $\{U\}^{(i)}$ of $[B]_p$ for the inelastic region are different from those for the elastic region due to the changes in the $[B]_e$ matrix.

Coordinate x for each region is measured from the origin of that region.

Consider now an inelastic region in the laminate, extending over a length of α from the notch. Equations (A11) and (A18) are the displacement solutions for the elastic and inelastic regions. The boundary conditions for the problem are:

$$u_1^p(0) = u_2^p(0) = 0$$

$$\frac{du_{0i}^p(0)}{dx} = 0 \; ; \; i = 1,3$$

$$u_{0i}^p(\alpha) = u_{0i}^e(0)$$

$$u_1^p(\alpha) = u_1^e(0) \qquad \text{(A20)}$$

$$u_2^p(\alpha) = u_2^e(0)$$

$$\frac{du_{0i}^p(\alpha)}{dx} = \frac{du_{0i}^e(0)}{dx} \; ; \; i = 1,3$$

$$\frac{du_1^p(\alpha)}{dx} = \frac{du_1^e(0)}{dx}$$

In addition to the above 14 boundary conditions, the inelasticity condition for the appropriate layer/interface at the junction of the two regions must be imposed for a unique F - α relationship.

REGION WITH AN INPLANE OR AN INTERLAMINAR CRACK ($0 < x < \zeta$)

The governing equations for a region with a crack are obtained by imposing the stress-free conditions on the cracked inplane or interlaminar surface. For an inplane crack in the top layer, for example, equations (A1) and (A4) are modified to:

$$\frac{d^2u_{01}}{dx^2} - \frac{G_{xz12}}{E_{x1}h_1d_1}(u_{01} - u_{02}) = 0 \qquad (A21)$$

$$\frac{d^2u_1}{dx^2} + \frac{2G_{xy2}h_2}{E_{xu1}a_0^2h}(u_{02} - u_1) + \frac{G_{xy3}h_3}{E_{xu1}a_0^2h}(u_{03} - u_1)$$

$$- \frac{G_{xy12}}{E_{xu1}a_0^2}(u_1 - u_2) = 0 \qquad (A22)$$

Equations (A2), (A3) and (A5) remain unchanged.

If, on the other hand, there is a debond between layers 1 and 2, equations (A1) and (A2) take the form:

$$\frac{d^2u_{01}}{dx^2} - \frac{2G_{xy1}}{E_{x1}aa_0}(u_{01} - u_1) = 0 \qquad (A23)$$

$$\frac{d^2u_{02}}{dx^2} - \frac{2G_{xy2}}{E_{x2}aa_0}(u_{02} - u_1) - \frac{G_{xz23}}{E_{x2}h_2d_2}(u_{02} - u_{03}) = 0 \qquad (A24)$$

Equations (A3), (A4) and (A5) remain unchanged.

For either type of crack, the governing equations take the form of equation (A7), and the solutions, the form of equation (A9). Introducing new constants,

$$\frac{d^2\{u\}_c}{dx^2} - [B]_c\{u\} = (Fx + C_{25})\{D\} \qquad (A25)$$

$$\{u\}_c = (C_{21}e^{-m_9 x} + C_{26}e^{m_9 x})\{U\}^{(1)} + (C_{22}e^{-m_{10} x} + C_{27}e^{m_{10} x})\{U\}^{(2)} + (C_{23}e^{-m_{11} x} + C_{28}e^{m_{11} x})\{U\}^{(3)} + (C_{24}e^{-m_{12} x} + C_{29}e^{m_{12} x}\{U\}^{(4)} + (Fx + C_{25})\{S\}_c \quad (A26)$$

where $\{S\}_c = -[B]_c^{-1} D$ (A27)

and the superscript or subscript "c" represents the cracked region.

The boundary conditions for a problem with a cracked region, an inelastic region, and an elastic region could be written in a manner similar to equations (A20). For a unique F - α - ζ relationship, the criterion for crack initiation will also have to be imposed at the crack tip.

DEGENERATE CASES

The various regions in the laminate as described above are determined by the sequence in which defects are likely to be initiated with an increase in the applied load. However, more than one defect could initiate and grow simultaneously. For some widely used laminate constructions, certain sequences of defect formation could cause the nature of the above solutions to change. Such a situation will arise (i) when two or more inelastic zones (inplane/interlaminar) appear simultaneously, or (ii) when one or more laminae act as non-load carrying members undergoing rigid body displacements. The first type of degeneracy occurs for elastic-plastic behavior in inplane/interlaminar shear, and the degenerate layer/layers have a linear variation of axial strain. The second type of degeneracy is more likely to occur in an elastic analysis with a shear behavior governed by a secant modulus approach. The degenerate layer/layers in this case are essentially "carried" by the load-carrying adjacent regions.

Simultaneous Inelastic Inplane and Interlaminar Shear Stress Transfer for a Lamina

Consider, for example, the first type of degeneracy when inelastic zones have initiated simultaneously in the surface layer 1 (inplane shear mode) and at the interface between layers 1 and 2 (interlaminar shear mode). Equation (A1) takes the form:

$$\frac{d^2u_{01}}{dx^2} = \frac{2\bar{\tau}_{xy1}}{E_{x1}a} + \frac{\bar{\tau}_{xz12}}{E_{x1}h_1} = R_1 \tag{A28}$$

Integrating this equation with respect to x twice, one obtains

$$u_{01}(x) = R_1 \frac{x^2}{2} + C_{30}x + C_{31} \tag{A29}$$

If the boundary of this region for x = 0 is the notch surface, then C_{30} vanishes. Equation (A29) then becomes:

$$u_{01}(x) = R_1 \frac{x^2}{2} + C_{31} \tag{A30}$$

Equation (A2) is then modified to:

$$\frac{d^2u_{02}}{dx^2} - \frac{2G_{xy2}}{E_{x2}aa_0}(u_{02} - u_1) - \frac{G_{xz23}}{E_{x2}h_2d_2}(u_{02} - u_{03})$$

$$= \frac{\bar{\tau}_{xz12}}{E_{x2}h_2} \tag{A31}$$

and equation (A4) assumes the form:

$$\frac{d^2u_1}{dx^2} + \frac{2G_{xy2}h_2}{E_{xu1}a_0^2h}(u_{02} - u_1) + \frac{G_{xy3}h_3}{E_{xu1}a_0^2h}(u_{03} - u_1)$$

$$- \frac{G_{xy12}}{E_{xu1}a_0^2}(u_1 - u_2) = - \frac{2\bar{\tau}_{xy1}h_1}{E_{xu1}a_0h} \qquad \text{(A32)}$$

Upon utilizing the solution in equation (A30), equation (A6) becomes

$$2a_2hE_{xu2}u_2(x) = Fx + C_{35} - ah_1E_{x1}x^2\left(\frac{2\bar{\tau}_{xy1}}{E_{x1}a} + \frac{\bar{\tau}_{xz12}}{E_{x1}h_1}\right)$$

$$- 2ah_2E_{x2}u_{02}(x) - ah_3E_{x3}u_{03}(x)$$

$$- 2a_0hE_{xu1}u_1(x)$$

or

$$2a_2hE_{xu2}u_2(x) = Fx + C_{35} - (2\bar{\tau}_{xy1}h_1 + \bar{\tau}_{xz12}a)x^2$$

$$- 2ah_2E_{x2}u_{02}(x) - ah_3E_{x3}u_{03}(x)$$

$$- 2a_0hE_{xu1}u_1(x) \qquad \text{(A33)}$$

Substituting equation (A33) into equation (A32), and considering equations (A31) and (A3), the governing equations for the degenerate region are written as:

$$\frac{d^2\{u\}_d}{dx^2} - [B]_d\{u\}_d = (Fx + C_{35})\{D\}_d + \{Dx2\}_dx^2 + \{R\}_d \qquad \text{(A34)}$$

where $\{u\}_d = \lfloor u_{02}\ u_{03}\ u_1 \rfloor^T$ (A35)

and the subscript or superscript "d" refers to the degenerate solution(s). The solution to equation (A34) is:

$$\{u\}_d = (C_{32}e^{-m_{13}x} + C_{36}e^{m_{13}x})\{U\}^{(1)} + (C_{33}e^{-m_{14}x} + C_{37}e^{m_{14}x})\{U\}^{(2)} + (C_{34}e^{-m_{15}x} + C_{38}e^{m_{15}x})\{U\}^{(3)} + \{F\}_d x^2 + (Fx + C_{35})\{S\}_d + \{T\}_d \quad \text{(A36)}$$

where $\{F\}_d = -[B]_d^{-1}\{Dx2\}_d$ (A37)

$$\{S\}_d = -[B]^{-1}\{D\}_d \quad \text{(A38)}$$

$$\{T\}_d = -[B]^{-1}(\{R\} - 2\{F\}). \quad \text{(A39)}$$

The boundary conditions for a laminate with a degenerate region are written in the same form as before.

Simultaneous Inplane and Interlaminar Cracking for a Lamina

If, instead of the elastic-plastic approach, an elastic secant modulus approach is chosen to predict the "peeling off" of the surface lamina(e) in a laminate, the above solutions could be modified accordingly. Considering the same example presented earlier, the surface ply degeneracy of the second type changes equations (A30) through (A33) by eliminating all the terms with yield stresses. The governing equations then reduce to the form:

$$\frac{d^2\{u\}_d}{dx^2} - [B]_2\{u\}_d = (Fx + C_{35})\{D\}_d \quad \text{(A40)}$$

The solution to equation (A40) is:

$$\{u\}_d = (C_{32}e^{-m_{13}x} + C_{36}e^{m_{13}x})\{U\}^{(1)} + (C_{33}e^{-m_{14}x} + C_{37}e^{m_{14}x})\{U\}^{(2)} + (C_{34}e^{-m_{15}x} + C_{38}e^{m_{15}x})\{U\}^{(3)} + (Fx + C_{35})\{S\}_d \quad \text{(A41)}$$

It is seen that a single ply degeneracy reduces the number of coupled equations by one, as reflected by the matrix $[B]_d$. If a group of layers has a degenerate solution in a region of the laminate, the $[B]_d$ matrix reduces in size further. The equations and the solutions for these cases could then be written as above.

Simultaneous Inplane Plasticity in All Layers

An extreme case of inplane inelasticity in all the layers over a region ($0 < x < \alpha$) of the laminate is not uncommon. In that region, the core region (see fig. 1) experiences a plastic flow. Mathematically, this uncouples the core displacement equations from those for the u_1 and u_2 displacements. Equation (A4) for this region is:

$$\frac{d^2u_1}{dx^2} - \frac{G_{xy12}}{E_{xu1}a_0^2}(u_1 - u_2) = -(2\bar{\tau}_{xy1}h_1 + 2\bar{\tau}_{xy2}h_2 + \tau_{xy3}h_3)/(E_{xu1}a_0h)$$

or

$$\frac{d^2u_1}{dx^2} - \frac{G_{xy12}}{E_{xu1}a_0^2}(u_1 - u_2) = -\frac{b_1}{E_{xu1}a_0h} \quad \text{(A42)}$$

where $b_1 = 2\bar{\tau}_{xy_1} h_1 + 2\bar{\tau}_{xy2} h_2 + \bar{\tau}_{xy3} h_3$. (A43)

Equation (A6) becomes:

$$2a_2 h E_{xu2} u_2 = Fx + C_{40} - b_1 x^2 - 2a_0 h E_{xu1} u_1 \quad \text{(A44)}$$

The last two equations can be solved simultaneously for $u_1(x)$ and $u_2(x)$ in the degenerate region of the laminate.

The core displacements in this region are governed by the plastic flow equations. Each layer has an inplane shear force that is proportional to α, and an interlaminar shear strain that maintains the value at $x = \alpha$. Therefore, the total axial force in each layer, or the axial strain in that layer, varies linearly with respect to x. That is,

$$\frac{du_{0i}}{dx} = E_i x \ , \quad i = 1,3 \quad \text{(A45)}$$

where $E_{x1} a h_1 E_1 = 2\bar{\tau}_{xy1} h_1 + \tau_{xz12}(\alpha) a$ (A46)

$$E_{x2} a h_2 E_2 = 2\bar{\tau}_{xy2} h_2 - \tau_{xz12}(\alpha) a + \tau_{xz23}(\alpha) a \quad \text{(A47)}$$

and $E_{x3} a h_3 E_3 = 2\bar{\tau}_{xy3} h_3 - 2\tau_{xz23}(\alpha) a$ (A48)

The core displacement solutions for the degenerate region are dependent on the displacement solutions of the adjacent region (along the x-axis) through the $\tau_{xz12}(\alpha)$ and $\tau_{xz23}(\alpha)$ terms. In other words,

$$\tau_{xz12}(\alpha)/\text{degenerate region} = \tau_{xz12}(0)/\text{adjacent region}$$
$$\tau_{xz23}(\alpha)/\text{degenerate region} = \tau_{xz23}(0)/\text{adjacent region} \quad \text{(A49)}$$

When an elastic analysis with a secant modulus shear behavior is carried out, a region ($0 < x < \zeta$) of through-the-thickness crack might be predicted. For this region, equations (A42) and (A44) become:

$$\frac{d^2u_1}{dx^2} - \frac{G_{xy12}}{E_{xu1}a_0^2}(u_1 - u_2) = 0 \quad \text{(A50)}$$

$$2a_2hE_{xu2}u_2 = Fx + C_{40} - 2a_0hE_{xu1}u_1 , \quad \text{(A51)}$$

respectively. The above equations yield solutions for $u_1(x)$ and $u_2(x)$ for the region $0 < x < \zeta$.

The core, in this case, moves as a rigid body, and the displacements are those of the adjacent region along the x-axis.

$$u_{0i}/\text{degenerate region} = u_{0i}(0)/\text{adjacent region}, \; i = 1,3 \quad \text{(A52)}$$

APPENDIX B
TEST SPECIMEN DESIGN

The objective of the experimental program is primarily to perform exploratory tests for determining basic data required as input into the failure model. After considering the deficiencies in the data during the previous analytical/experimental correlation study (ref. 2) and the needs for the modified basic failure model with interlaminar effects, the following tests were identified:

(i) $[\pm 45]_s$ laminate uniaxial compression/compression fatigue tests to determine the nature of the interaction between inplane shear and transverse compression in a lamina and to compare the wearout rate with that of a $[\pm 45]_s$ uniaxial tension/tension fatigue test;

(ii) $[0_i/90_j]_s$ laminate unaxial compression/compression fatigue tests to ascertain the effect of transverse restraint (provided by the 90 degree laminae) on the failure mode and the wearout rate for a unidirectional lamina in compression/compression fatigue;

(iii) $[\pm 25_2/90]_s$ laminate specimen to obtain the S-N curve for interlaminar normal tensile stress and

(iv) Partially notched $[\pm 45_i/0_j]_s$ laminate for determining the behavior of interlaminar shear stress in fatigue.

With regard to the design of all specimens subjected to compression, dimensions were chosen such that failure would not occur prematurely due to instability. For the $[0_i/90_j]_s$ specimens, the stacking sequence was $[0/90/0]_{2s}$. This would avoid any interlaminar edge failures due to compression loading. The design of the $[\pm 25_2/90]_s$ laminate was taken from reference This particular stacking sequence results in a high value of the interlaminar normal tensile stress when the specimen is subjected to tension loading. This ensures edge failure due to interlaminar normal stress. Finally, a partially notched $[\pm 45_i/0_j]_s$

laminate, with the notch in the 0 degree layers, was designed to investigate the interlaminar shear behavior.

Figure B1 illustrates a partially notched $[\pm 45_i/0_j]_s$ laminate with the notch in the 0 degree layers across the width of the specimen. Consideration of equilibrium in the x-direction results in the following differential equations:

$$\frac{E_1 h_1}{2} \frac{d^2 u_1}{dx^2} + \frac{u_2 - u_1}{d} G_{xz} = 0 \qquad \text{(B1)}$$

$$E_2 h_2 \frac{d^2 u_2}{dx^2} - \frac{u_2 - u_1}{d} G_{xz} = 0 \qquad \text{(B2)}$$

where 'd' is the width of the interlaminar shear transfer zone. Subscripts 1 and 2 correspond to the 0 degree and ±45 degree plies, respectively. Also, force equilibrium at any cross section of the laminate results in the following expression for the displacement u_2:

$$u_2 = \left[\frac{Fx}{2w} - C_1 - \frac{E_1 h_1 u_1}{2}\right] \frac{1}{E_2 h_2} \qquad \text{(B3)}$$

where the constant $C_1 = - \frac{E_1 h_1 u_1(0)}{2}$ and F is the applied laminate force. Upon substitution of equation (B3) in equation (B1) and the subsequent solution of the resulting differential equation, one obtains

$$u_1 = C_2 e^{-\alpha x} + Ax + B \qquad \text{(B4)}$$

where C_2 is a constant of integration,

$$\alpha^2 = \frac{2G_{xz}}{E_1 h_1 d}\left[1 + \frac{E_1 h_1}{2E_2 h_2}\right] \tag{B5}$$

$$A = \frac{FG_{xz}}{WE_1E_2h_1h_2\alpha^2 d} \text{ and } B = \frac{-2C_1G_{xz}}{E_1E_2h_1h_2d\alpha^2} \tag{B6}$$

The boundary condition ensuring the finiteness of the force for large x has already been considered by eliminating exponential terms of the type $e^{\alpha x}$. Consideration of the boundary condition $\frac{du}{dx} = 0$ at $x = 0$ yields

$$C_2 = A/\alpha \tag{B7}$$

and consequently,

$$C_1 = \frac{-FG_{xz}}{2W\alpha(E_2h_2d\alpha^2 - G_{xz})} \tag{B8}$$

An expression for the displacement u_2 can be obtained from equations (B4), (B6) and (B3). Having known the displacements u_1 and u_2, the interlaminar shear stress can be calculated as

$$\tau_{xz}(x) = G_{xz}\left[\frac{u_1(x) - u_2(x)}{d}\right] \tag{B9}$$

The objective of the above analysis is to determine the percentage of the 0 degree layers in the $[\pm 45_i/0_j]_s$ laminate such that failure occurs due to the interlaminar stress τ_{xz} in the vicinity of the notch and not due to overstress in the ±45° layers. Also failure should not occur in the

unnotched portion of the laminate.

Table (B1) shows the results of the analysis. Assuming that the ultimate value of the interlaminar stress τ_{xz} is 68.94 MN/M^2 (10 ksi), the 40%/60% $[\pm 45/0]_s$ laminate appears to be the logical choice. A problem associated with the stacking sequence for this laminate is that for tension loading, the interlaminar normal stress at the free edge would be tensile. The effect of a tensile σ_z can be alleviated by choosing a wider specimen (say, 3.81 cm or 1-1/2 in).

REFERENCES

1. McLaughlin, P. V., Jr., Kulkarni, S. V., Huang, S. N., and Rosen, B. W., Fatigue of Notched Fiber Composite Laminates, Part I: Analytical Model, NASA CR-132747, March 1975.
2. Kulkarni, S. V., McLaughlin, P. V., Jr., and Pipes, R. B., Fatigue of Notched Fiber Composite Laminates, Part II: Analytical and Experimental Evaluation, NASA CR-145039, April 1976.
3. Kulkarni, S. V. and Rosen, B. W., Evaluation of Fracture in Notched Composite Laminates, Final Report, NASA Contract No. NAS2-9069 with MSC, October 1976.
4. Pipes, R. B., Interlaminar Stresses in Composite Laminates, AFML-TR-72-18, May 1972.
5. Bathe, K. J., Wilson, E. L., and Peterson, F. E., SAP IV - A Structural Analysis Program for Static and Dynamic Response of Linear Systems, Report EERC 73-11, Univ. of California, Berkeley, April 1974.
6. Armen, H., Pifko, A., and Levine, M. S., PLANE Program, from Finite Element Analysis of Structures in the Plastic Range, NASA CR-1649, 1971.
7. Advanced Composites Design Guide. Volume IV: Materials, prepared under Contract No. F33615-74-C-5075 by Rockwell International Corporation, Los Angeles Aircraft Division, January 1977.
8. Hill, R., The Mathematical Theory of Plasticity, Oxford University Press, London, 1950.
9. Durchlaub, E. C. and Freeman, R. B., Design Data for Composite Structure Safelife Prediction, AFML-TR-73-225, March 1974.
10. Kulkarni, S. V., Rice, J. S., and Rosen, B. W., "An Investigation of the Compressive Strength of Kevlar-49/Epoxy Composites," Composites, Sept. 1975, pp. 217-225.
11. Pagano, N. J. and Pipes, R. B., "Some Observations on the Interlaminar Strength of Composite Laminates," Int. J. Mechanical Sciences, Vol. 15, pp. 679-688, 1973.

Table 1. Unidirectional T-300/5208 Lamina Properties and Some Laminate Data Used in the Current Study

	Elastic-Plastic Approach		Secant Modulus Approach
Property	Trial Data	Actual Data	Actual Data
$G_{xy}(0°)$ in GPa	6.550	6.550	3.283
$G_{xy}(\pm45°)$ in GPa	35.935	35.935	35.935
$G_{xy}(90°)$ in GPa	6.550	6.550	3.283
G_{xy} in GPa	3.275	5.516	5.516
$E_x(0°)$ in GPa	137.896	137.896	137.896
$E_x(\pm45°)$ in GPa	22.394	22.394	22.394
$E_x(90°)$ in GPa	10.342	10.342	10.342
a (mm)	6.350	6.350	6.350
a_o (mm)	2.540	3.332	3.332
W (mm)	40.640	38.100	38.100
$d=d_1=d_2$ (mm)	0.070	0.014	0.014
$\bar{\tau}_{xz}$ in MPa	68.948	68.948	68.948
$\bar{\tau}_{xy}$ (0°) in MPa	68.948	68.948	68.948
$\bar{\tau}_{xy}$ (±45°) in MPa	448.162	723.954	723.954
$\bar{\tau}_{xy}$ (90°) in MPa	68.948	68.948	873.709
$\sigma_T(0/\pm45/90)_s$ in MPa	4481.620	482.636	482.636
$\sigma_T(0/0/\pm45)_s$ in MPa	4481.620	689.480	689.480
γ^u_{xy} (0°)	0.021	0.021	-
γ^u_{xy} (±45°)	0.1	0.0206	-
γ^u_{xy} (90°)	1.29	1.6914	-
γ^u_{xz}	0.025	0.025	-

Table 2. Stresses in a $[0_2/\pm45/\bar{0}]_s$ T-300/5208 Laminate For Different Interlaminar Boundary Layer Thicknesses

	d (mm)		
	0.070	0.035	0.014
$\alpha_{xyl,3}{}^{>0}$			
τ_{xyl} (MPa)	68.95	68.95	68.95
τ_{xy2} (MPa)	366.78	372.21	375.57
τ_{xy3} (MPa)	67.51	68.18	68.60
τ_{xz12} (MPa)	19.15	20.22	21.17
τ_{xz23} (MPa)	-5.97	-5.98	-5.93
SCF (Stress Concentration Factor)	2.113	2.116	2.117
$\alpha_{xyl,3}{}^{>0};\ \alpha_{xy2}{}^{\geq 0}$			
τ_{xyl} (MPa)	68.95	68.95	68.95
τ_{xy2} (MPa)	448.16	448.16	448.16
τ_{xy3} (MPa)	68.95	68.95	68.95
τ_{xz12} (MPa)	23.48	24.44	25.34
τ_{xz23} (MPa)	-7.32	-7.23	-7.11
$\alpha_{xyl,3}$ (mm)	0.52	0.48	0.45
SCF	2.1098	2.113	2.114
$\alpha_{xyl,3}{}^{>0};\ \alpha_{xy2}{}^{>0};\zeta_{xyl,3}{}^{\geq 0}$			
$\alpha_{xyl,3}$ (mm)	1.93	1.92	1.92
α_{xy2} (mm)	1.30	1.36	1.40
τ_{xyl} (MPa)	68.95	68.95	68.95
τ_{xy2} (MPa)	448.16	448.16	448.16
τ_{xy3} (MPa)	68.95	68.95	68.95
τ_{xz12} (MPa)	36.13	38.07	40.11
τ_{xz23} (MPa)	-11.25	-11.27	-11.40

Table 3. Stresses in a $[\pm 45/0_2/\overline{0}]_s$ T-300/5208 Laminate For Different Interlaminar Boundary Layer Thicknesses

	d (mm) 0.07	0.035	0.014
$\alpha_{xy2,3} > 0$			
τ_{xy1} (MPa)	361.07	369.17	374.45
τ_{xy2} (MPa)	68.44	68.67	68.84
τ_{xy3} (MPa)	68.95	68.95	68.95
τ_{xz12} (MPa)	-23.99	-25.41	-26.63
τ_{xz23} (MPa)	-4.45	-4.81	-5.21
SCF (Stress Concentration Factor)	2.109	2.114	2.117
$\alpha_{xy2,3} > 0$; $\alpha_{xy2} \geq 0$			
τ_{xy1} (MPa)	448.16	448.16	448.16
τ_{xy2} (MPa)	68.95	68.95	68.95
τ_{xy3} (MPa)	68.95	68.95	68.95
τ_{xz12} (MPa)	-29.88	-30.96	-32.00
τ_{xz23} (MPa)	-5.54	-5.86	-6.18
$\alpha_{xy2,3}$ (mm)	0.54	0.49	0.45
SCF	2.106	2.111	2.114
$\alpha_{xy2,3} > 0$; $\alpha_{xy2} > 0$; $\zeta_{xy1,3} \geq 0$			
$\alpha_{xy2,3}$ (mm)	1.91	1.91	1.91
α_{xy1} (mm)	1.24	1.32	1.38
τ_{xy1} (MPa)	448.16	448.16	448.16
τ_{xy2} (MPa)	68.95	68.95	68.95
τ_{xy3} (MPa)	68.95	68.95	68.95
τ_{xz12} (MPa)	-45.32	-47.91	-50.29
τ_{xz23} (MPa)	-8.41	-9.05	-9.60

NOTES FOR TABLE 2 AND TABLE 3

TABLE 2:

- a_o, width of the average stress concentration region = 1.27 mm.
- In-plane shear yield stresses = 68.95 MPa for a 0^0 layer
  448.16 MPa for a $\pm 45^0$ layer
- Interlaminar shear yield stresses = 68.95 MPa
- Subscripts 1, 2 and 3 refer to the 0_2, ±45 and $\overline{0}$ laminae, respectively
- Stress Concentration Factor (SCF) is the normal stress in the average stress concentration region divided by the gross applied stress

TABLE 3:

- Subscripts 1, 2 and 3 refer to the ±45, 0_2 and $\overline{0}$ laminae, respectively.

Table 4. Damage Growth in a $[0/\pm45/90]_s$ T-300/5208 Laminate for Different Interlaminar Boundary Layer Thicknesses (Secant Modulus Approach)*

d = 0.00140 cm.		d = 0.00279 cm.		d = 0.00699 cm.	
Force (KN)	ζ (cm.)	Force (KN)	ζ (cm.)	Force (KN)	ζ (cm.)
25.94	0.0**	25.96	0.0**	26.03	0.0**
27.25	.0254	27.23	.0254	27.19	.0254
27.60	.0635	27.90	.1016	27.87	.1016
28.12	.1270	28.69	.2032	28.67	.2032
29.04	.2540	29.41	.3048	29.39	.3048
29.88	.3810	30.77	.5080	30.78	.5080

*The applied laminate stress, σ_T, at which transverse crack propates from the notch tip is assumed to be very large.

**Inplane crack initiates in the 0° and ±45° layers.

Table 5. Input Data for Different Laminates for a Two-Dimensional Elastic-Plastic Analysis (PLANE Finite Element Program)

Laminate	E_x (GPa)	E_y (GPa)	G_{xy} (GPa)	ν_{21}	σ_x^y (MPa)	σ_y^y (MPa)	σ_z^y (MPa)	τ_{xy}^y (MPa)
$[0]_s$	137.9	10.3	6.55	.019	1448	207	207	62
$[0/90]_s$	74.5	74.5	6.55	.035	724	276	207	62
$[0/\pm 45]_s$	61.5	27.0	26.13	.290	483	197	207	225
$[0/\pm 45/90]_s$	54.7	54.7	21.24	.289	483	276	207	183
$[0_2/\pm 45]_s$	81.0	24.5	21.24	.188	724	194	207	183

Table 6. Load at Initiation of Plasticity for Various Laminates

Laminate	P_{cr}
[0]	20.82 E3
$[0/90]_s$	17.54 E3
$[0_2/\pm 45]_s$	30.85 E3

Table 7. Variation of Stress Concentration Factor for Various Laminates as a Function of Applied Load

Laminate	Applied Load	$\frac{\text{Stress in Element 12}}{\text{Applied Load}}$
[0]	20.82	1.87
	29.15	1.92
	33.32	2.0
$[0/90]_s$	17.54	1.77
	21.04	1.77
	28.06	1.65
$[0_2/\pm 45]_s$	30.85	2.98
	43.19	2.43
	49.37	2.14

Table 8. Various Tests and Specimen Geometries

Laminate	Type of Test	Specimen Size*(mm)	Objective	Remarks
$[0]$	Uniaxial Compression (S/F)**	165x6.4x2.3 (15.9)***	Unconstrained Uniaxial Compression Lamina Data	
$[0/90/0]_{2s}$	"	165x19.1x1.7 (19.1)***	Constrained Uniaxial Compression Lamina Data	
$[\pm 45_{16}]_s$	"	165x19.1x4.5 (19.1)***	In-plane Shear Data	
$[\pm 45/0_3]_s$	Uniaxial Tension (S/F)	229x25.4x1.4	Interlaminar Shear Data	Slit Notch in the 0° Layers
$[\pm 25_2/90]_s$	"	229x25.4x1.4	Interlaminar Normal Stress Data	

*Length x Width x Thickness
**S-Static; F-Fatigue
***Unsupported Length of Specimen

Table 9. NARMCO T-300/5208 Graphite Epoxy Unidirectional Laminate Tension Properties

Specimen	E_x (GPa)	ν_{xy}	σ_x^t (MPa)	ε_x^t
L2	137.9	.293	1606.7	11,000
R3	137.9	.313	1661.1	11,700
L1	143.4	.237	1669.2	10,930
R4	146.9	.310	1735.3	11,220
Average	141.6	.288	1668.1	11,210

Table 10. $[\pm 45_{16}]_s$ T-300/5208 Laminate Static Test Data for Uniaxial Tension and Compression

Specimen	Type of Test	σ_x (MPa)	E_x (GPa)	ν_{xy}
1BR1	Uniaxial Compression	202.8	-	-
1BR5	"	206.3	19.8	.7645
1BR2	"	192.5	18.0	.7565
1CC1	"	203.5	-	-
1CC2	"	202.0	-	-
1CC3	"	202.9	-	-
	Average	201.7	18.9	.7605
1BR6	Uniaxial Tension	171.7	19.4	0.6795
6AR1	"	155.1	19.0	.8000
6AR2	"	150.3	19.5	.7400
6AR3	"	143.8	18.4	.7500
	Average	155.2	19.0	.7420

Table 11. T-300/5208 $[\pm 45_{16}]_s$ Laminate Fatigue Compression Data (R = 0.1, f = 30 Hz)

			Residual Compression Test		
Specimen	S	N(cycles)	σ_x^c(MPa)	E_x(GPa)	ν_{xy}
1BR3	.80	12,490			
1BL1	.80	4,450			
1BL3	.80	7,200			
Avg.					
1AC3	.67	2,146,700			
1BR4	.67	15,450			
1CL3	.67	55,650			
1AC4	.67	1,308,130			
1CL1	.67	500,000	199.9	17.58	.781
1BL6	.67	500,000	195.4	16.55	.808
1AL5	.67	500,000	201.7	17.44	.866
			Avg. 199.0	17.17	.818
1CL4	.67	150,000	200.4	--	--
1AC5	.67	150,000	197.7	17.65	.788
1BL4	.67	150,000	192.8	14.55	.827
			Avg. 197.0	16.13	.808
1CL6	.50	10,000,000	201.5	18.68	.819
1AL6	.50	10,000,000	200.5	17.65	.871
1AL4	.50	10,000,000	198.7	17.51	.777
			Avg. 200.2	17.93	.822
1AL2	.50	1,000,000	198.0	17.10	.827
1AC6	.50	1,000,000	198.3	20.20	.775
1BL5	.50	1,000,000	194.2	18.00	.700
			Avg. 196.8	18.41	.767

Table 12. Static Test Data for $[\pm 25_2/90]_s$ T-300/5208 Laminates

Specimen	Type of Test	σ_x^{t*}, (MPa)	σ_x^{t**}, (MPa)
2AR1	Uniaxial Tension	206	179
2BL3	"	224	226
2AL3	"	228	210
		Avg. 219	205

*Determined from Acoustic Emission

**Obtained from Load-Displacement Chart

Table 13. Tension/Tension Lifetime Fatigue Test Data for $[\pm 25_2/90]_s$ T-300/5208 Laminates (f = 30Hz, R = 0.1)

Specimen	S	N (cycles)
2BL2	0.8	4510
2AR2	0.8	5550
2AL1	0.8	3120
2AL2	0.7	7600
2BR3	0.7	8400
2BL1	0.7	8000
2AR3	0.6	48,660
2BR2	0.6	205,550
2BR1	0.6	794,050
2CR1	0.6	2,061,580
2DL1	0.6	155,600

Table 14. Static Test Data for $[\pm 45/0_3]_s$ Partially Notched T-300/5208 Laminate

Specimen	Type of Test	σ_x^t (MPa)
3AR2	Uniaxial Tension	104.1
3AL2	"	77.2
3AL3	"	92.4
		Avg. 91.01

Table 15. Tension/Tension Lifetime Fatigue Data for $[\pm 45/0_3]_s$ Partially Notched T-300/5208 Laminate (R = 0.1, f = 30Hz)

Specimen	S	N (cycles)	σ_x^t (MPa)
3AR1	0.8	530,450	
3AL1	0.8	82,120	
3C2	0.8	8,910	
3BL3	0.7	504,210	
3BL2	0.7	2,957,100	
3BR3	0.7	617,740	
3BR2	0.6	4,397,520	
3BL1	0.6	$5x10^6$ (runout)	113*
3C1	0.6	$5x10^6$ (runout)	-

*Residual

Table 16. Uniaxial Compression Static Test Data for [0] T-300/5208 Laminate

Specimen	σ_x^t (MPa)	E_x (GPa)
7D3	1262.4	-
7D4	1108.7	-
7D5	1234.9	-
7D6	1421.0	131.7
7E1	1538.2	-
7D7	1367.2	134.4
7E2	1611.3	135.1
7E3	1234.2	131.7
Avg.	1347.2	133.1

Table 17. Uniaxial Compression Static Test Results for $[0/90/0]_s$ T-300/5208 Laminate

Specimen	σ_x^c (MPa)	E_x (GPa)	ν_{xy}
5BC1	1061.5	87.6	0.066
5AC5	1038.4	97.9	0.091
5AL5	867.0	91.0	0.056
5AC4	1000.8	93.1	0.105
5BL1	913.2	91.7	0.067
5AC6	1172.1 / 1008.7	- / 92.4	- / 0.077

Table 18. Uniaxial Compression/Compression Lifetime and Residual Strength/Stiffness Data for [0] T-300/5208 Laminate (f = 30Hz, R = 10)

Specimen	S	N, Cycles	Residual Strength σ_x^c (MPa)	Residual Modulus E_x (GPa)
7D14	0.8	1,420	1418*	
7D15	"	1,470	FF	
7D16	"	850	1146*	
7D25	"	4,240	1217*	
7D26	"	4,110	1656*	
7D27	"	3,350	1628*	
7D11	0.67	10^6	1274*	
7D12	"	94,510	1243*	
7D13	"	4,677,110	1192*	
7D22	"	10,300	1772*	
7D23	"	10,240	1487*	
7D24	"	7,780	1573*	
7D21	0.5	108,200	FF	
7D8	"	5×10^6	1288	-
7D9	"	5×10^6	1513	140
7D10	"	5×10^6	1578	137
			Avg. 1460	138.5
7D18	"	10^6	1682	125
7D19	"	10^6	1650	130
7D20	"	10^6	1378	129
			Avg. 1570	128

FF Fatigue Failure

*Residual Strength Tests Conducted After N Cycles

Table 19. Uniaxial Compression/Compression Lifetime and Residual Strength/Stiffness Data for $[0/90/0]_{2s}$ T-300/5208 Laminate (f=30Hz, R=10)

Specimen	S	N,Cycles	Residual Strength σ_x^c (MPa)	Residual Modulus E_x (GPa)	Poisson's Ratio ν_{xy}
5BC5	0.8	150			
5BC4	"	640			
5AL1	"	15,800			
5AL4	"	10			
5BC6	"	2,770			
5AL2	"	1,110			
5BL4	0.67	5,920			
5BC2	"	25,290			
5AL6	"	$5x10^{6*}$	816	97	0.172
5CL1	"	2,009,050	1061	79	0.05
5BL2	"	$5x10^{6}$	966	93	0.03
5AL3	"	2,470	-	-	-
			Avg. 1014	86	0.04
5BL6	0.5	$5x10^{6*}$	829	83	0.183
5AC3	"	$5x10^{6*}$	872	87	0.06
5BL3	"	$5x10^{6*}$	988	87	0.092
			Avg. 897	86	0.112
5AL1	"	10^{6}	852	97	0.072
5BL5	"	10^{6}	865	93	0.044
5AC2	"	10^{6}	842	90	0.109
			853	93	0.075

*Runout

Table B1. Design of a Partially Notched $[\pm 45_i/0_j]_s$ Laminate to Assure Failure due to Interlaminar Stress τ_{xz}

% of 0° Layers	40%	60%	80%
Initial Failure Stress for Laminate (MPa) (±45° Layers in Shear)	393.0	554.7	730.8
Ultimate Failure Stress for Laminate from Netting Analysis (MPa) (0° Layer in Tension)	579.2	868.7	1158.3
Failure Stress of ±45° Laminate in the Notched Area (MPa)	124.1	124.1	124.1
Corresponding Force $F_{\pm 45°}$ (N) (Specimen Width=25.4mm)	2642.2	1761.5	880.7
Value of the Force, F_s, when Failure Occurs by Interlaminar Shear (N) (for max. τ_{xz}=68.95MPa)	2139.6	1347.8	653.9
$F_{\pm 45°}/F_s$	1.23	1.31*	1.35

*The 60% configuration is chosen for the experiments.

Note: All failure stresses are for uniaxial tension.
Lamina Thickness = 0.14 mm

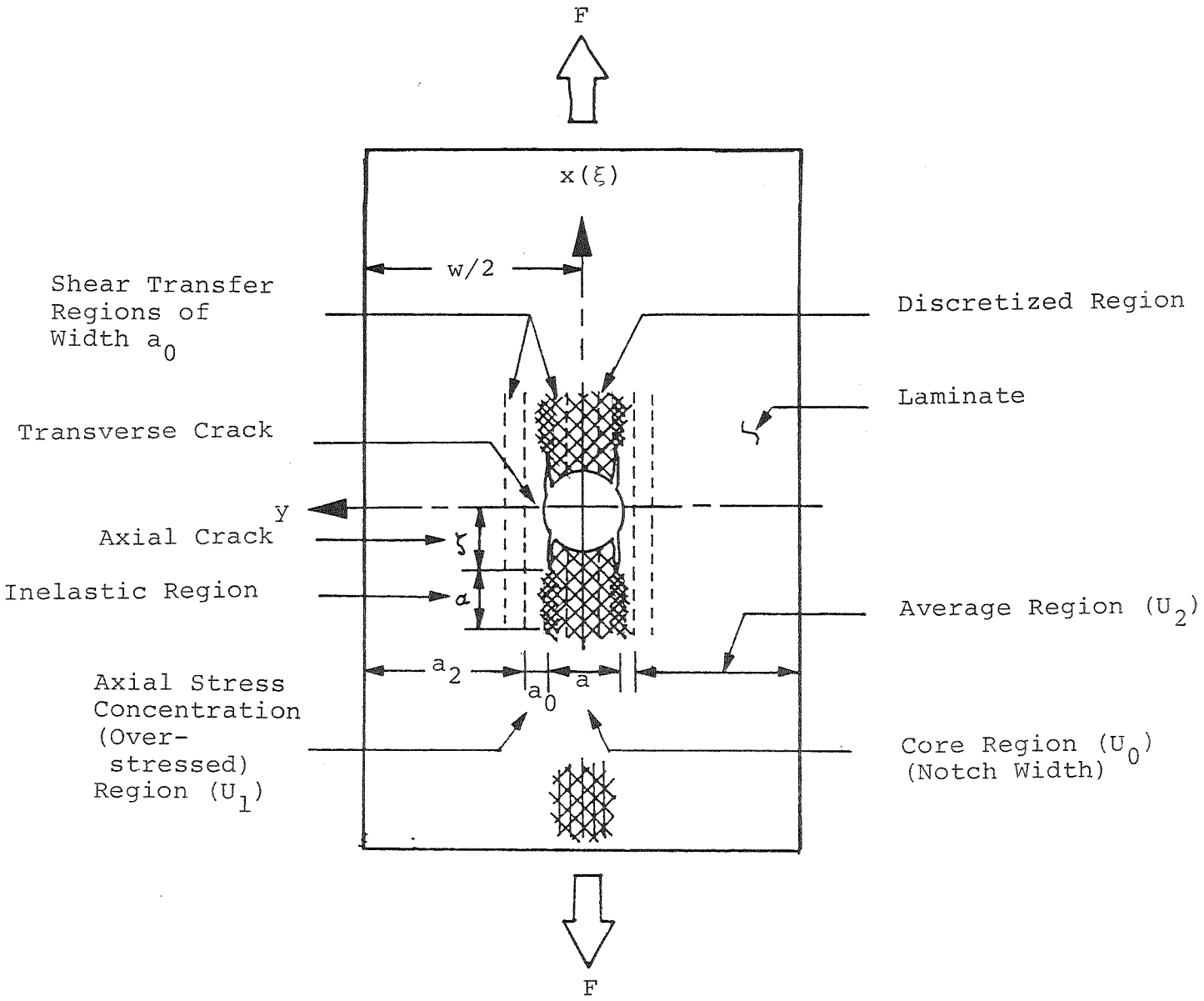

Figure 1. Minimechanics Model for a Notched Laminate

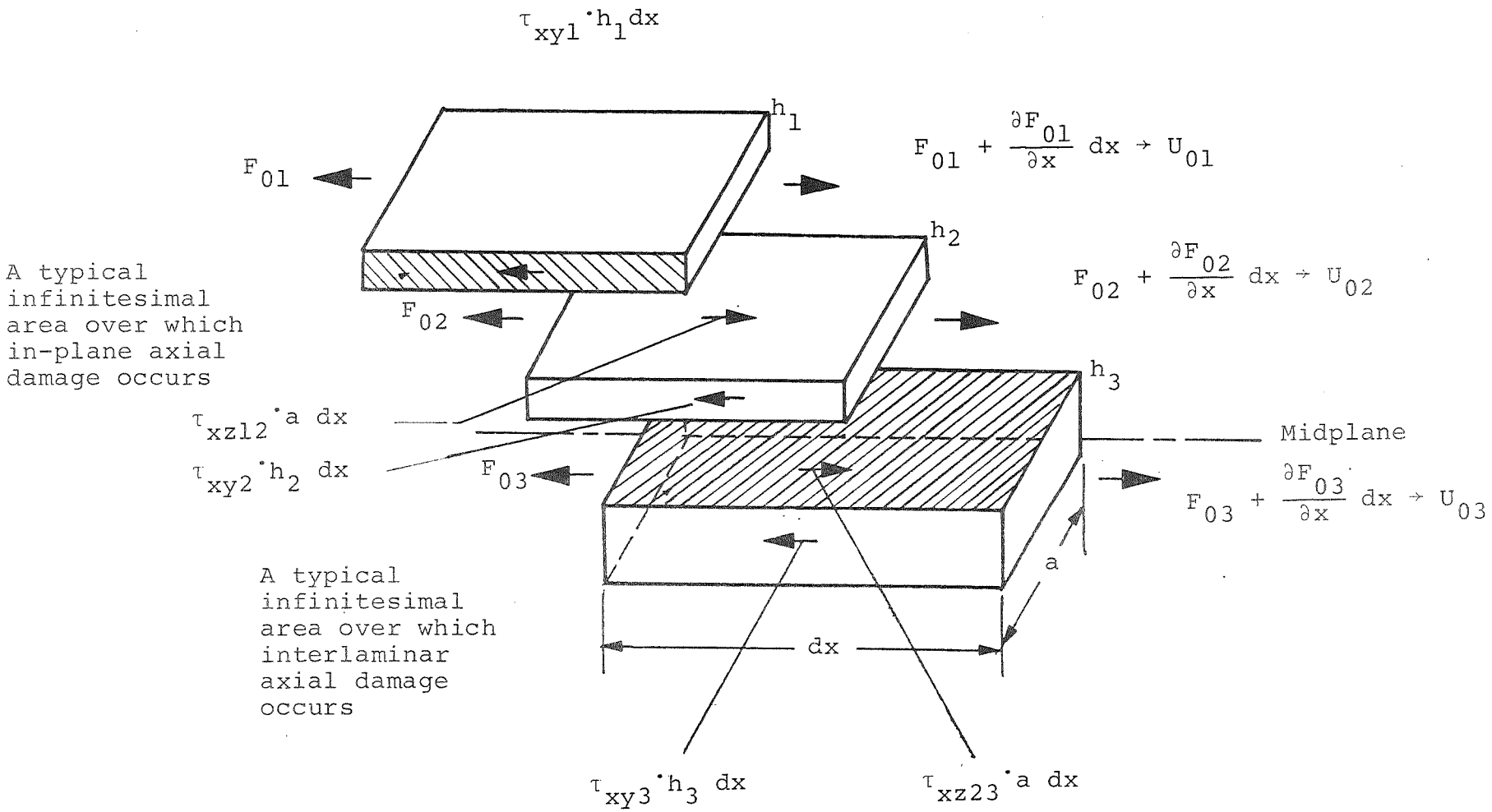

Figure 2. Discretized Core Region

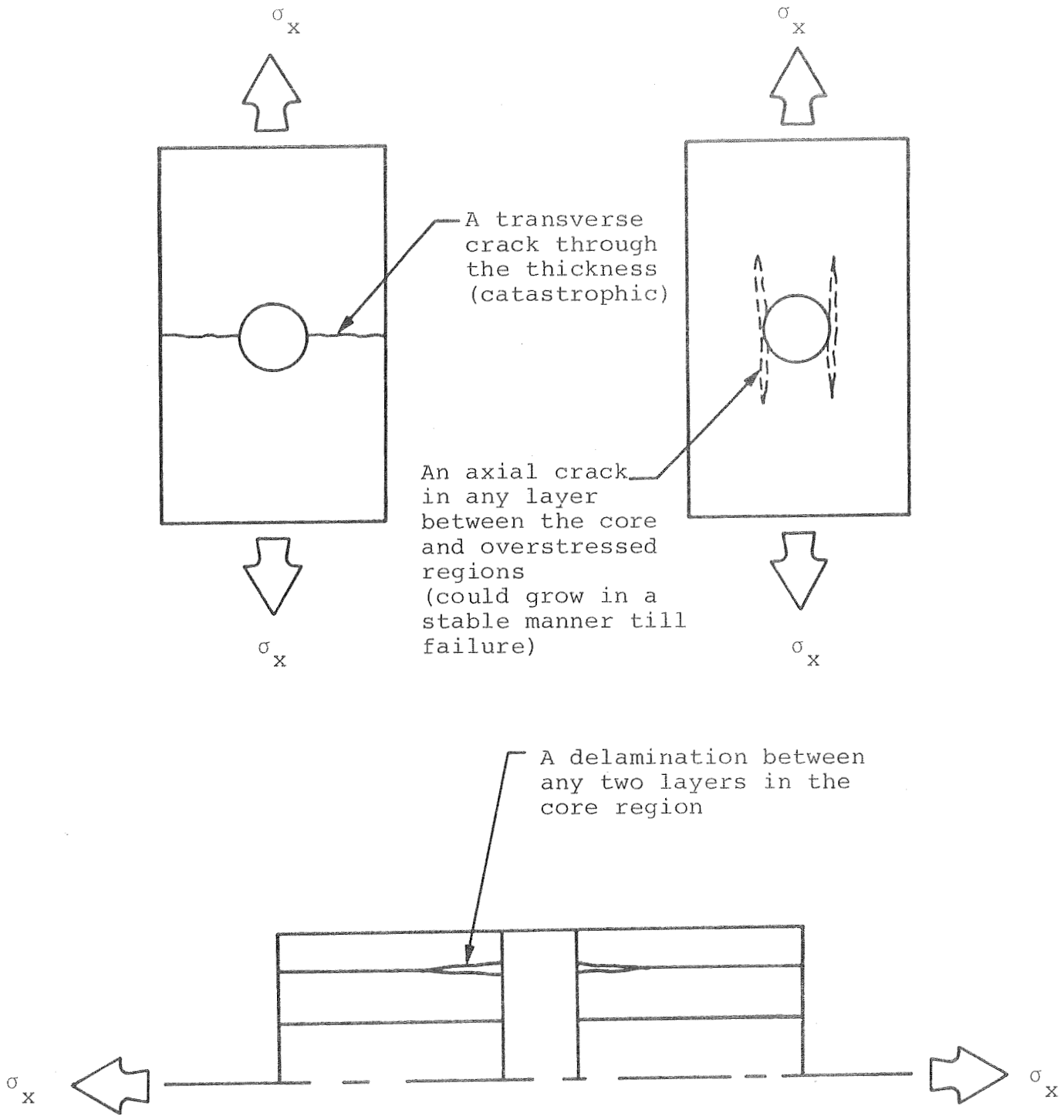

Figure 3. The Various Failure Modes in a Notched Laminate

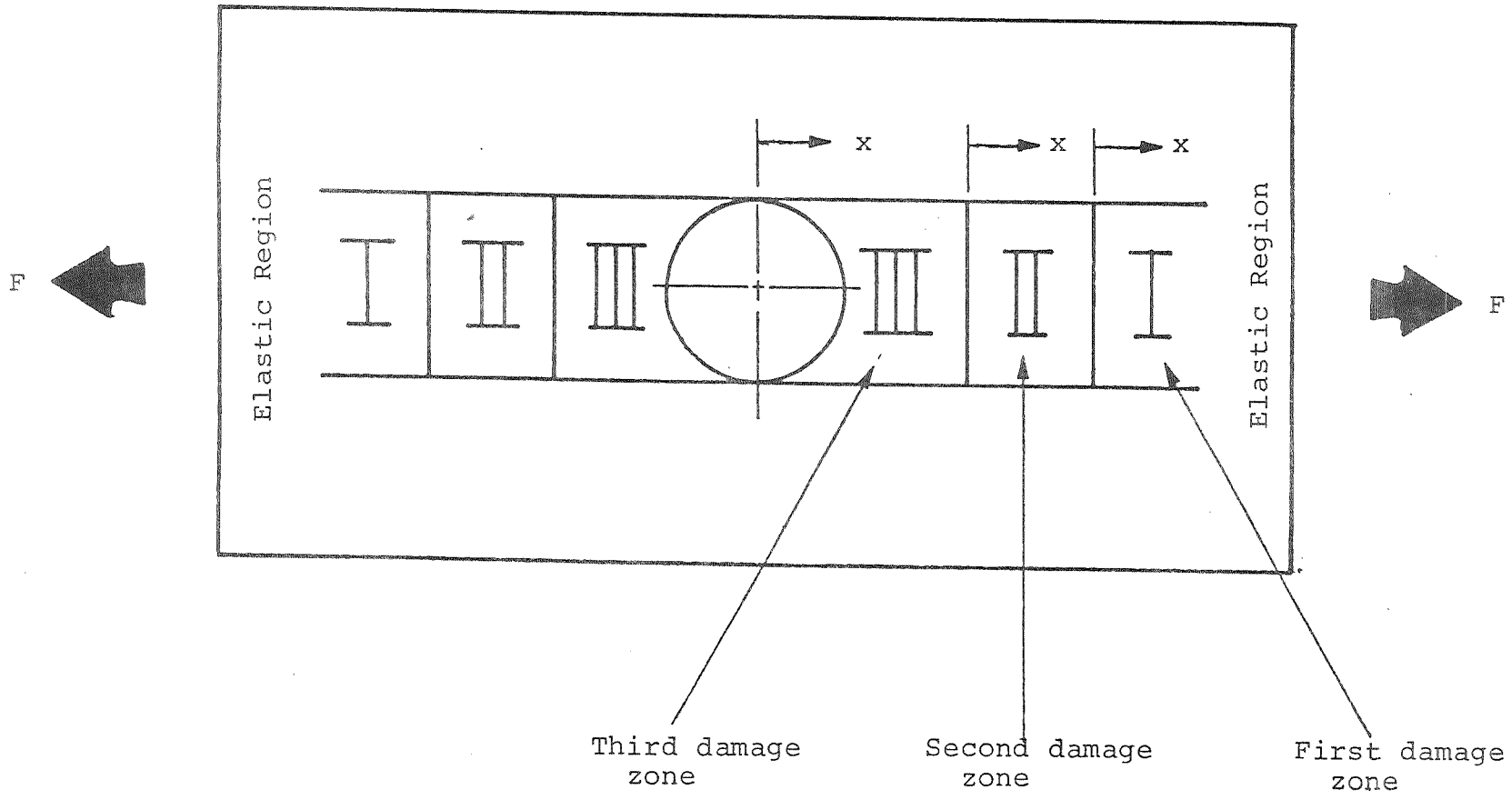

Figure 4 . Damage Zone Sequence and Local Coordinates

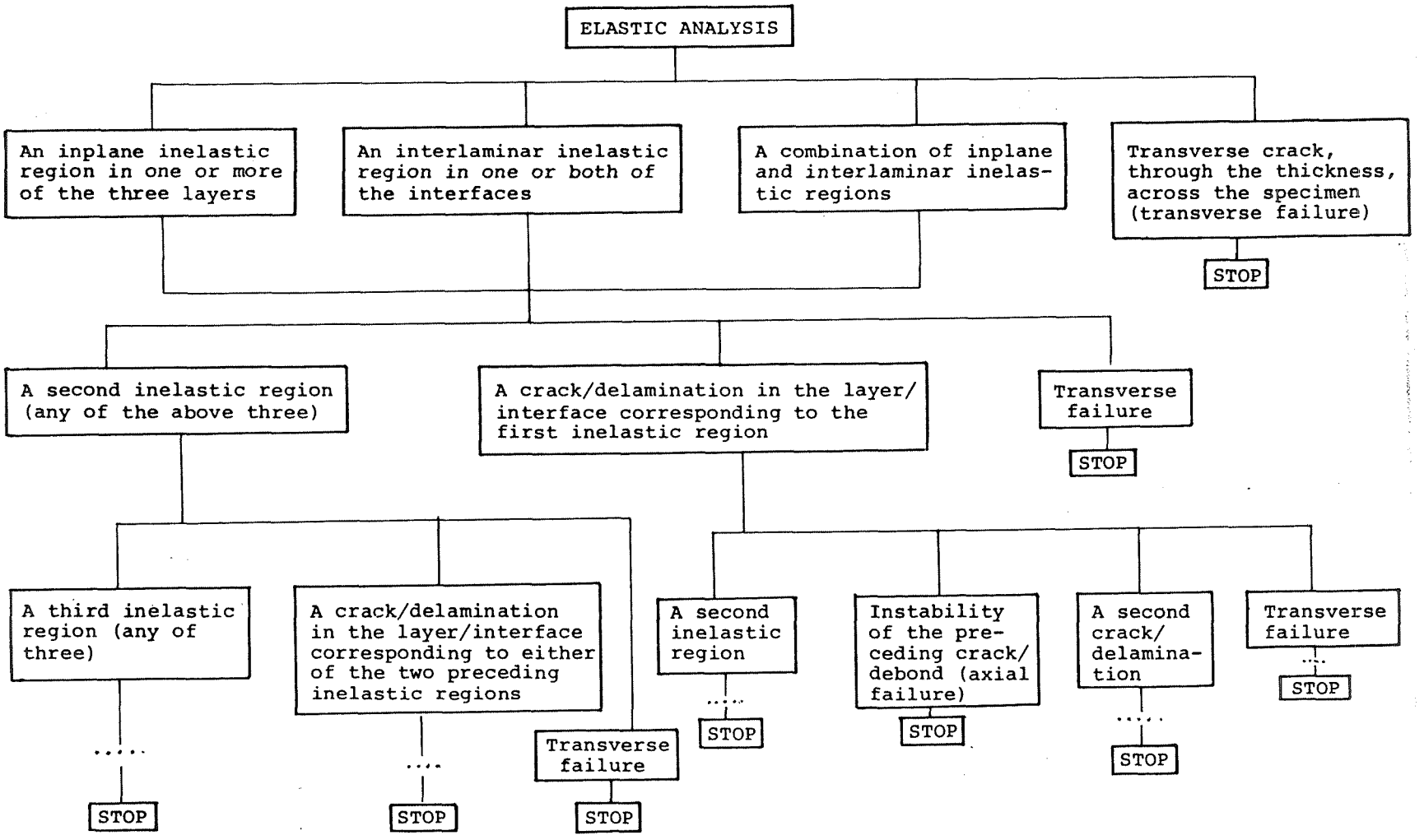

Figure 5. Various Damage Growth Combinations in a Notched Laminate.

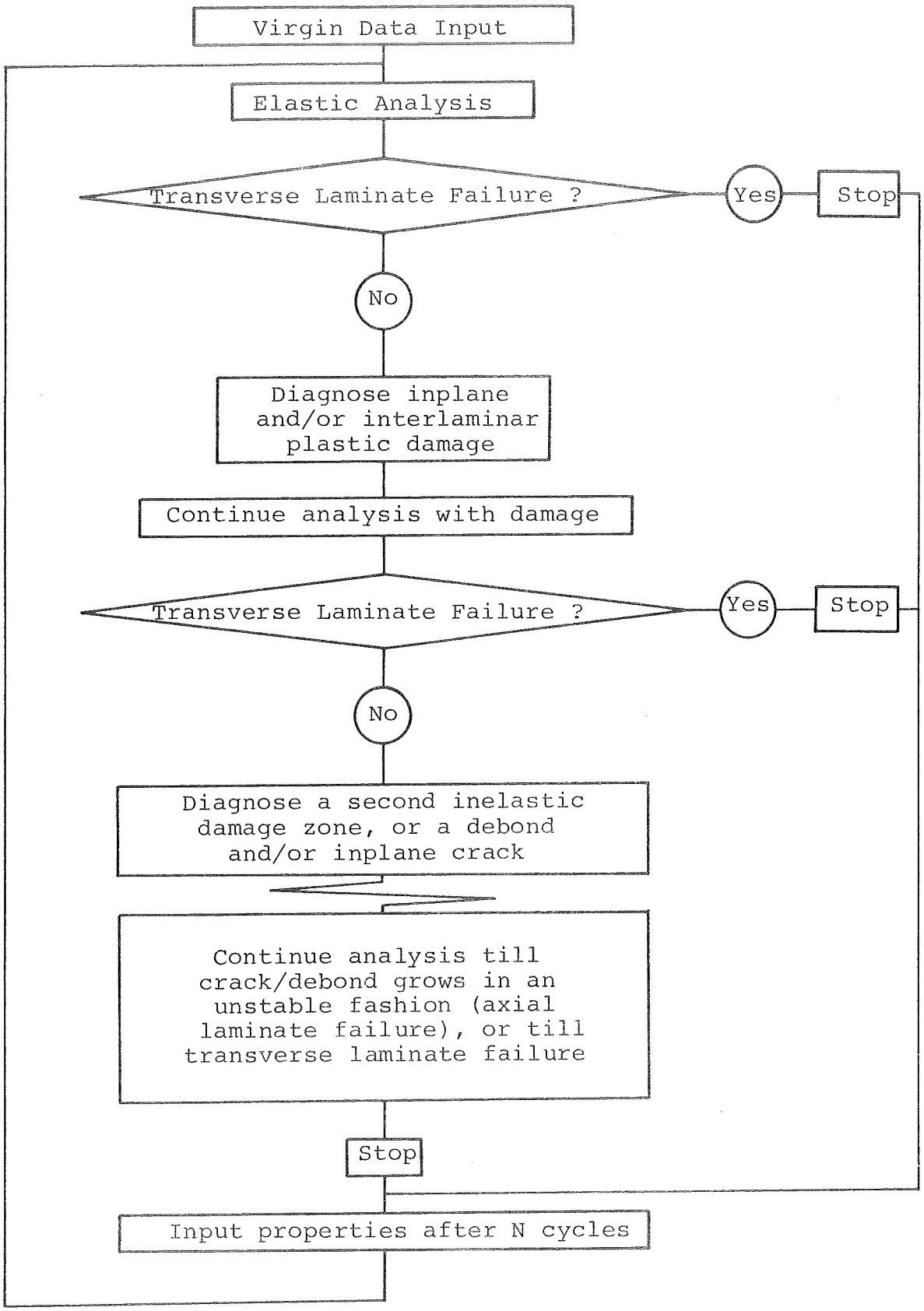

Figure 6. Flow Chart for Failure Mode and Strength Predictions.

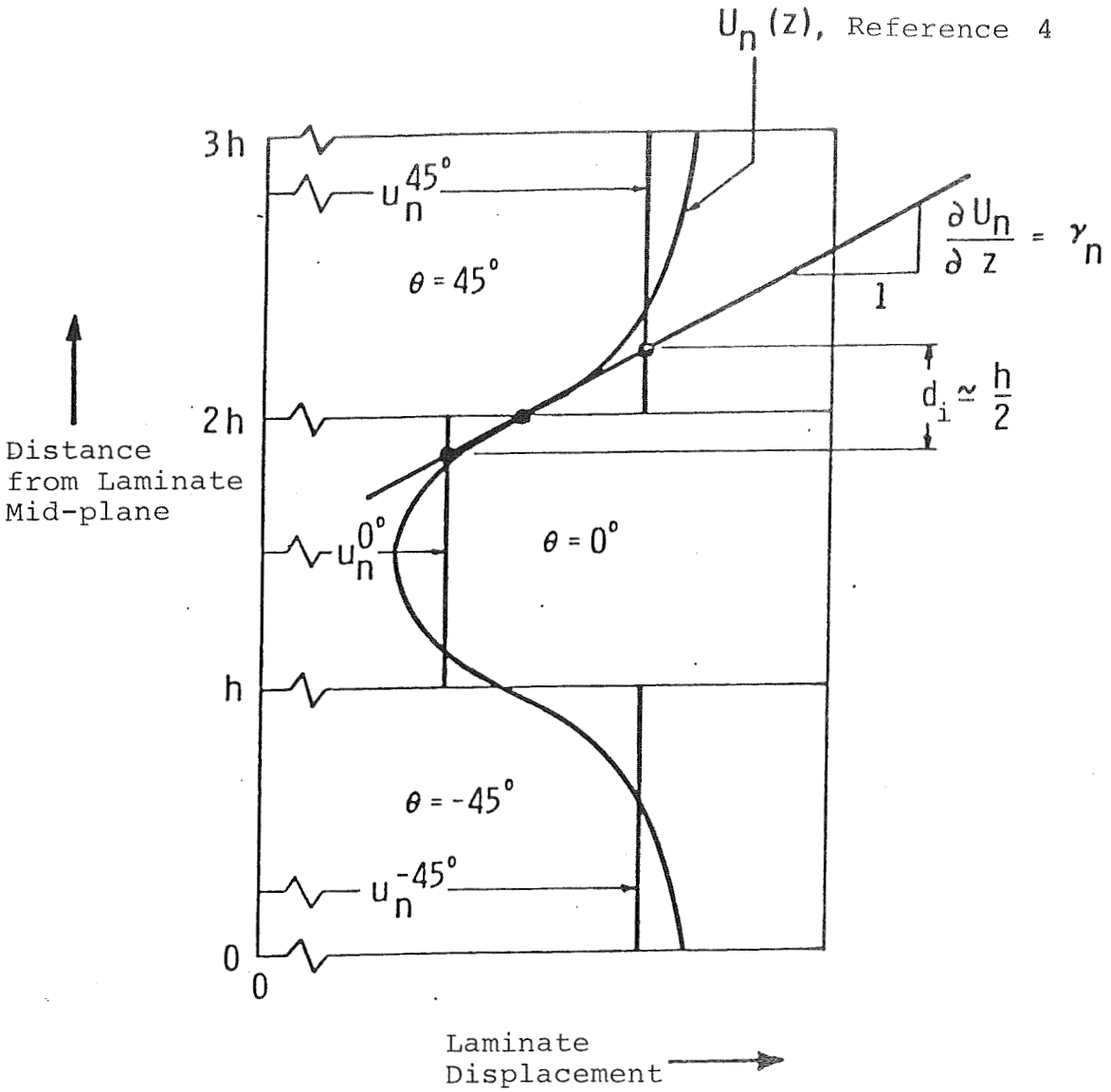

Figure 7 . Transverse Displacement Distributions Near Specimen Edge, $[45/0/-45]_s$ Laminate (ref. 4), Showing Average Lamina Displacements, u_n, First Interlayer Shear Strain, γ_n, and Determination of Parameter d.

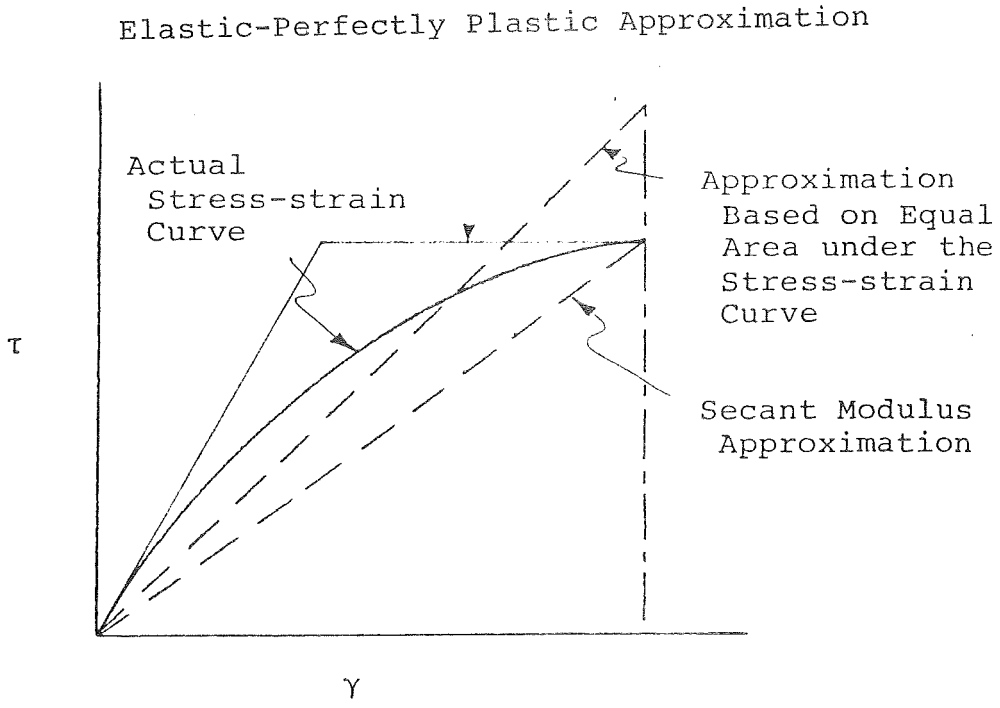

Figure 8. Different Linear Approximations of the In-Plane and Interlaminar Shear Strain Curve

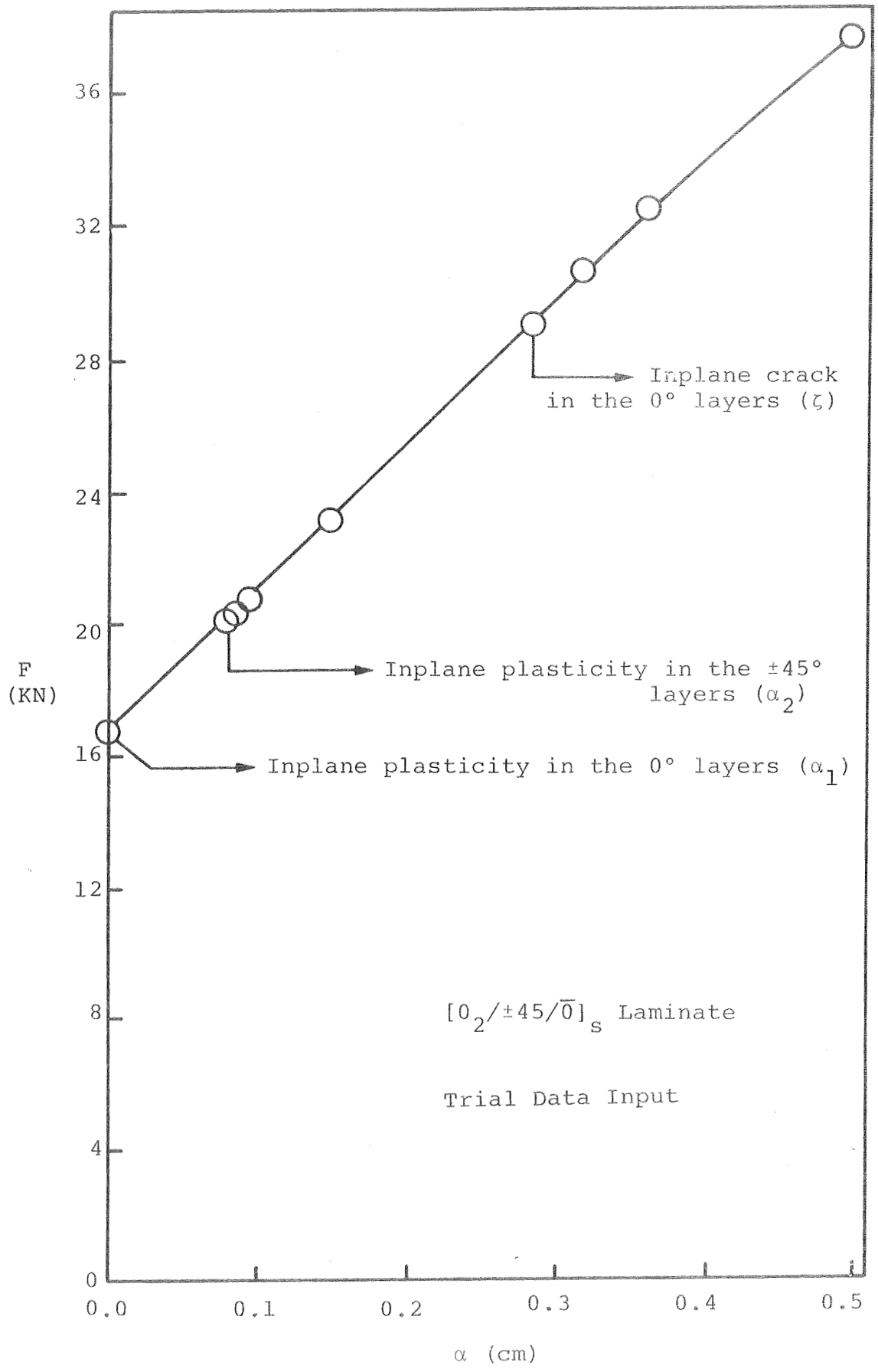

Figure 9. Variation of Applied Laminate Force with the Total Axial Damage Zone Size

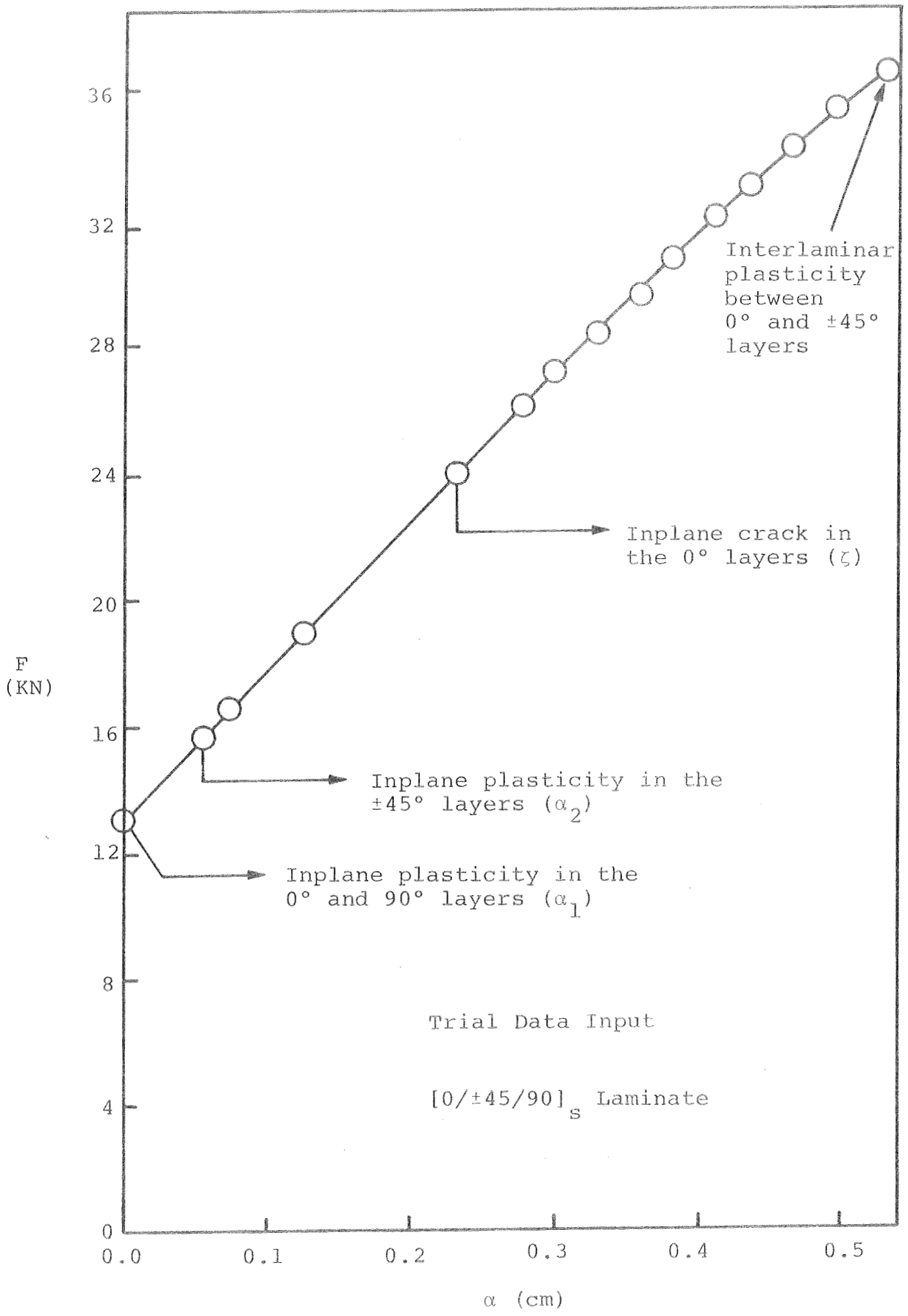

Figure 10. Variation of Applied Laminate Force with the Total Axial Damage Zone Size

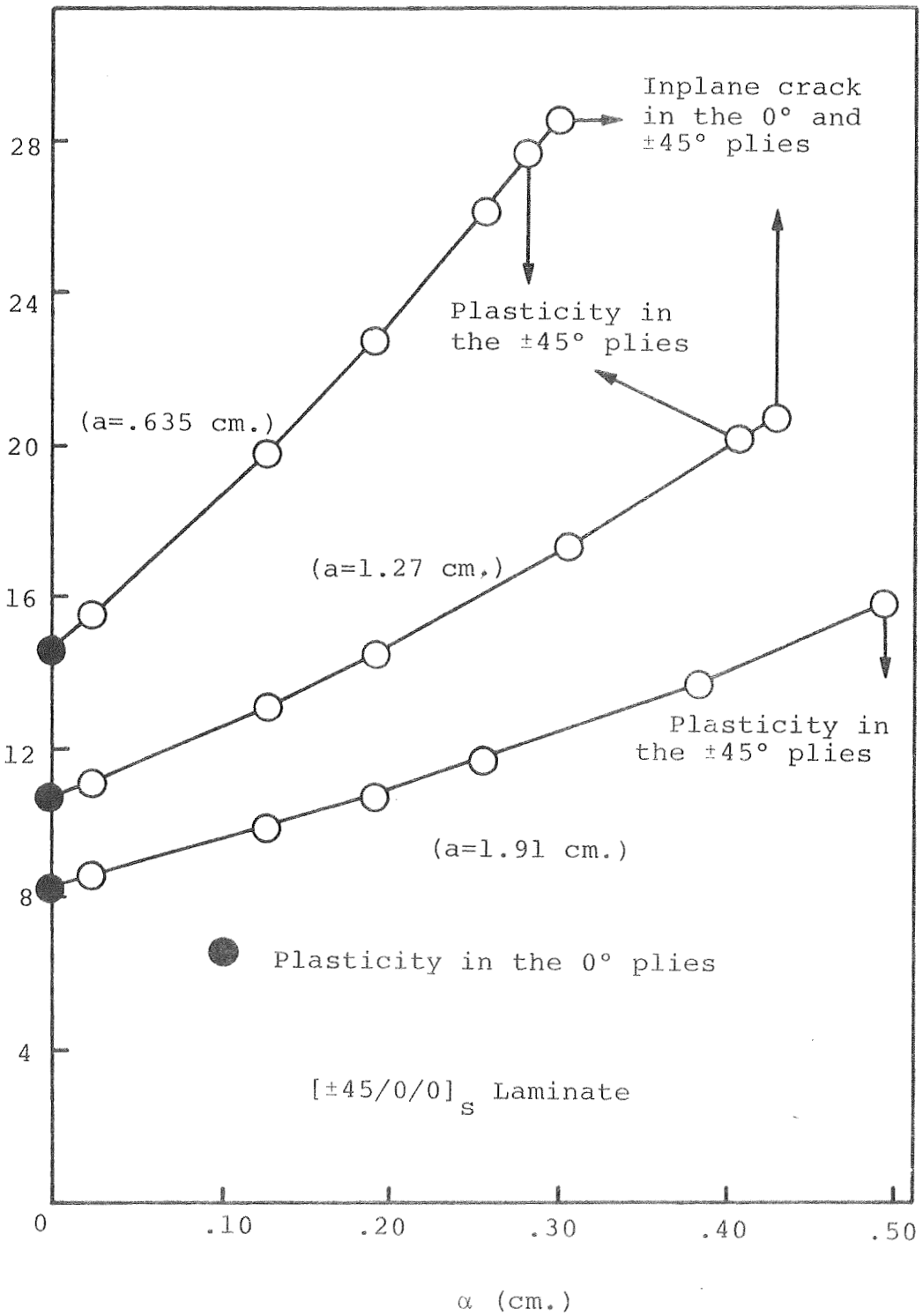

Figure 11. Damage Growth in a $[\pm 45/0/0]_s$ Laminate for the Trial Data Input

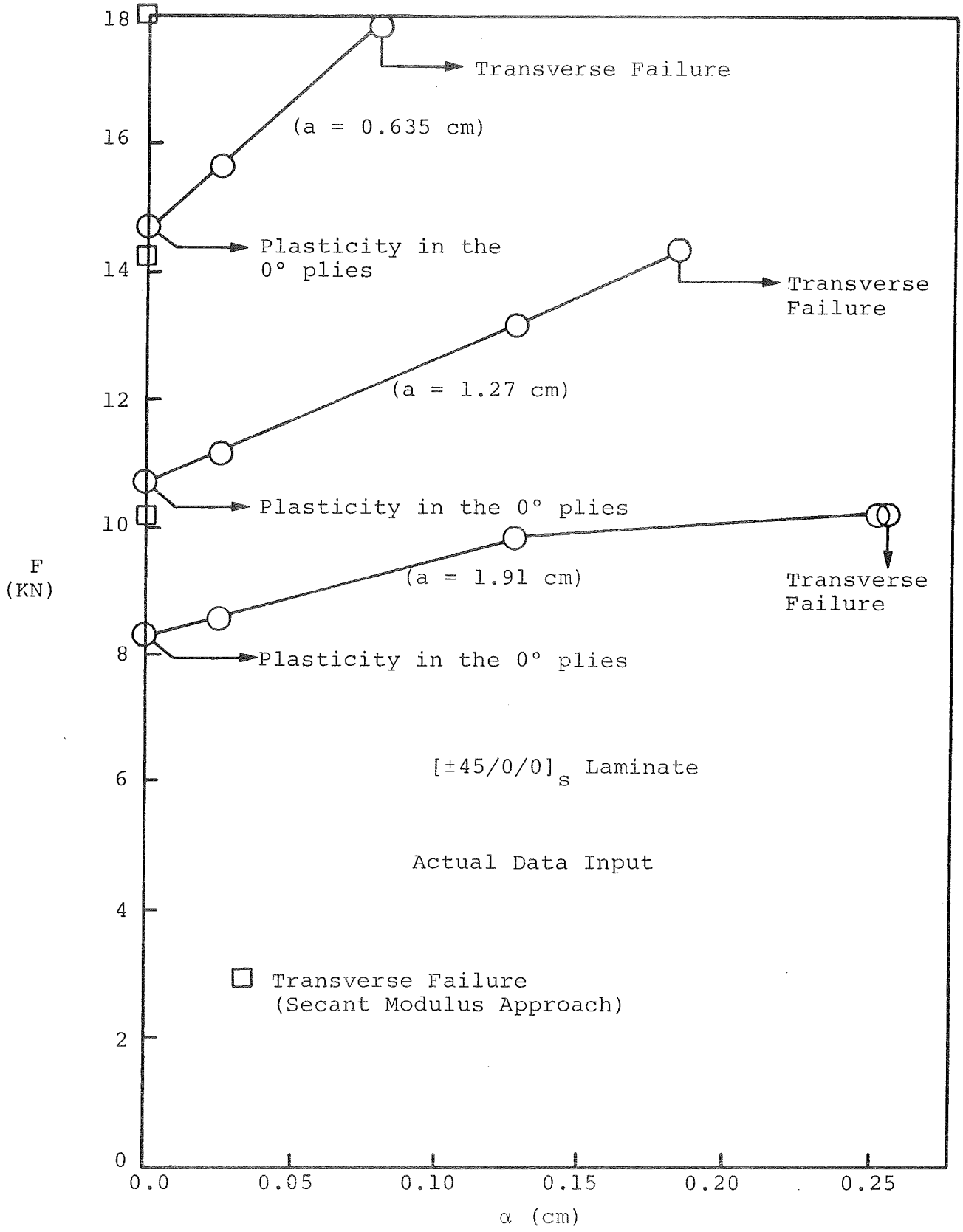

Figure 12. Variation of Applied Laminate Force with the Total Axial Damage Zone Size

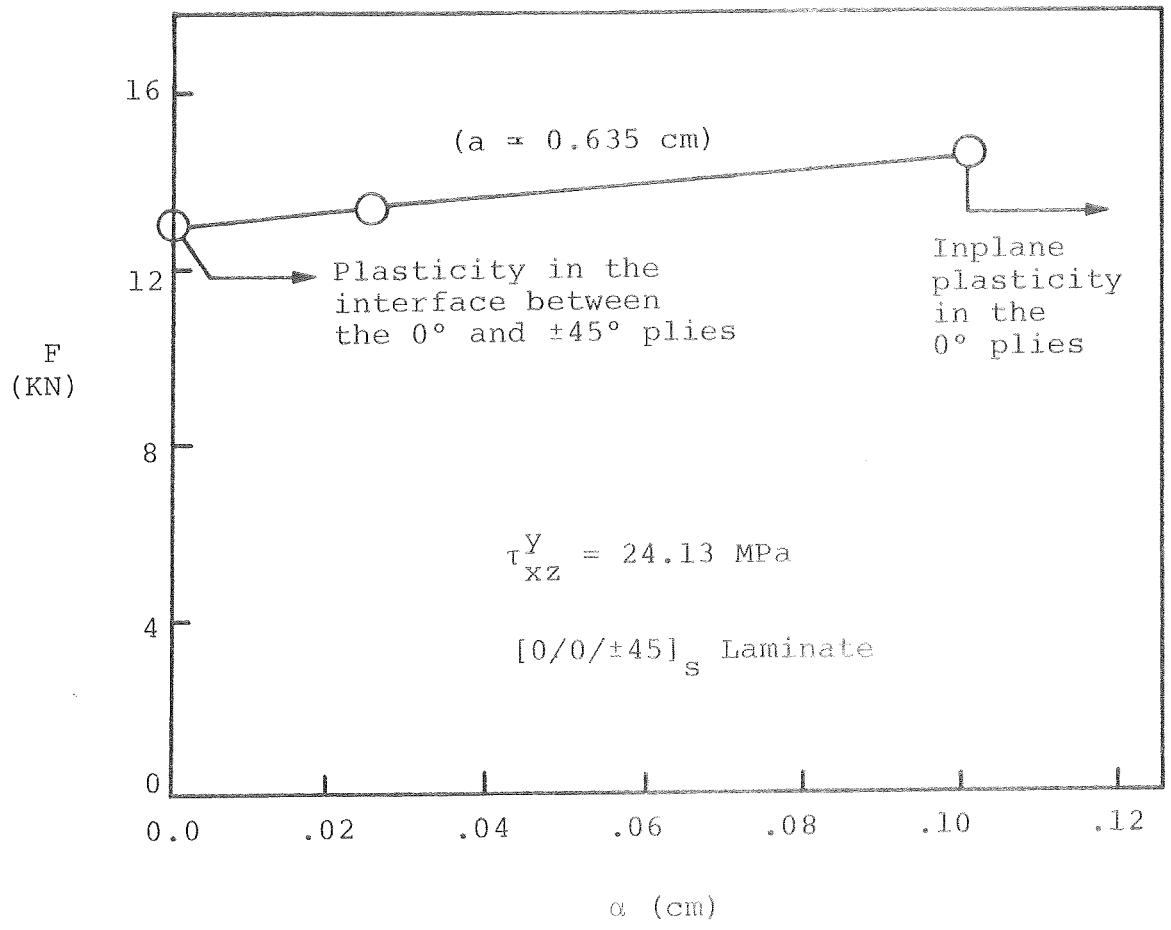

Figure 13. Variation of Applied Laminate Force with Axial Damage Zone Size

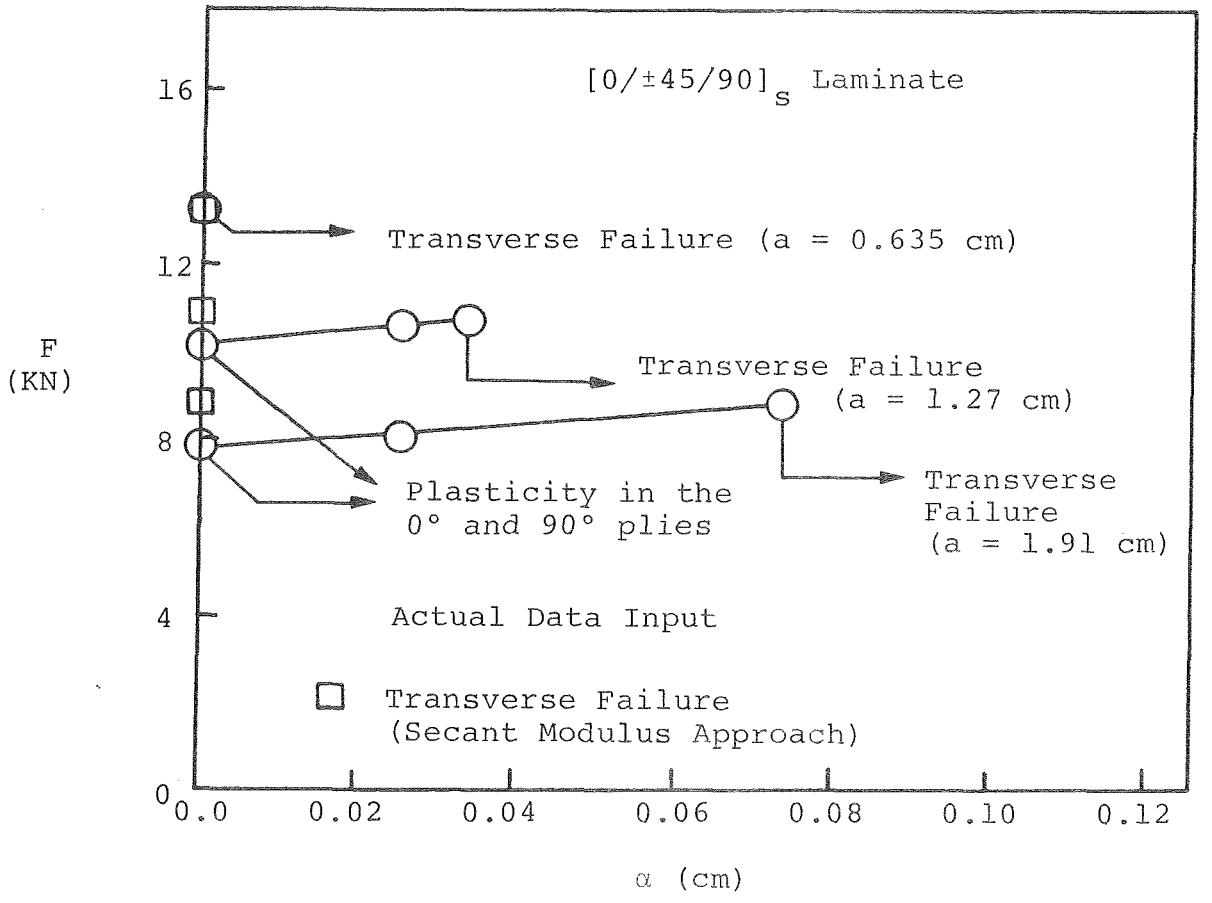

Figure 14. Variation of Applied Laminate Force with Total Axial Damage Zone Size

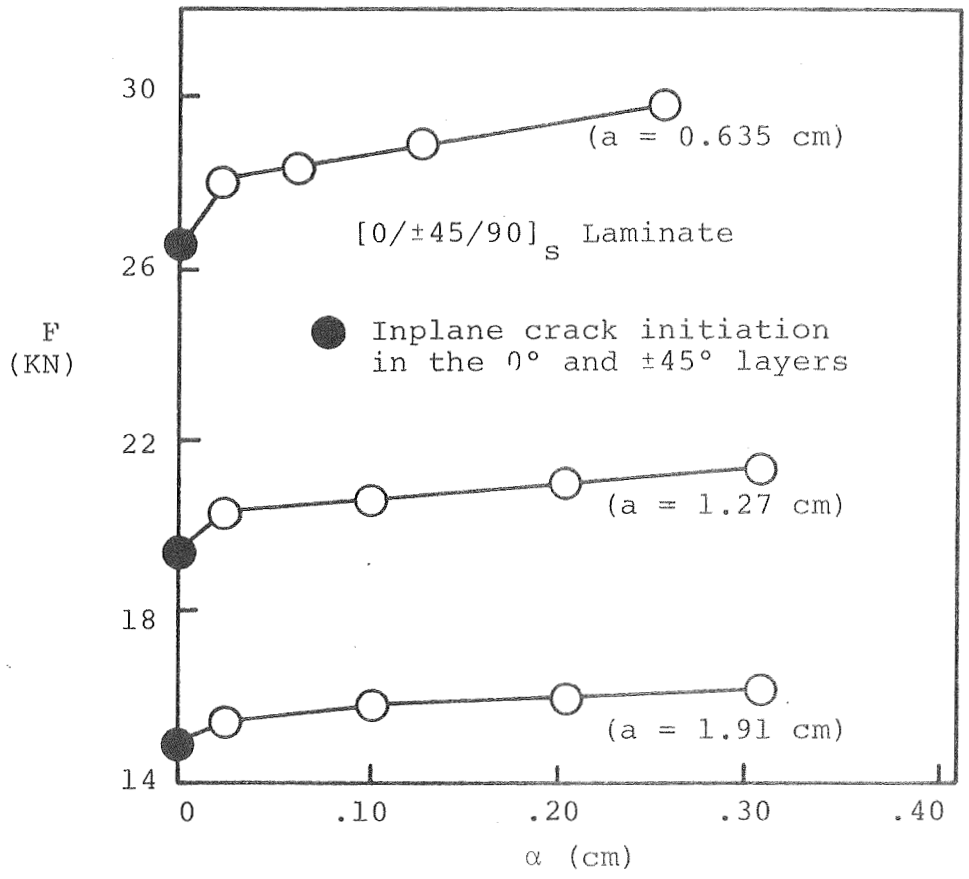

Figure 15. Variation of Applied Laminate Force with Axial Damage Zone Size (Secant Modulus Approach) for a Large Value of σ_T

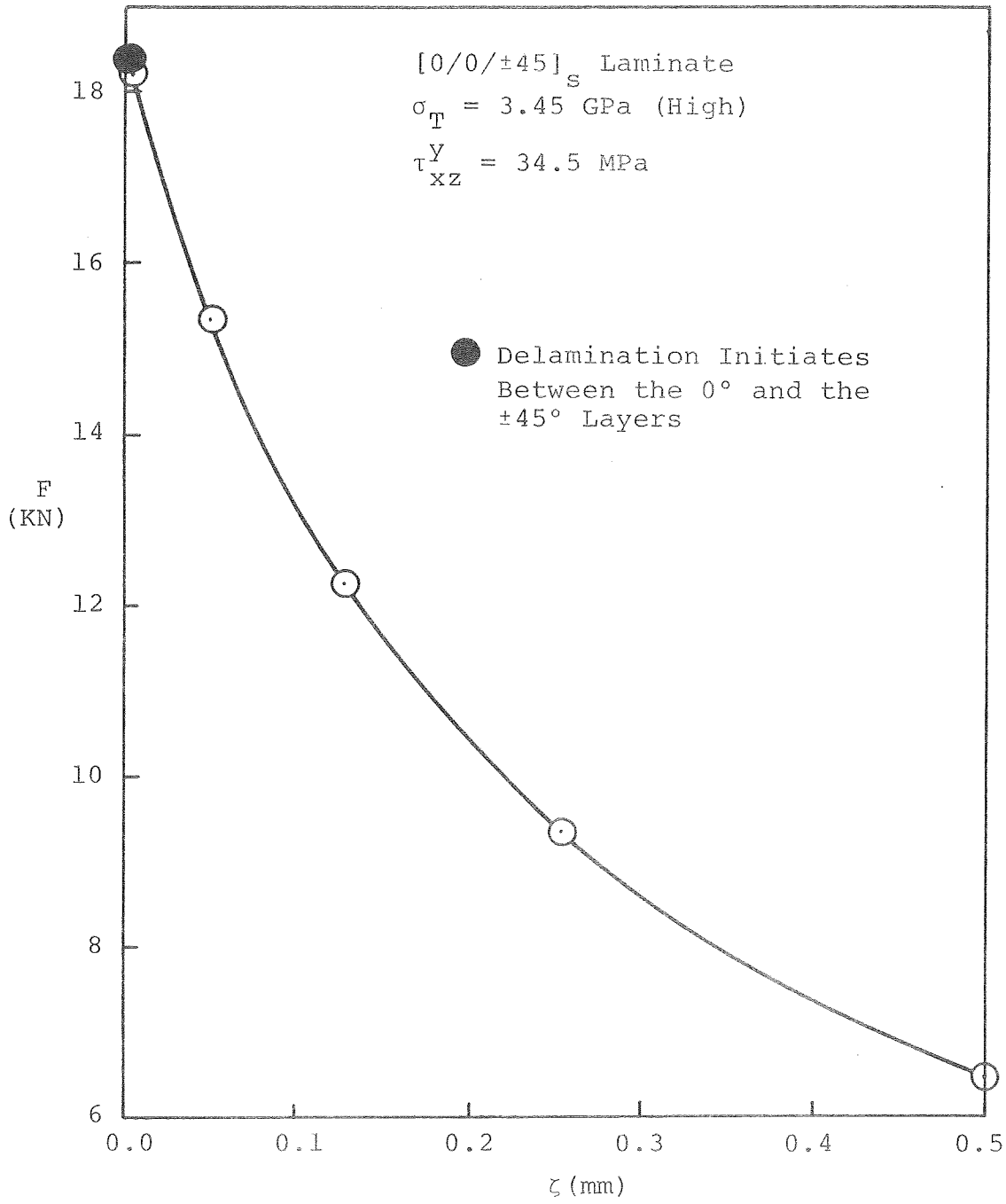

Figure 16. Unstable Growth of Delamination in a $[0/0/\pm45]_s$ Laminate (Secant Modulus Approach)

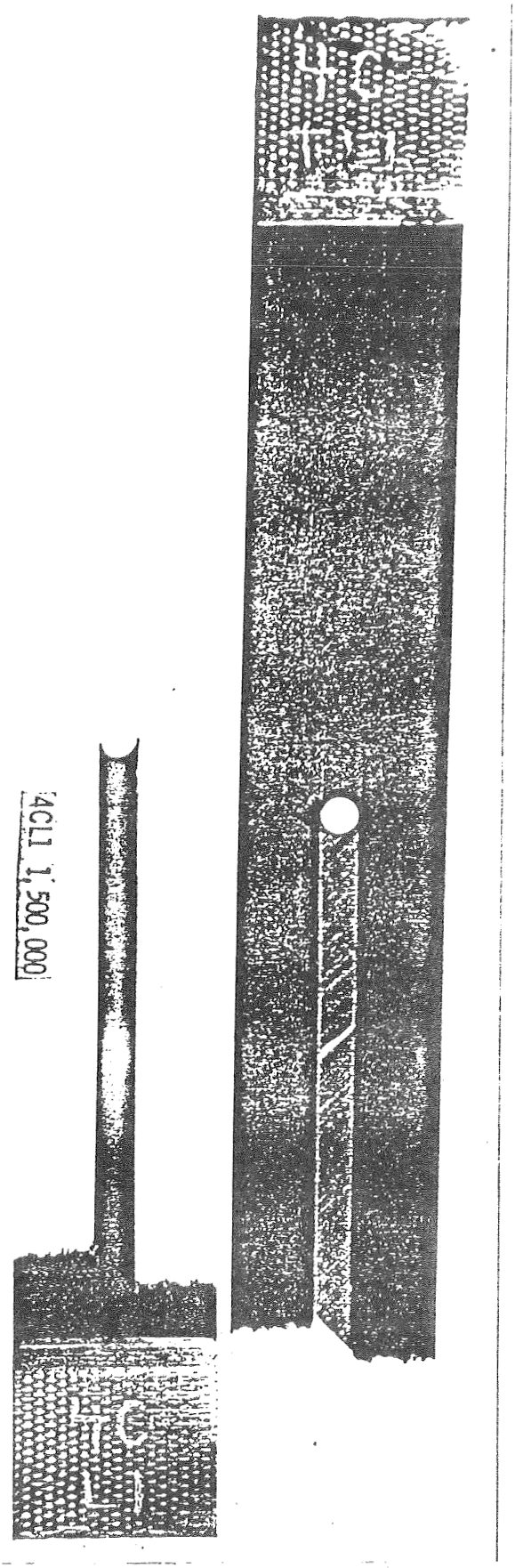

Figure 17. Fatigue Failure of a Notched $[0_2/\pm45]_s$ Boron/Epoxy Laminate Showing Delamination of the 0° Layers from the Laminate (S=.8) (ref. 2)

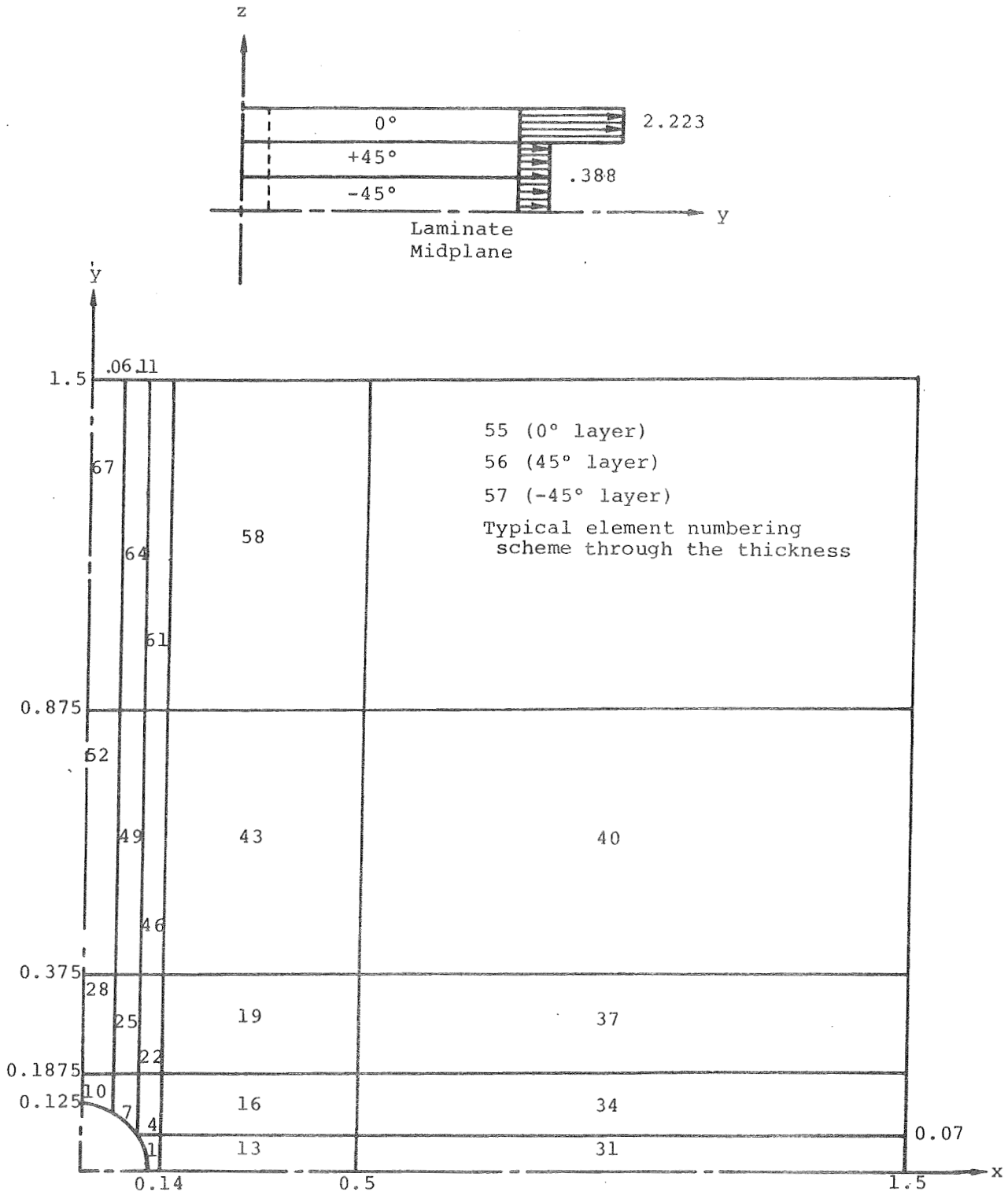

Figure 18. SAP-IV Finite Element Mesh for an Octant of a Notched Laminate

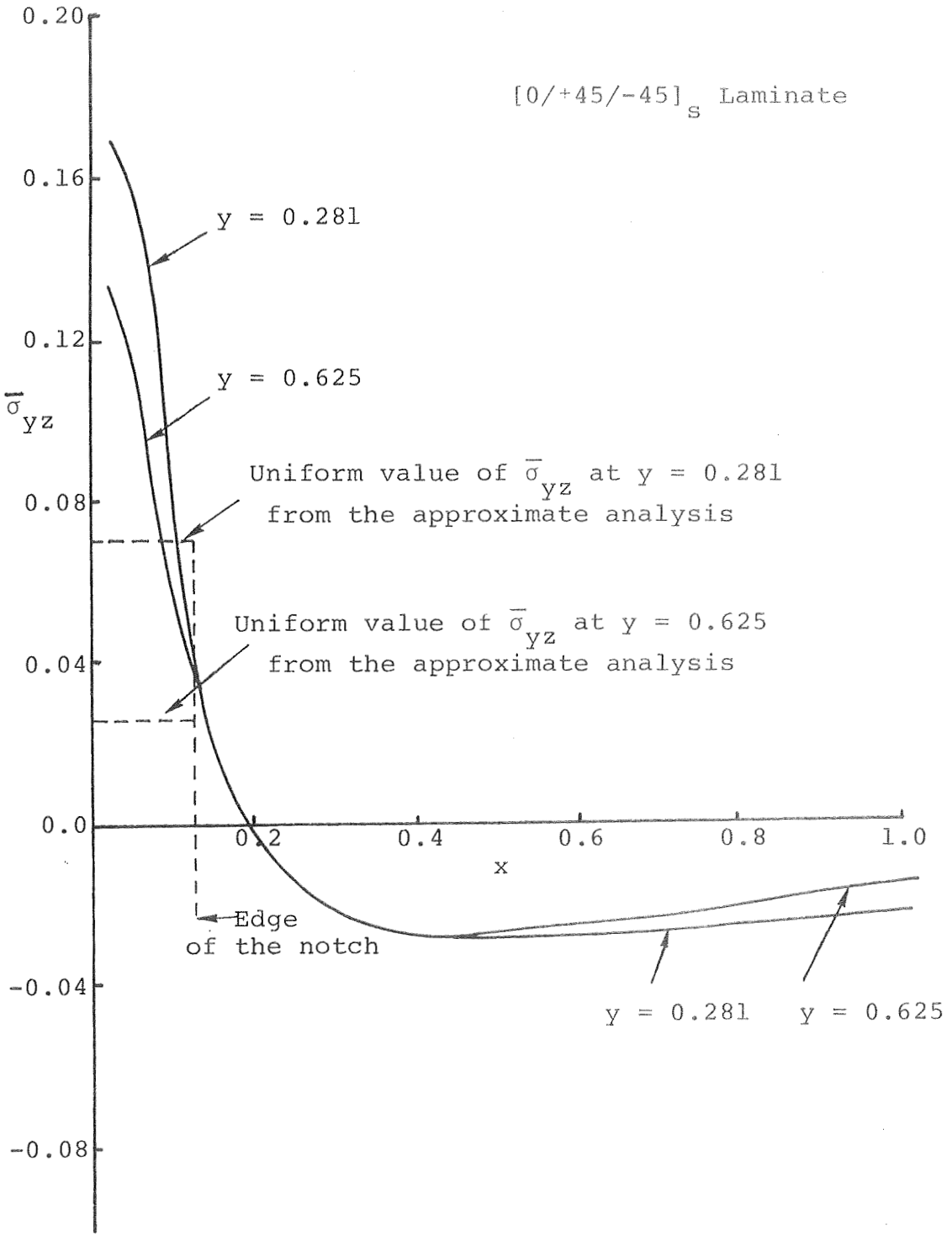

Figure 19. Average σ_{yz} for Unit Applied Average Stress at the Interface Between 0° and 45° Layers for Different Values of y.

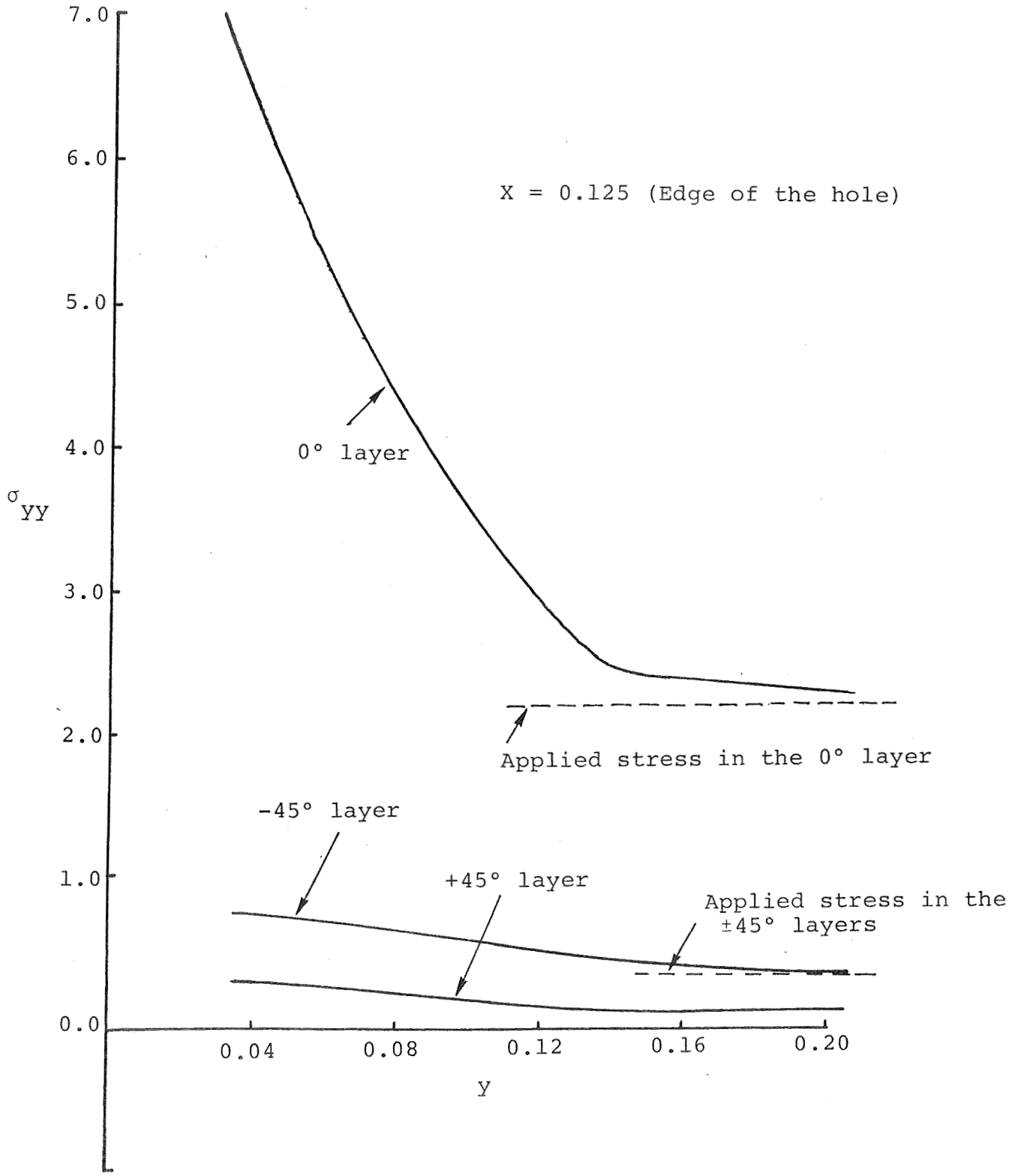

Figure 20. Element Centroidal σ_{yy} Values in the Different Layers for Different y Values from the Edge of the Hole

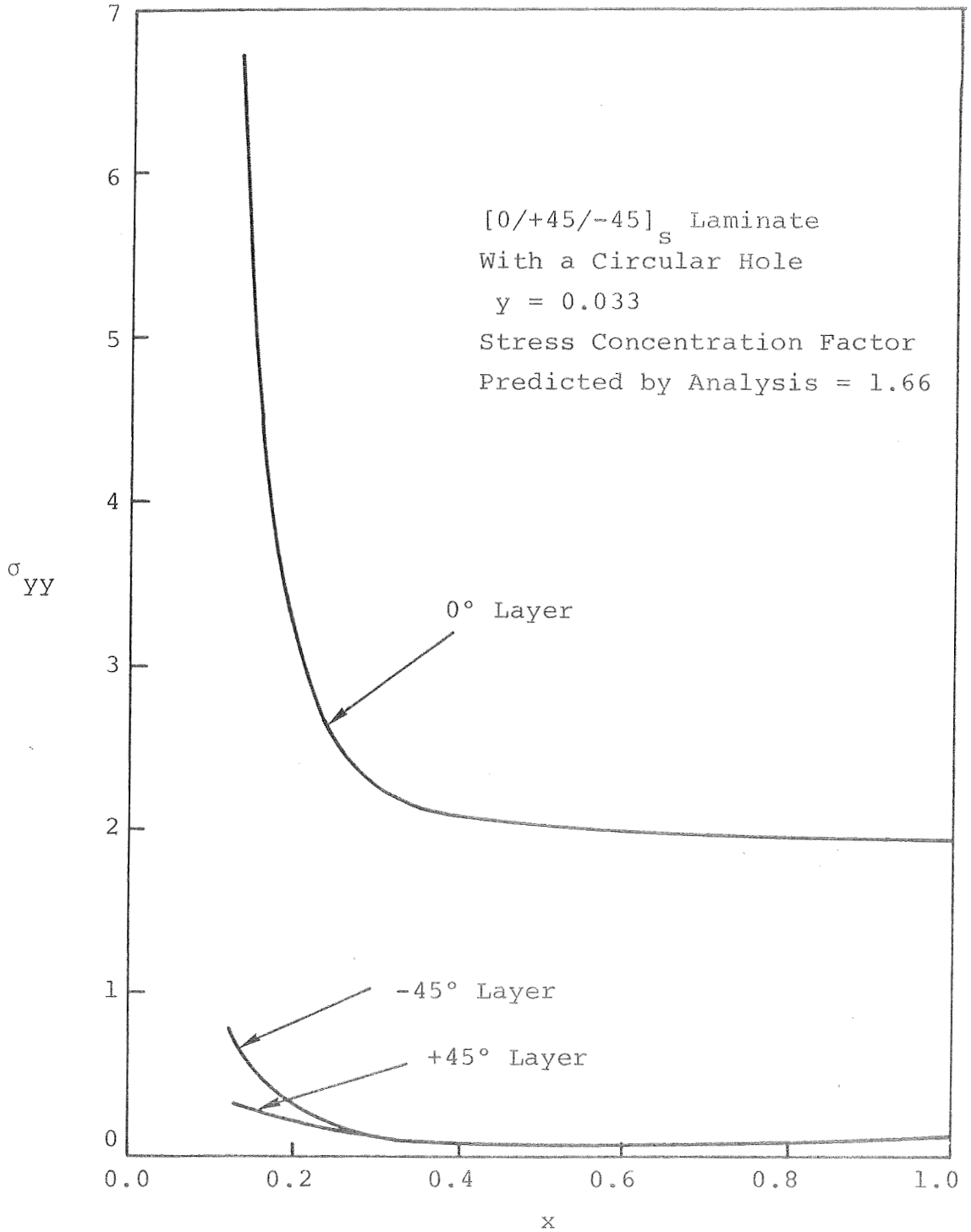

Figure 21. Variation of Element Centroidal σ_{yy} With x at y = 0.033

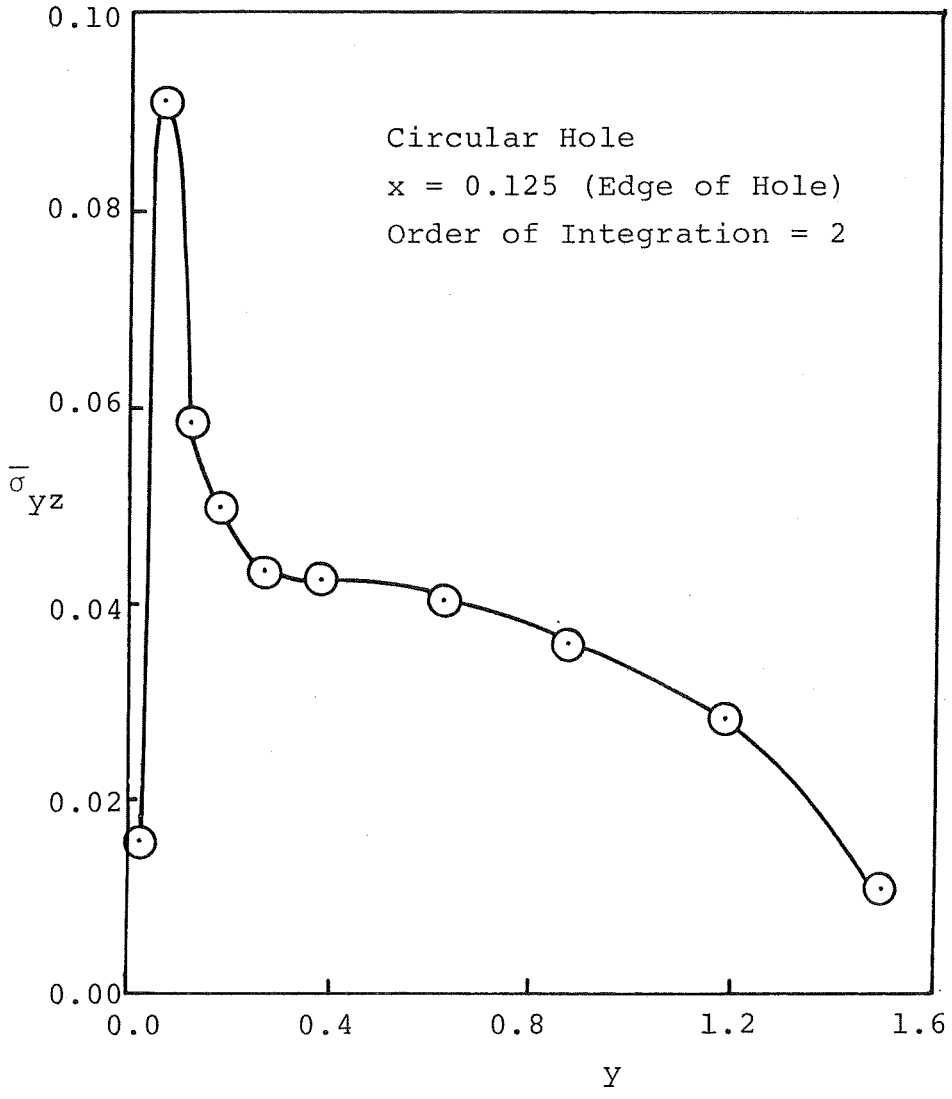

Figure 22. Variation of $\bar{\sigma}_{yz}$ with y at the 0/+45 Interface in a Notched $[0/+45/-45]_s$ Laminate

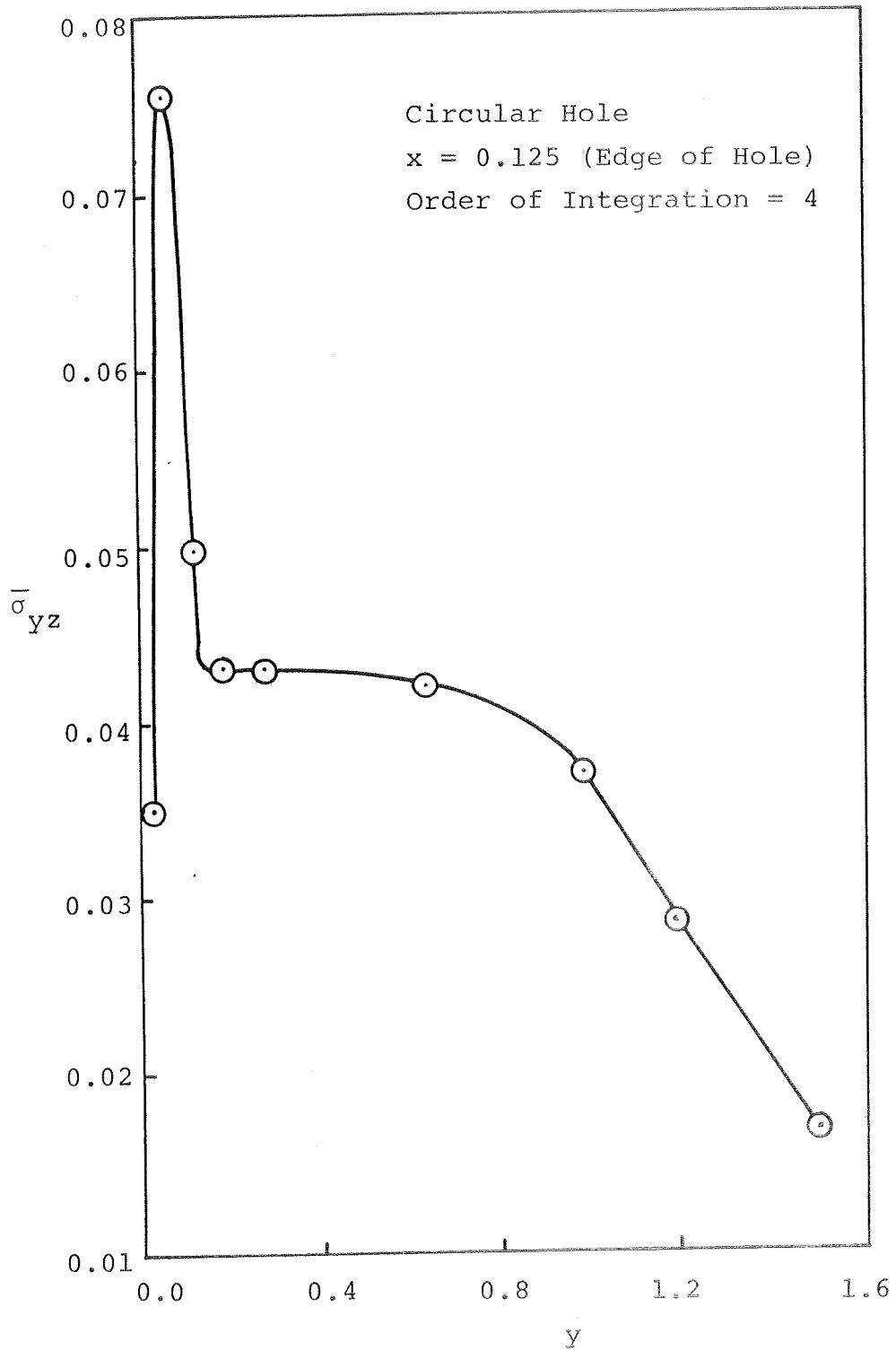

Figure 23. Variation of $\bar{\sigma}_{yz}$ with y at the 0/+45 Interface in a Notched $[0/+45/-45]_s$ Laminate

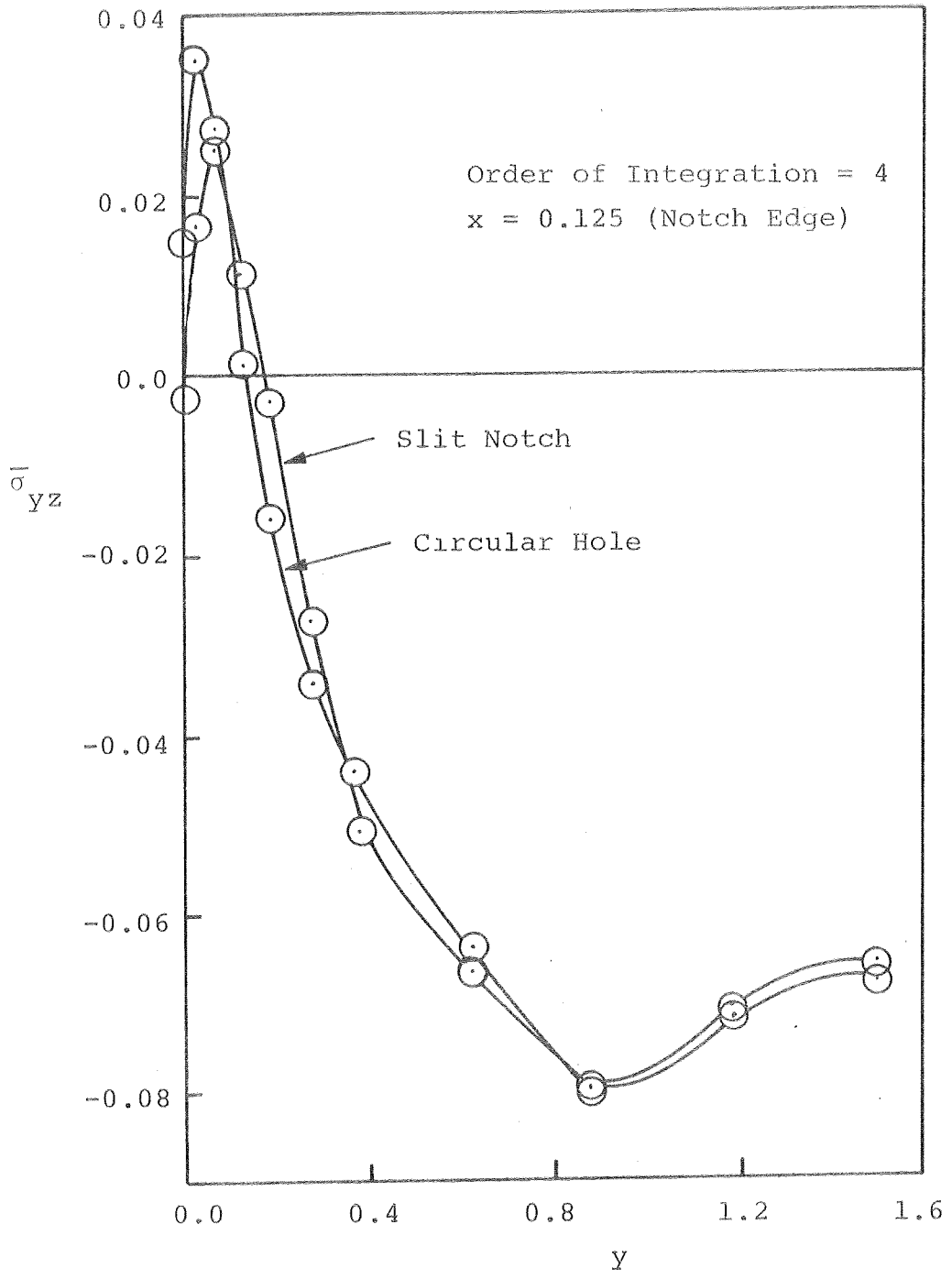

Figure 24. Variation of $\bar{\sigma}_{yz}$ with y at the +45/-45 Interface in Notched $[0/+45/-45]_s$ Laminates With a Circular Hole and a Slit Notch

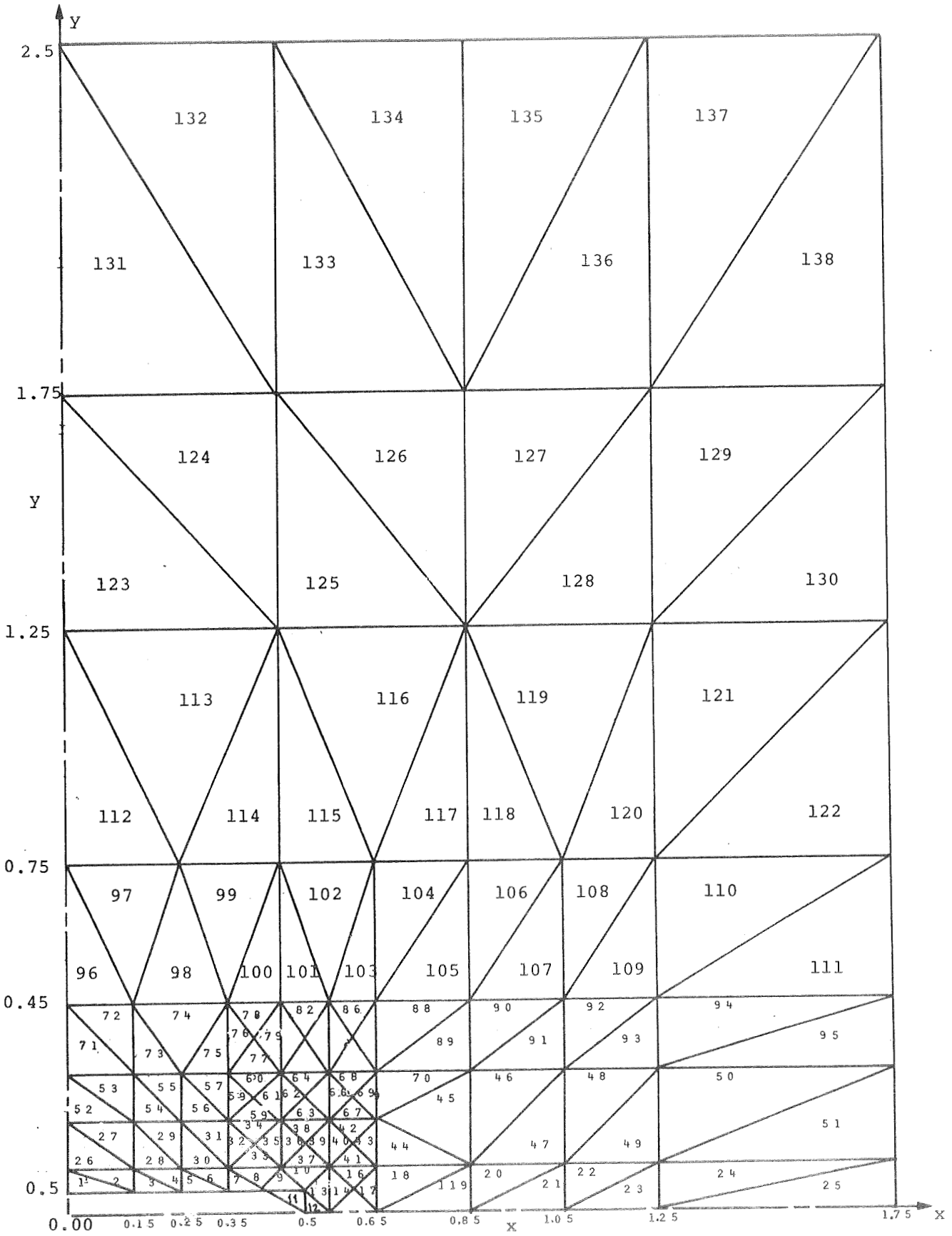

Figure 25. Mesh Geometry for the 2-D Elastic-Plastic Finite Element Analysis.

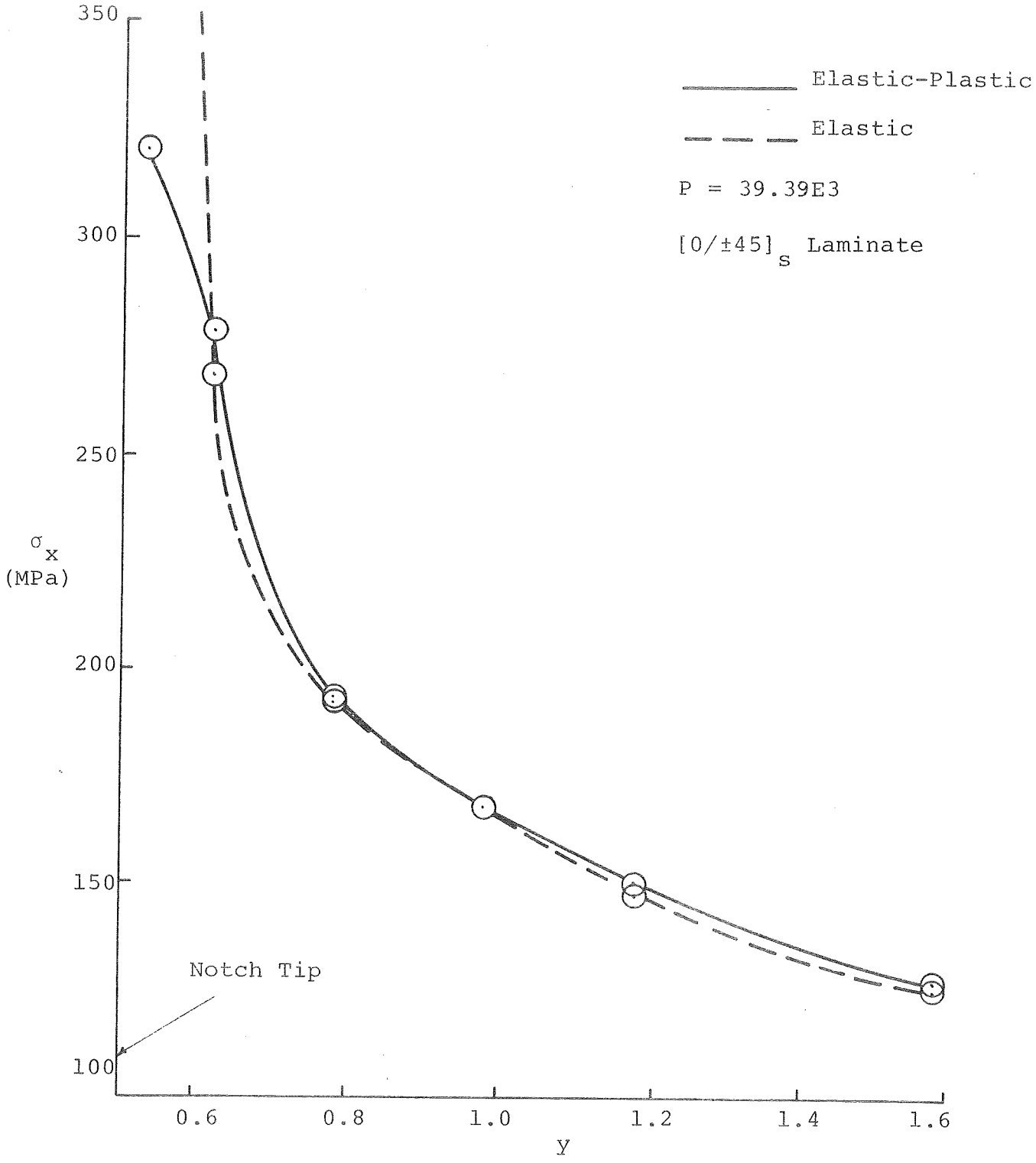

Figure 26. Variation of σ_x with y for P = 39.39E3

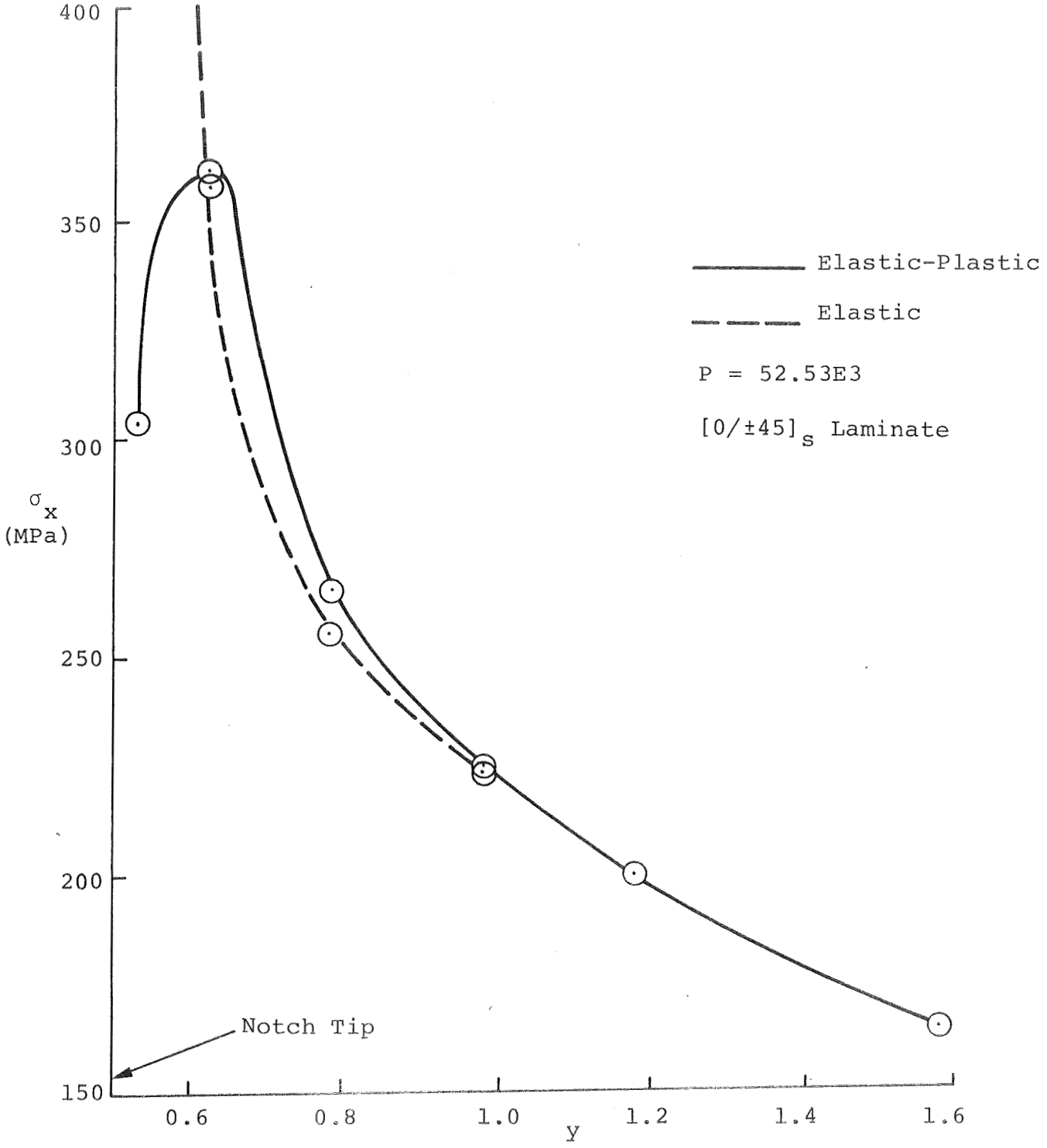

Figure 27. Variation of σ_x with y for P = 52.53E3

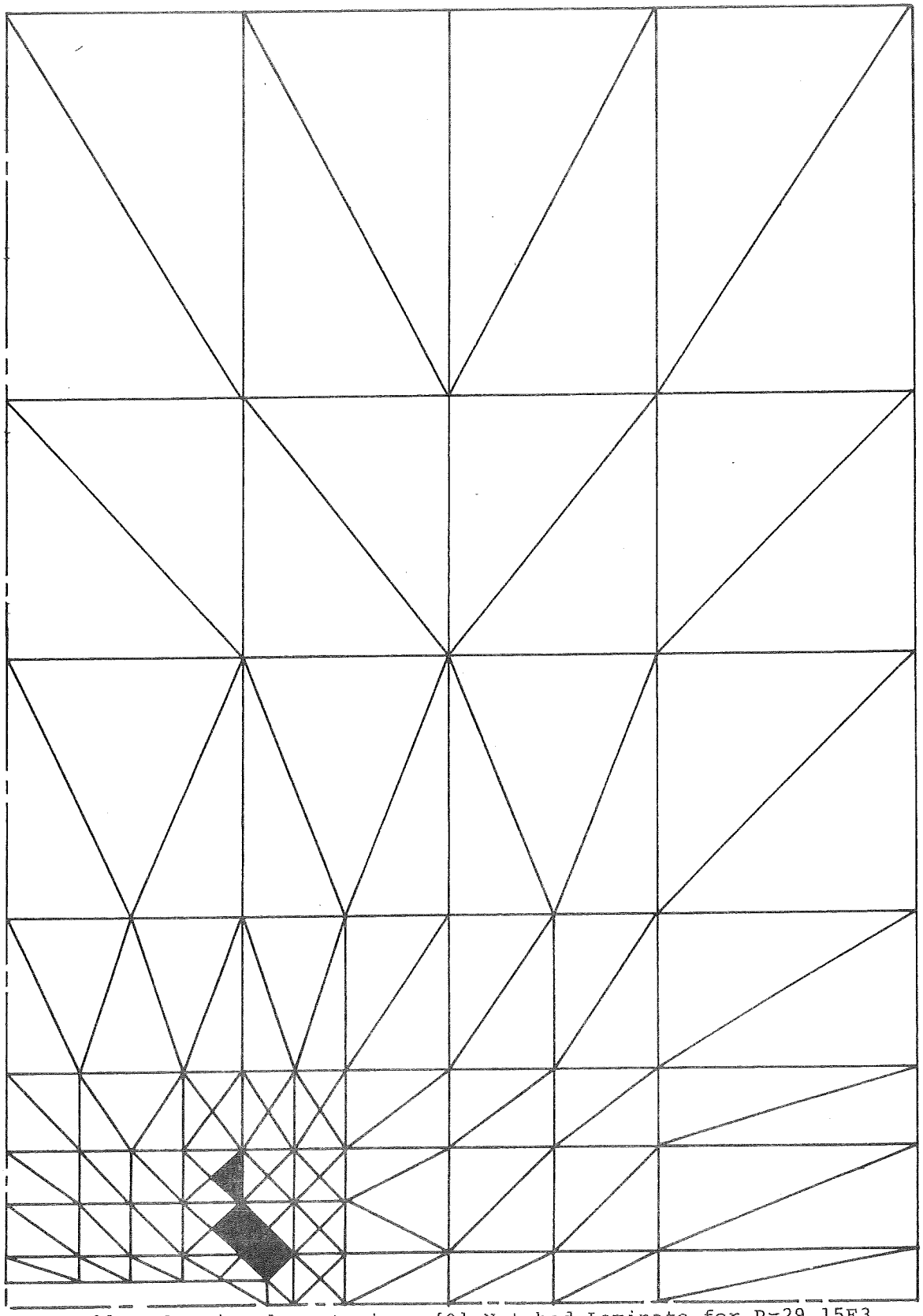

Figure 28. Plastic Elements in a [0] Notched Laminate for P=29.15E3

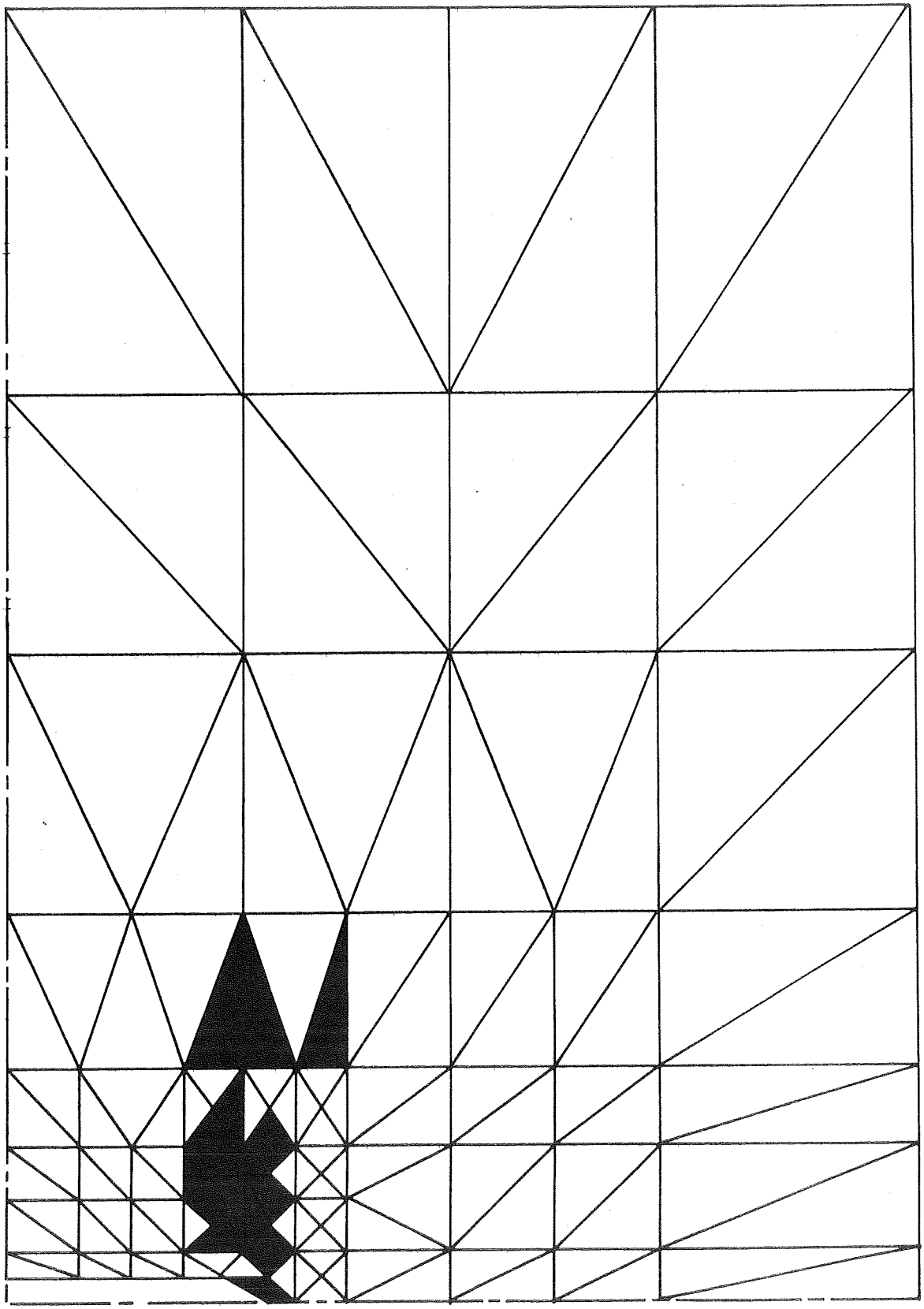

Figure 29. Plastic Elements in a $[0/90]_s$ Notched Laminate for P=28.06E3

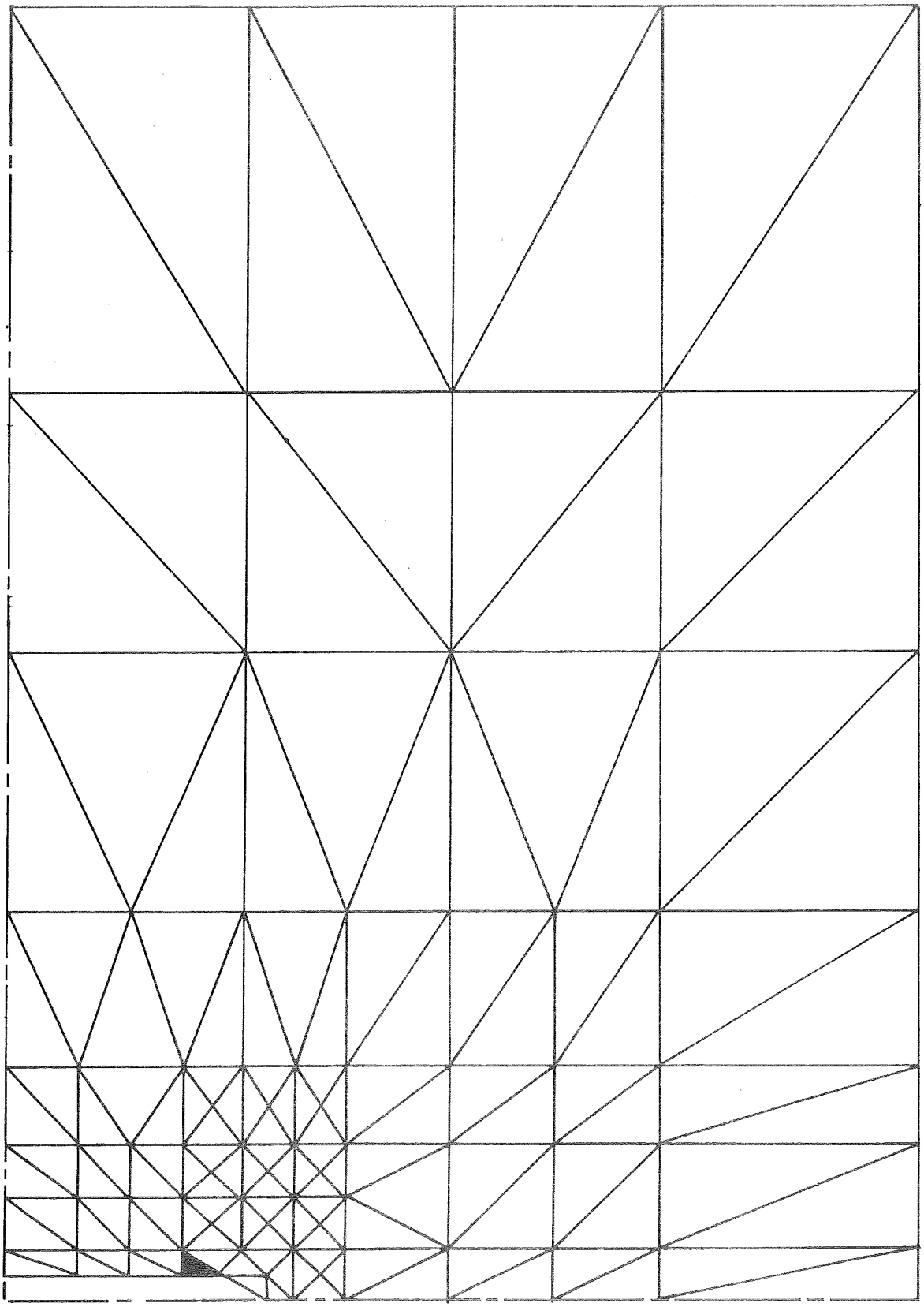

Figure 30. Plastic Elements in a $[0_2/\pm45]_s$ Notched Laminate for P=30.85E3

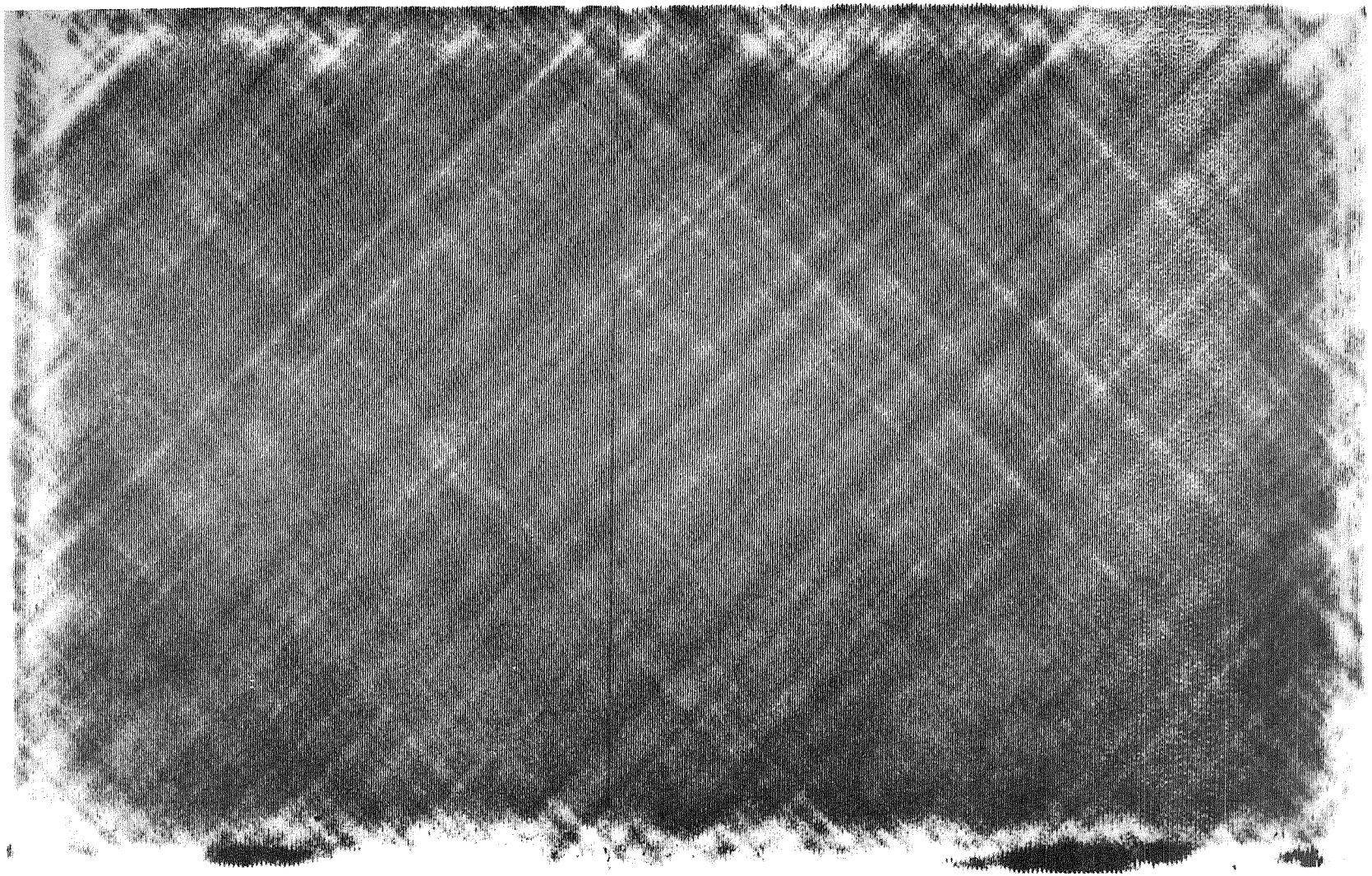

Figure 31. "C" Scans for a $[\pm 45]_s$ T-300/5208 Laminate Panel

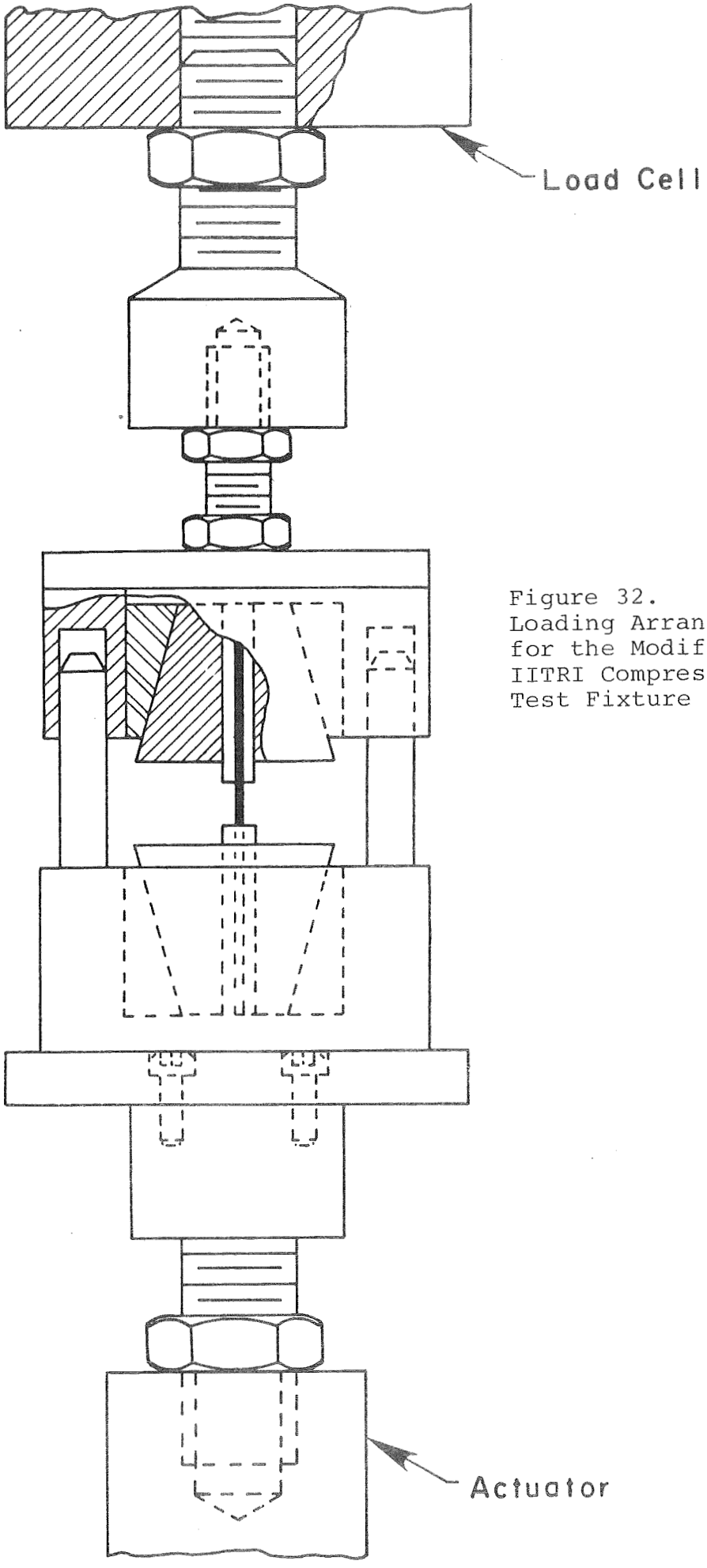

Figure 32.
Loading Arrangement
for the Modified
IITRI Compression
Test Fixture

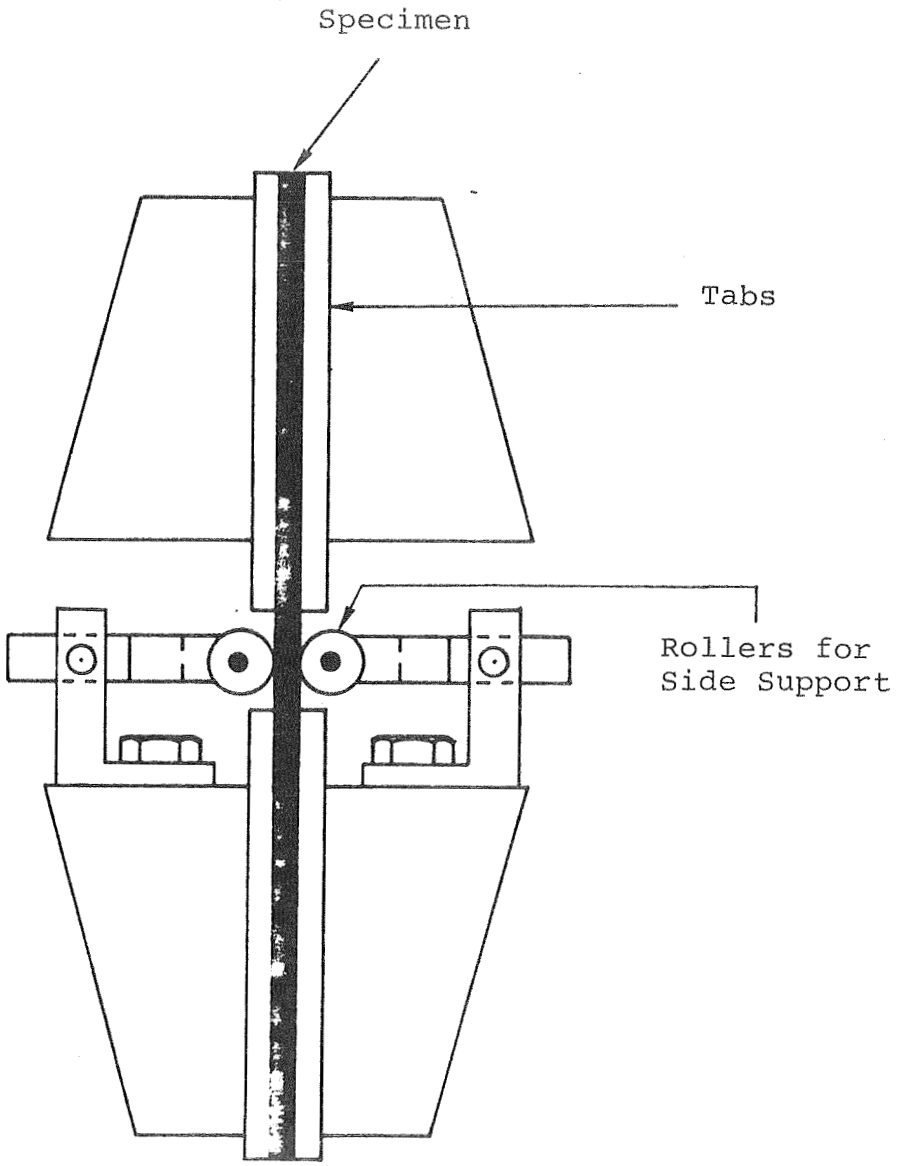

Figure 33. Modified IITRI Compression Test Fixture

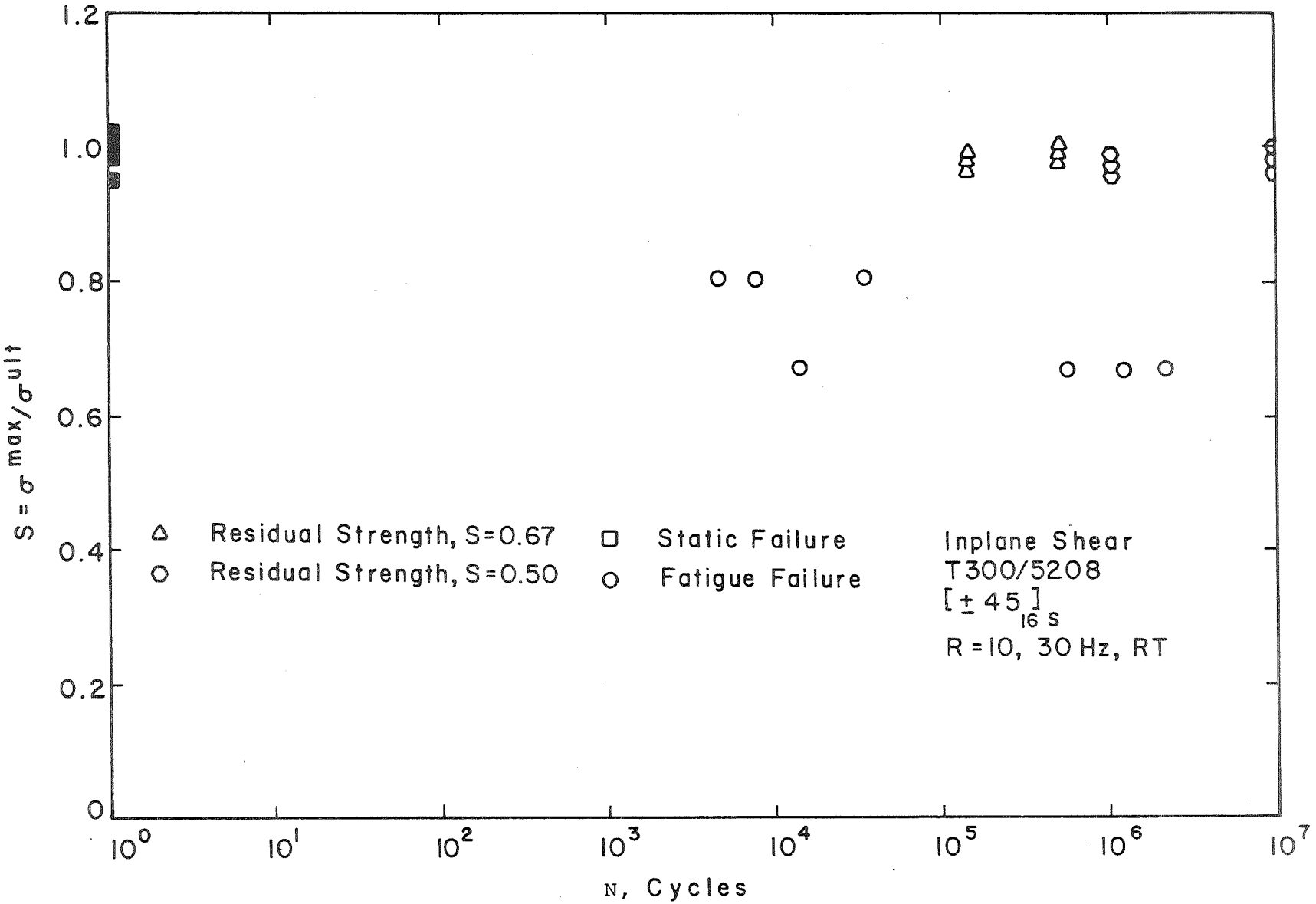

Figure 34. S-N and Residual Strength - N Data for $[\pm 45]_s$ T-300/5208 Compression/Compression Tests

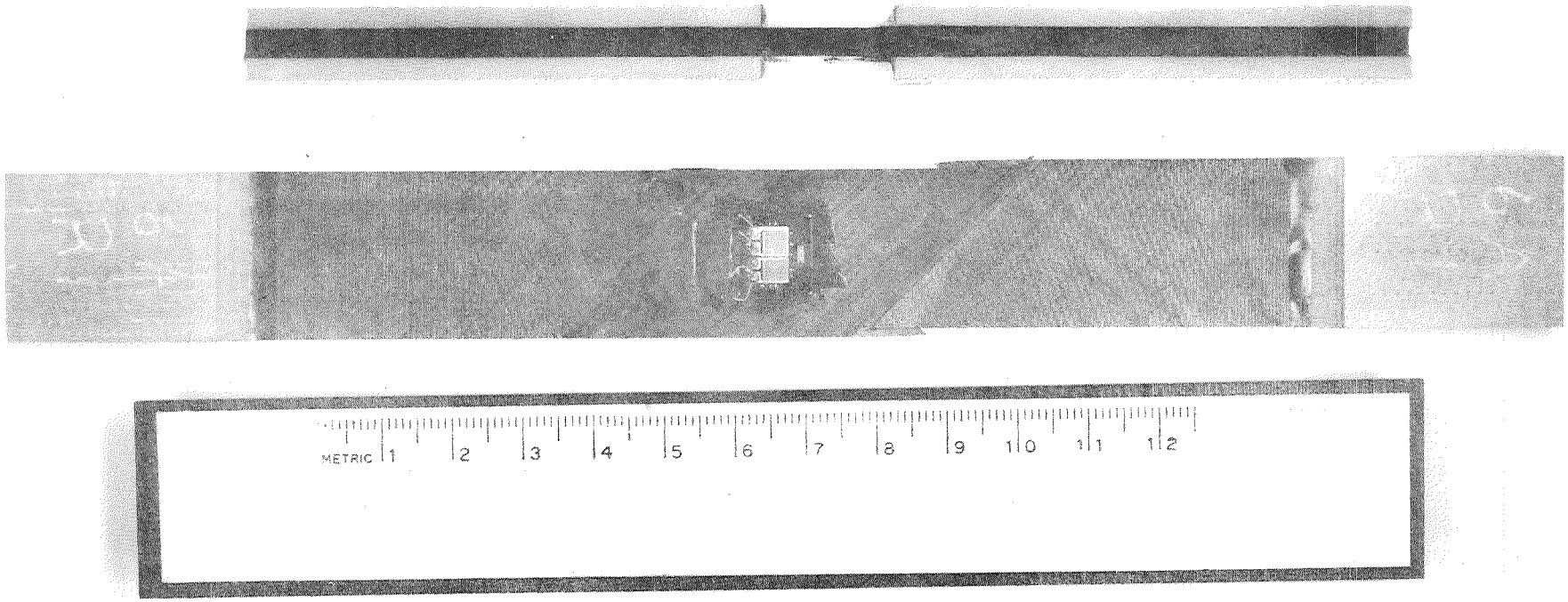

Figure 35. $[\pm 45]_s$ T-300/5208 Laminate Failure Modes for Uniaxial Tension for Two Different Specimen Geometries

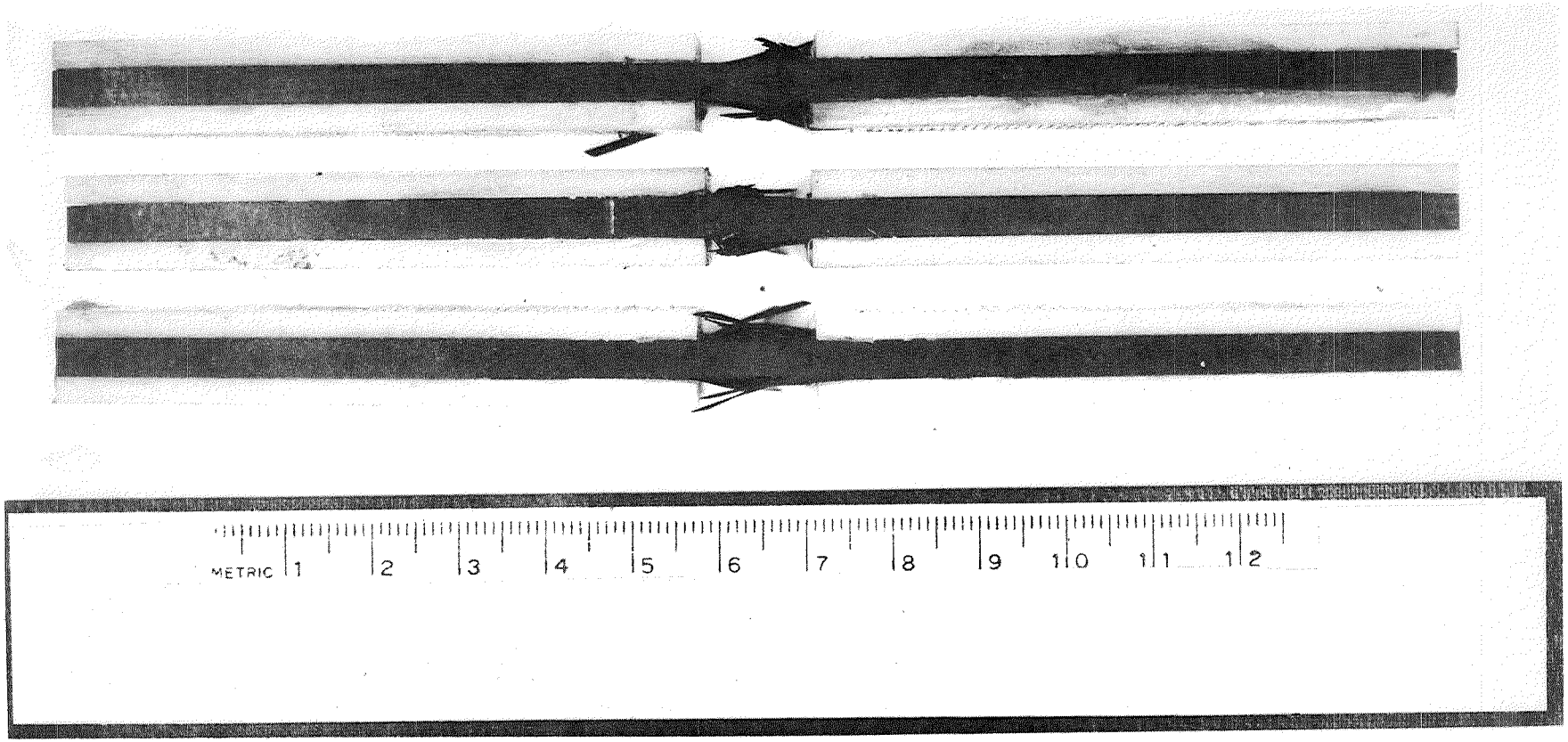

Figure 36. $[\pm 45_{16}]_s$ T-300/5208 Laminate Compression Failures Showing Microbuckling of Laminae

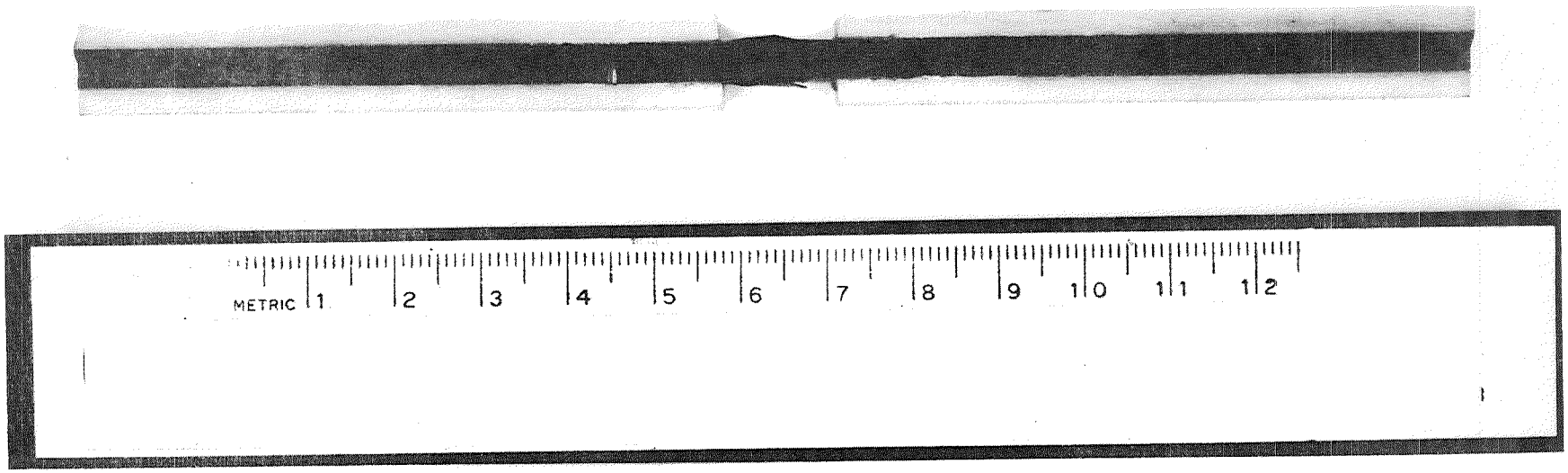

Figure 37. $[\pm 45_{16}]_s$ T-300/5208 Laminate Failure due to Surface Ply Buckling

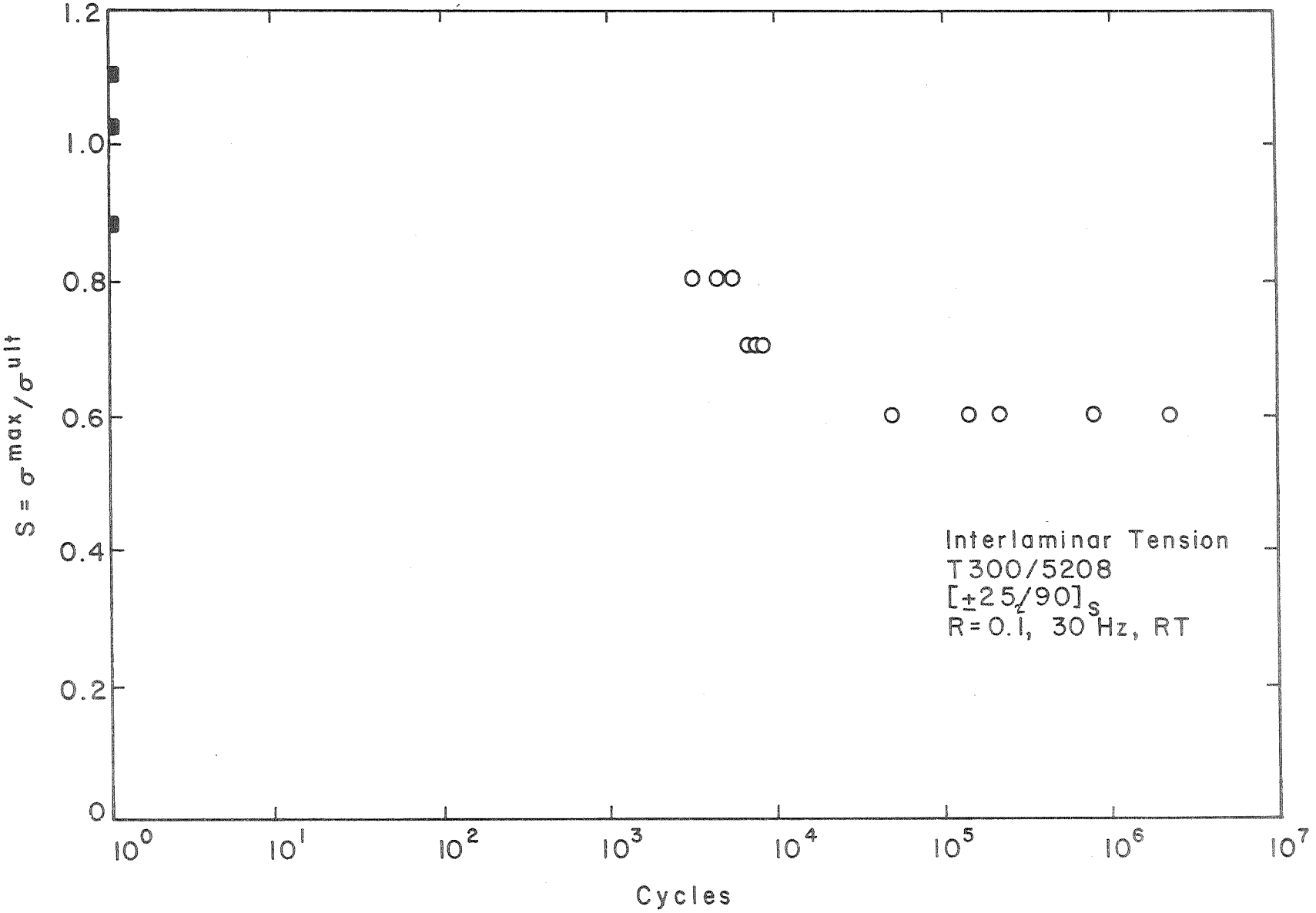

Figure 38. S-N Data for $[\pm 25_2/90]_s$ T-300/5208 Laminate

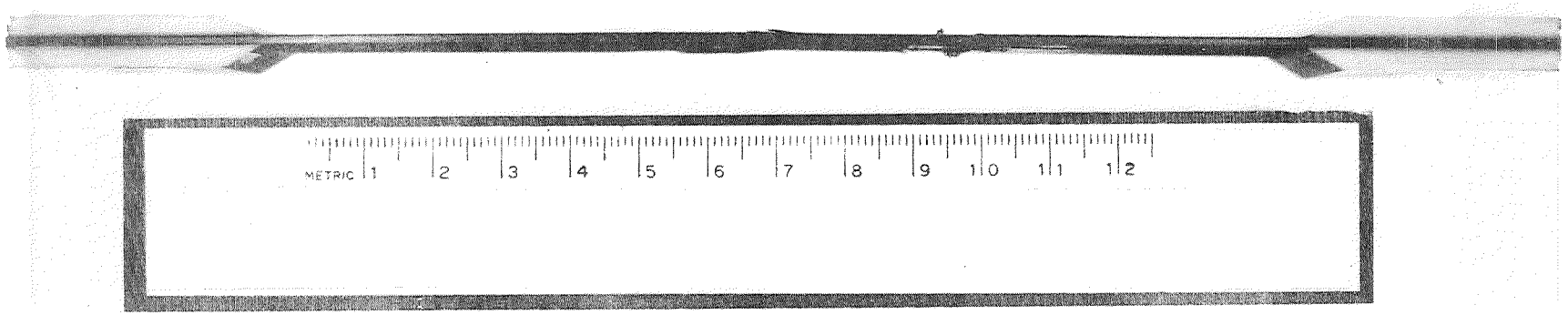

Figure 39. $[\pm 25_2/90]_s$ T-300/5208 Laminate Edge Failure due to Interlaminar Normal Stress

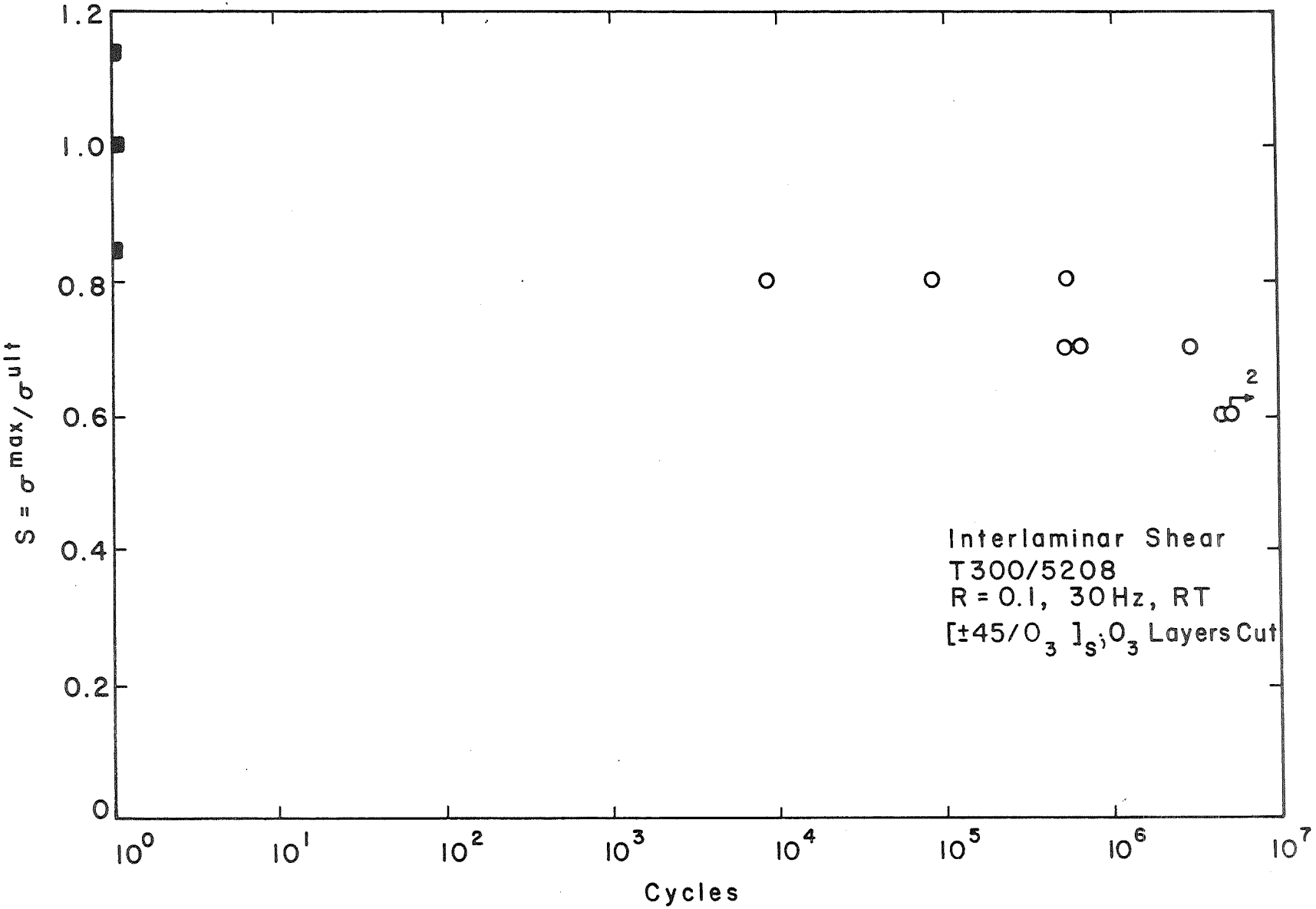

Figure 40. S-N Data for Partially Notched $[\pm 45/0_3]_s$ T-300/5208 Laminate

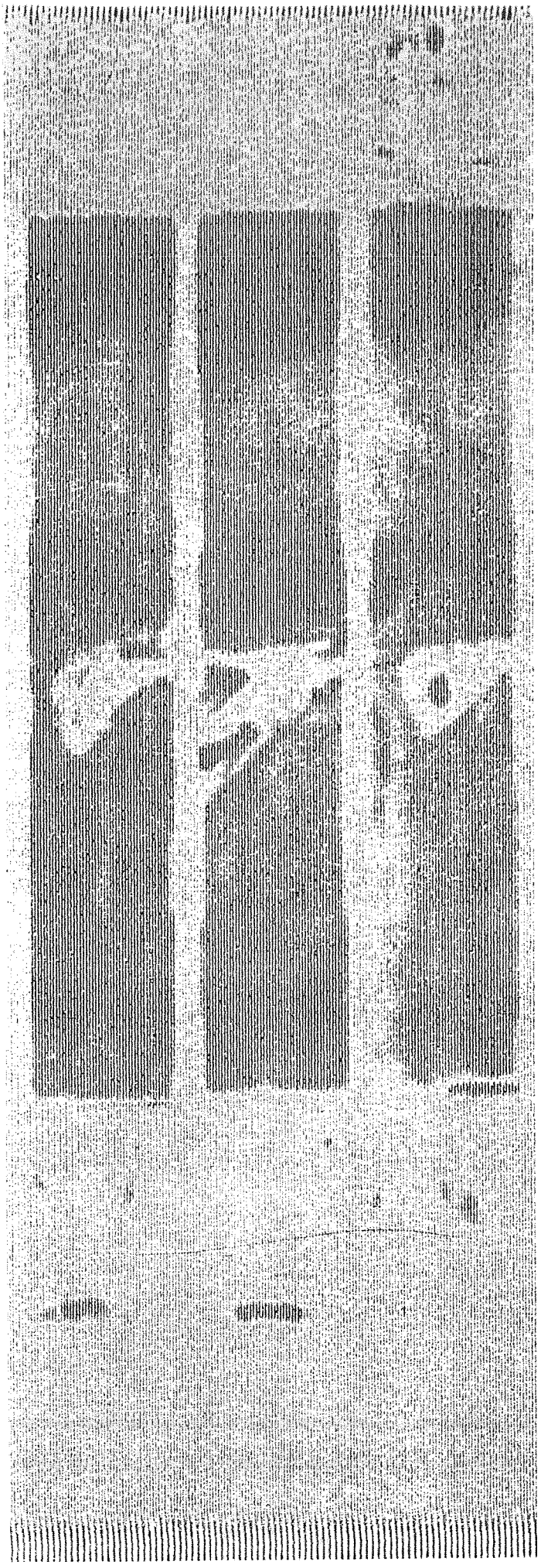

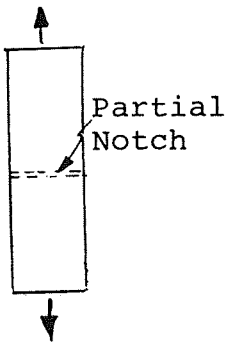

Figure 41.

C-Scans of Failed, Partially Notched $[\pm 45/0_3]_s$ T-300/5208 Laminates

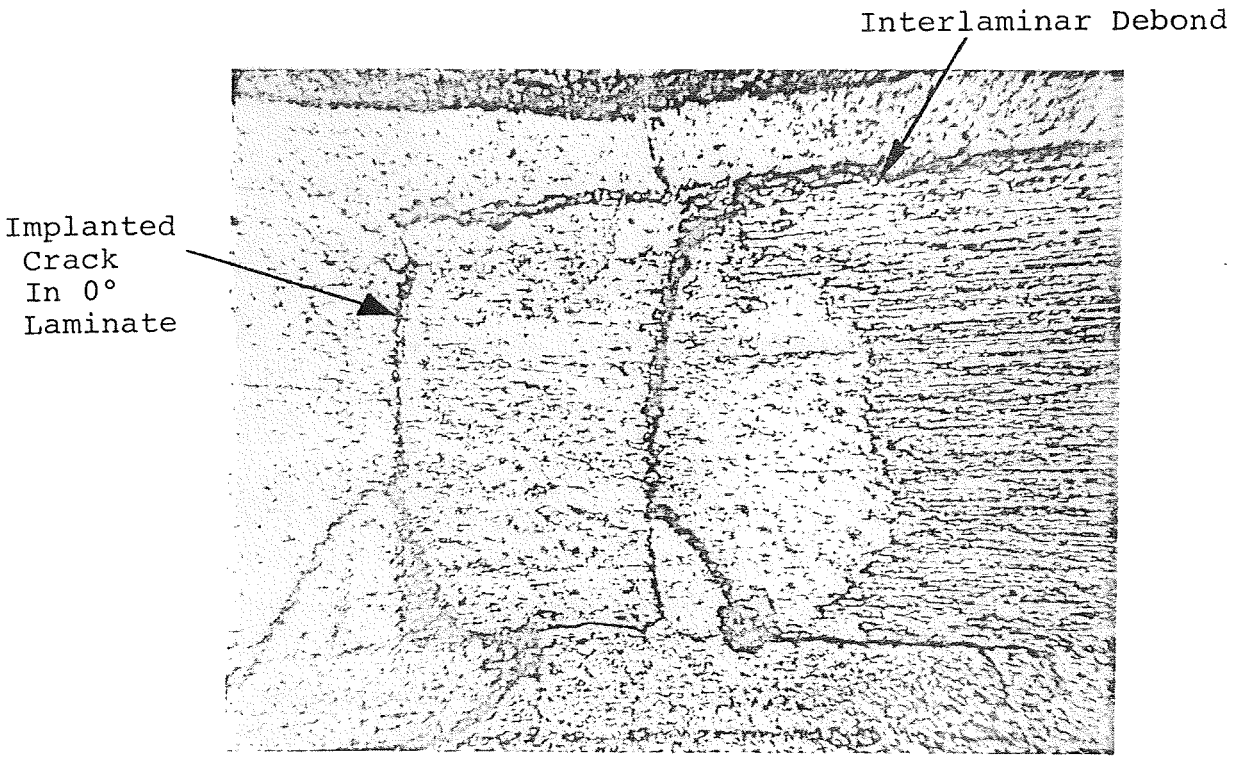

Figure 42. Photomicrograph of a Failed $[\pm 45/0_3]_s$ Partially Notched Laminate (x100)

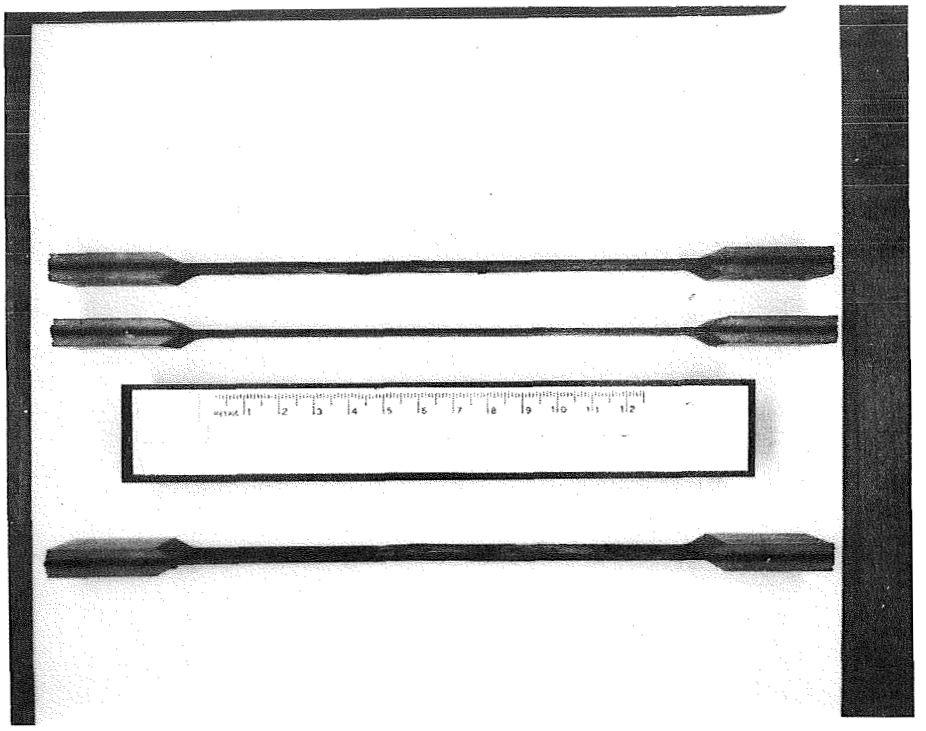

Figure 43. $[\pm 45/0_3]_s$ T-300/5208 Partially Notched Laminate Static and Residual Strength Test Failure Modes

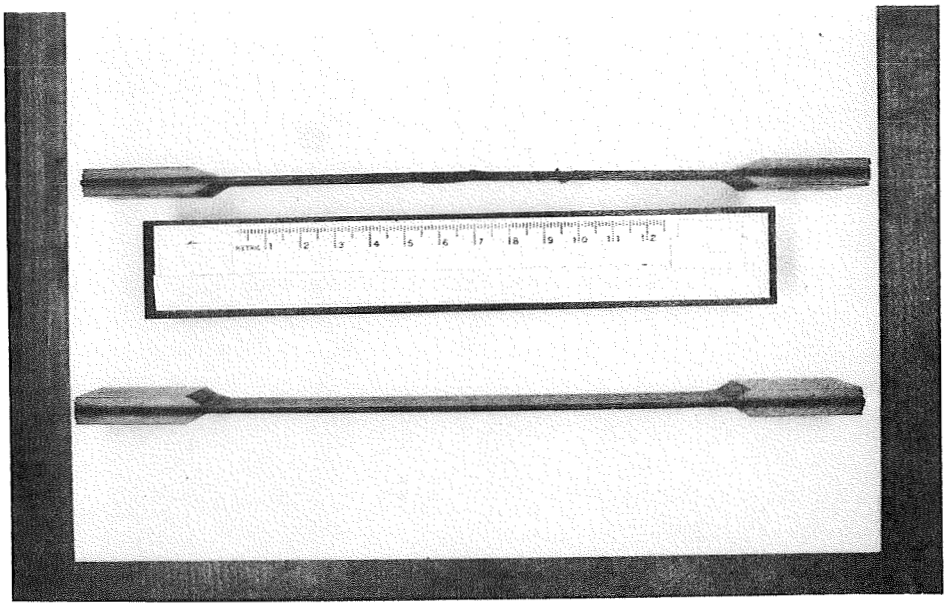

Figure 44. $[\pm 45/0_3]_s$ T-300/5208 Partially Notched Laminate Fatigue Failure Mode

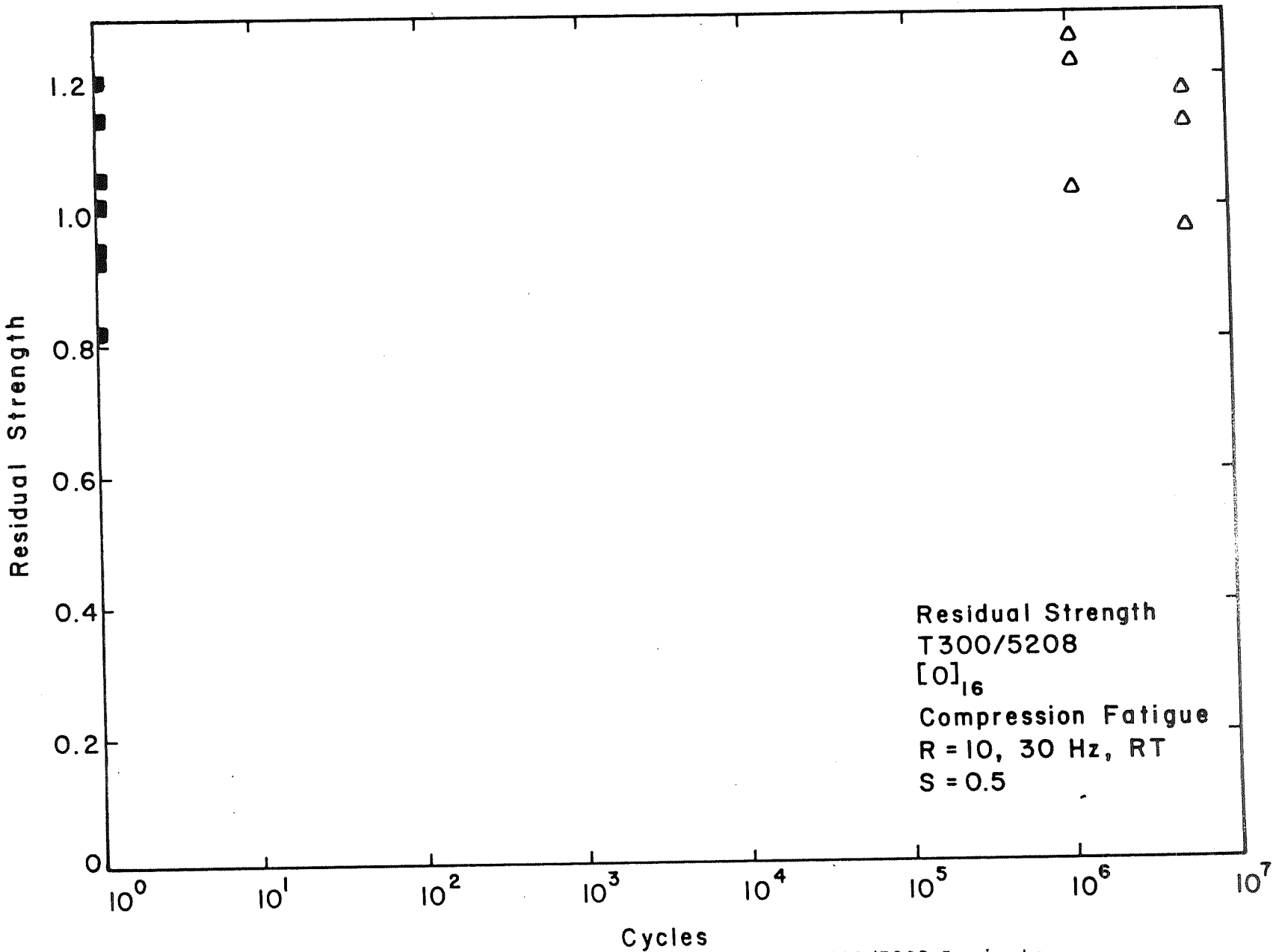

Figure 45. Residual Strength - N Data for [0] T-300/5208 Laminate

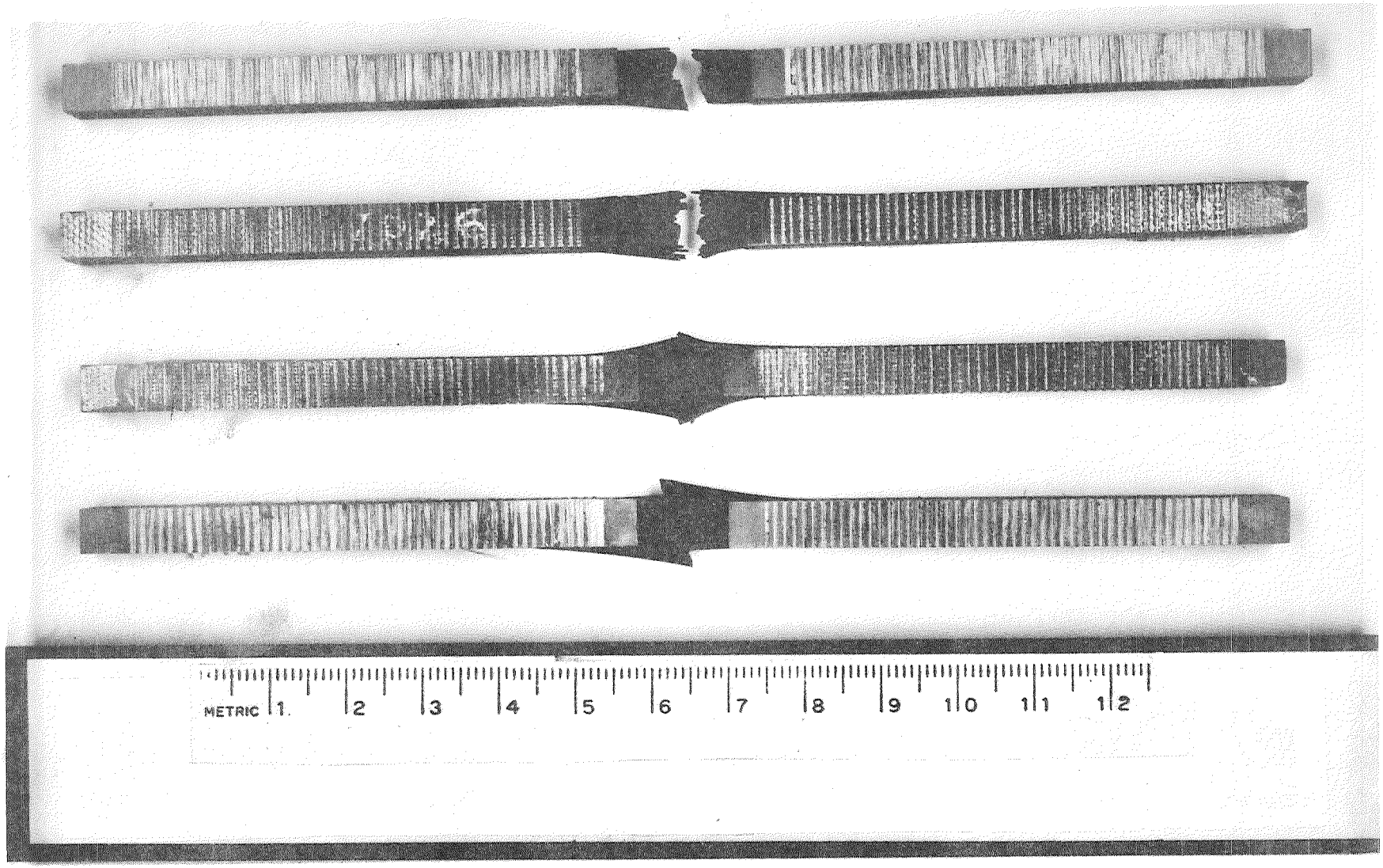

Figure 46. [0] T-300/5208 Laminate Compression Failures during Residual Strength Tests

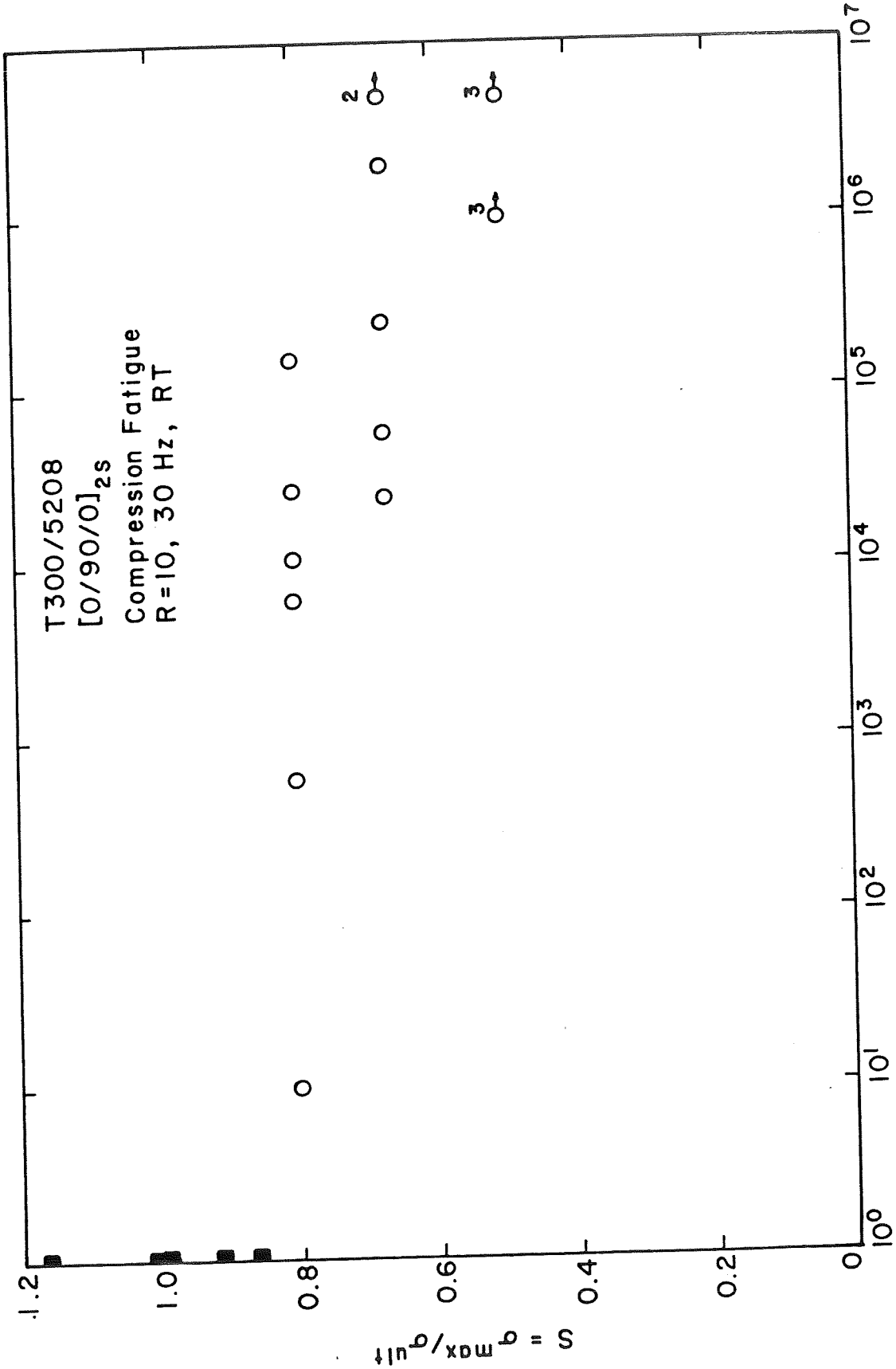

Figure 47. S-N Data for $[0/90/0]_{2s}$ T-300/5208 Laminate

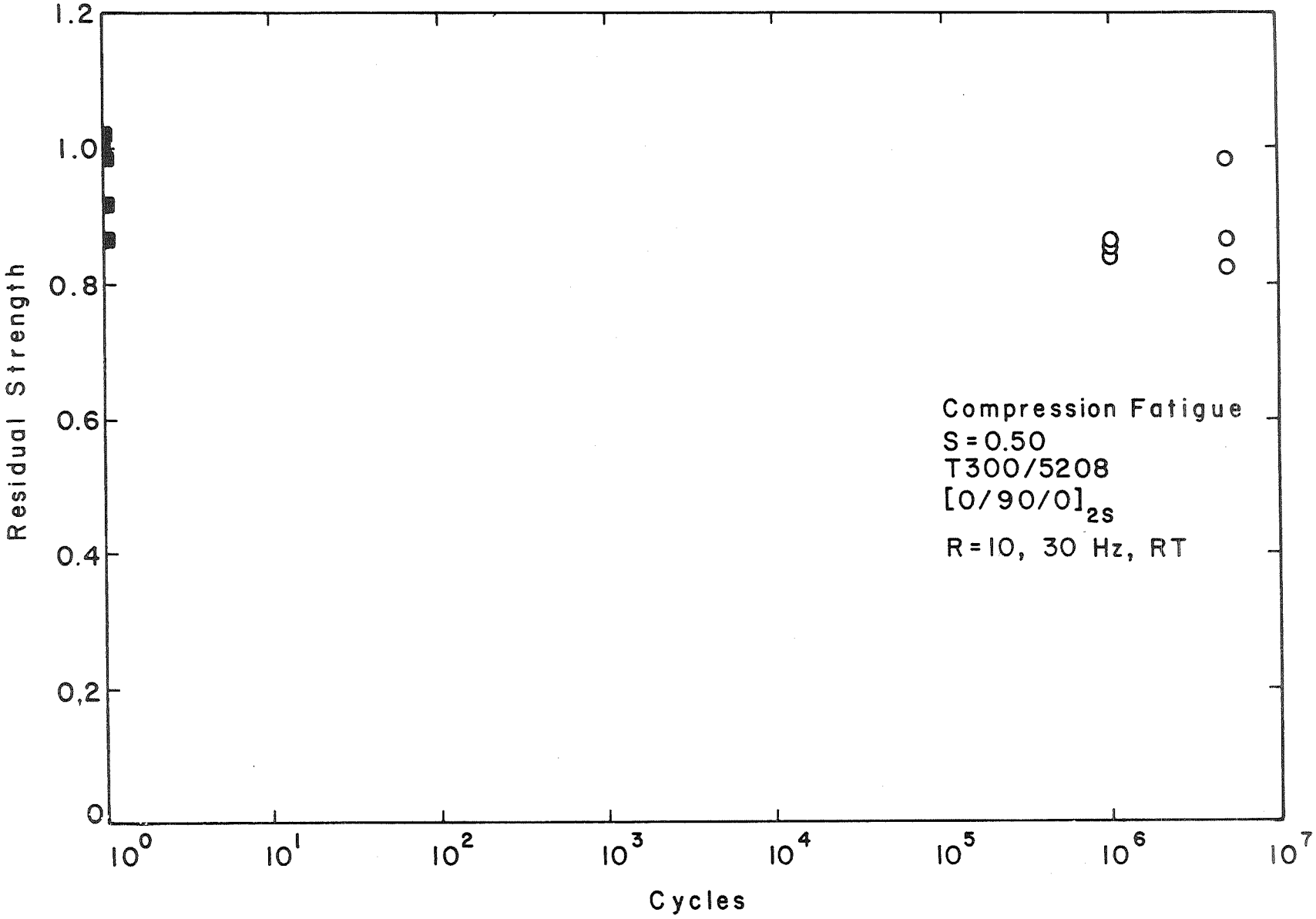

Figure 48. Residual Strength - N Data for $[0/90/0]_{2s}$ T-300/5208 Laminate

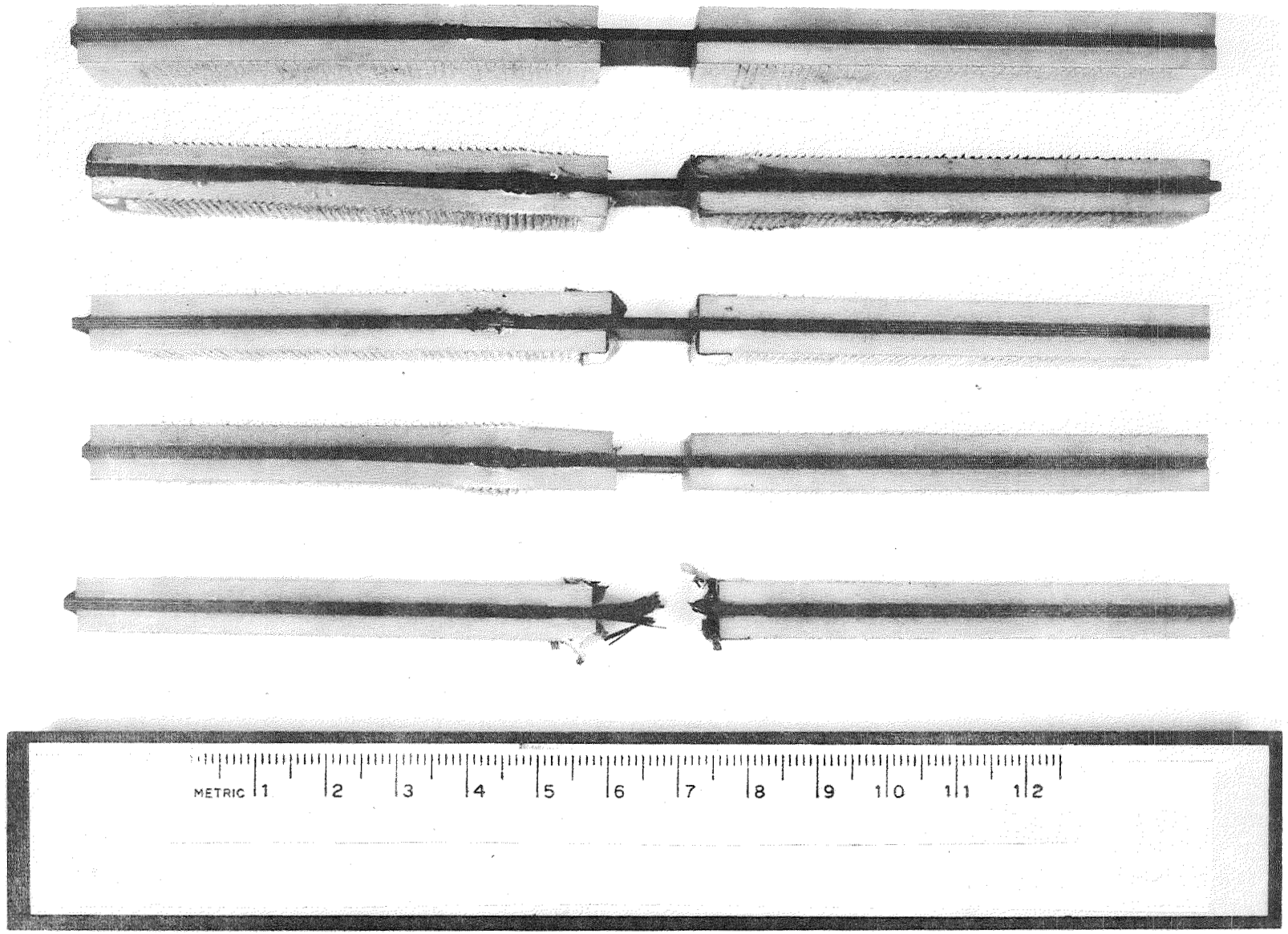

Figure 49. $[0/90/0]_{2s}$ T-300/5208 Laminate Failure Modes during Fatigue (Inside the Tabs for S=0.8) and during Residual Strength Tests

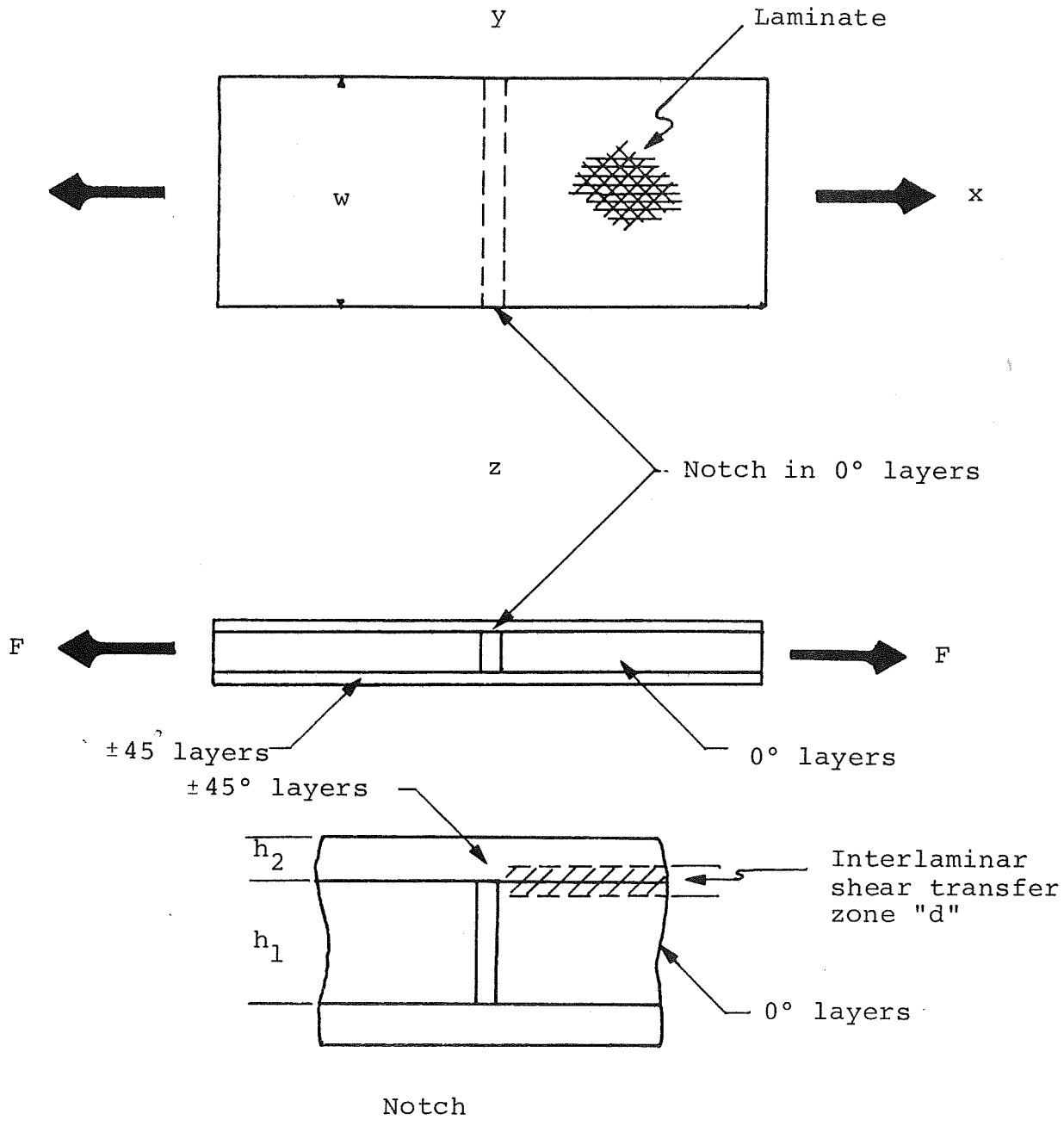

Figure B1. Partially Notched $[\pm 45_i/0_j]_s$ Laminate for Obtaining Interlaminar Shear Stress (τ_{xz}) Data (not to scale)

DISTRIBUTION LIST

	No. Copies
NASA Langley Research Center Hampton, VA 23665	
Attn: Report & Manuscript Control Office, Mail Stop 180A	1
Structures Laboratory, USARTL (AVRADCOM), Mail Stop 266	2
George L. Roderick, Mail Stop 188E	24
NASA Ames Research Center Moffett Field, CA 94035	
Attn: Library, Mail Stop 202-3	1
US Army Research & Technology Laboratories (AVRADCOM), Mail Stop 207-1	2
Aeromechanics Laboratory, USARTL (AVRADCOM), Mail Stop 215-1	2
NASA Dryden Flight Research Center P. O. Box 273 Edwards, CA 93523	
Attn: Library	1
NASA Goddard Space Flight Center Greenbelt, MD 20771	
Attn: Library	1
NASA Lyndon B. Johnson Space Center 2101 Webster Seabrook Road Houston, TX 77058	
Attn: JM6/Library	1
NASA Marshall Space Flight Center Marshall Space Flight Center, AL 35812	
Attn: Library, AS61L	1
Jet Propulsion Laboratory 4800 Oak Grove Drive Pasadena, CA 91103	
Attn: Library, Mail 111-113	1
National Aeronautics & Space Administration Washington, DC 20546	
Attn: RW	1
RWS/Dr. Michael Salkind	1
NASA John F. Kennedy Space Center Kennedy Space Center, FL 32899	
Attn: Library, IS-DOC-1L	1

	No. Copies
NASA Lewis Research Center 21000 Brookpark Road Cleveland, OH 44135	
Attn: Library, Mail Stop 60-3	1
Robert H. Johns, Mail Stop 49-3	1
Gordon T. Smith, Mail Stop 49-3	1
Propulsion Laboratory, USARTL (AVRADCOM), Mail Stop 500-317	2
University of Wisconsin Department of Engineering Mechanics Madison, WI 53706	
Attn: Professor R. E. Rowlands	1
United Aircraft Corporation Pratt & Whitney Aircraft East Hartford, CT 06118	
Attn: Dr. T. A. Cruse, Scientific Analysis Group	1
University of Wyoming Department of Mechanical Engineering Larmie, WY 82070	
Attn: Professor Donald F. Adams	1
University of Minnesota 107 Aeronautical Engineering Building Minneapolis, MN 55455	
Attn: Professor Phil Hodge	1
Northrop Corporation Aircraft Division 3901 W. Broadway Hawthorne, CA 90250	
Attn: Glen C. Grimes, Engineering Specialist Structures R&T, Dept. 3780/62	1
Kedwork, Kawa & Associates LTD 400 Kelvin Boulevard Winnipeg, Manitabo CANADA R3P 0j2	
Attn: Dr. Keith T. Kedwork	1
McDonnell Douglas Corporation P. O. Box 516 St. Louis, MO 63166	
Attn: Dr. Michael P. Renieri, Bldg. 34, Post 350	1
Dr. Gary D. Renieri, Bldg 106, Level 4, Post C-5	1

	No. Copies
Department of the Navy Office of Naval Research Arlington, VA 22217 Attn: Dr. Nicholas Perrone, Director, Structural Mechanics Program	1
National Science Foundation Washington, DC 20550 Attn: Dr. Clifford J. Astill, Solid Mechanics Program	1
Wright-Patterson Air Force Base, OH 45433 Attn: MBM/Dr. Nicholas J. Pagano	1
Air Force Flight Dynamics Laboratory Wright-Patterson Air Force Base, OH 45433 Attn: Dr. George P. Sendeckyj, Structures Division Dr. J. C. Halpin	1 1
Air Force Materials Laboratory Wright-Patterson Air Force Base, OH 45433 Attn: Dr. J. M. Whitney, Nonmetallic Materials Division Dr. H. T. Hahn, Nonmetallic Materials Division	1 1
University of Delaware Department of Mechanical & Aerospace Engineering 107 Evans Hall Newark, DE 19711 Attn: Dr. R. Byron Pipes	1
Battelle Columbus Laboratories 505 King Avenue Columbus, OH 43201 Attn: Dr. Edmund F. Rybicki	1
E. I. duPont de Nemours & Co., Inc. Experimental Station/B262 Wilmington, DE 19898 Attn: Dr. Carl H. Zweben, Textile Fibers	1
IIT Research Institute 10 West 35 Street Chicago, IL 60616 Attn: Dr. I. M. Daniel, Manager	1
General Dynamics Corporation Fort Worth, TX 76101 Attn: M. E. Waddoups	1

	No. Copies
McDonnell Douglas Corporation Douglas Aircraft Company 3855 Lakewood Boulevard Long Beach, CA 90846 Attn: Dr. Longin B. Greszczuk	1
Lockheed Aircraft Corporation Lockheed-California Company P. O. Box 551 Burbank, CA 91520 Attn: Larry R. Markham, Dept. 7572, Bldg. 63, Plant A1	1
Applied Technology Laboratory US Army Research & Technology Laboratories (AVRADCOM) Fort Eustis, VA 23604 Attn: J. Robinson/SAVDL-EU-SS	2
Department of the Army US Army Materials & Mechanics Research Center Waterton, MA 02172	1
Attn: Dr. E. Lenoe	1
Dr. J. Perkins	1
Picatinny Arsenal Materials Engineering Laboratory, Bldg. 183 Dover, NJ 07801 Attn: Charles Wright	1
NASA Scientific & Technical Information Facility 6571 Elkridge Landing Road Linthicum Heights, MD 21090	27 plus original